A Monte Carlo simulation study of the excitation of molecules in high-mass star forming regions

L Mfulwane

orcid.org 0000-0002-0823-1423

Dissertation accepted in partial fulfilment of the requirements for the degree *Master of Science in Astrophysical Sciences* at the North-West University

Supervisor:	Prof DJ van der Walt
Co-supervisor:	Prof JO Chibueze

Graduation May 2024

26730367

Declaration of Authorship

I, Lebogang Lenah Mfulwane, declare that this thesis titled, **A Monte Carlo simulation study of the excitation of molecules in high-mass star forming regions** and the work presented in it are my own. I confirm that:

- This work was done wholly or mainly while in candidature for a research degree at this university.
- Where any part of this thesis has previously been submitted for a degree or any other qualification at this university or any other institution, this has been clearly stated.
- Where I have consulted the published work of others, this is clearly attributed.
- Where I have quoted from the work of others, the source is always given. With the exception of such quotation, this thesis is entirely my work.
- I have acknowledged all main sources of help.
- Where the thesis is based on work done by myself jointly with others, I have made clear exactly what was done by others and what I have contributed myself.

Signed : L.L Mfulwane

Date : 02 February 2024

Acknowledgements

Before anything else, I would like to express my sincere gratitude to the National Astrophysics and Space Science Programme (NASSP) and the Centre for Space Research (CSR) at North-West University for supporting my work financially.

My absolute gratitude goes to my supervisor, Prof. Johan van der Walt, for the outstanding guidance and words of wisdom. It was a long journey, full of ups and downs; however, your guidance inspired me to keep going. Thank you so much! I would also like to thank Prof. James Chibueze for the support and advice to get me through. Many thanks to Ms J. Wessels for editing and critically reviewing this work. To the staff members, to mention a few, Ms L. van Wyk, Ms E. van Rooyen, Mr K. Tefo and Mr L. Fransman, I am grateful for the support.

I would also like to express my uttermost gratitude to a few individuals who supported me through this journey. Their contribution made this work possible and shaped who I am. My gratitude starts with God the Almighty for the strength for the strength to see me through to the end. A special thank you to my late parents, Mr Moses P. Mfulwane and Mrs Maria M. Mfulwane. Even when my mother didn't understand the career path I had chosen for myself, she still supported me until her last days. To my siblings, Marcus, Candis, Kgomotso, Dipuo and Lerato I am grateful for the emotional support. To friends and colleagues Mr A. Dzodzomenyo, Ms M. Seidu, Ms B. Homera and Mr D. Phuravhathu, thank you for the advice and chats to lift my spirit.

Abstract

Astronomical maser emission occurs in various astrophysical environments and can be used to infer the physical properties of the regions where they are excited. A key component of interpreting the presence of maser emission associated with a specific astrophysical environment is determining the pumping mechanism (radiative or collisional) for a particular maser. Baan et al. (2017) recently concluded that the extragalactic 4.8GHz formaldehyde megamasers are radiatively pumped, based on calculations, using the online Radex facility. The aforementioned is contrary to the conclusion of van der Walt (2014) that formaldehyde masers associated with high mass star forming regions are collisionally pumped. Since much of the interpretation of the maser emission depends on the pumping mechanism, we revisited the pumping of the formaldehyde masers to try to understand the results obtained by Baan et al. (2017).

A Monte Carlo model was built to investigate the pumping mechanism of this molecule. A single molecule is modelled as a system, and the rest of the molecules, H_2 molecules and the radiation represent the reservoir. The molecule is followed in time. The Monte Carlo simulation models the random walk of the molecule into various energy states according to the probabilities of radiative and collisional excitation processes. Two distributions are constructed as a result: the holding time distribution and the distribution of the number of visits.

The calculations show that understanding the roles of collisional and radiative excitation processes helps to determine the pumping scheme of a maser. The pumping scheme proposed explains why the collisional excitation process plays a prominent role in establishing an inversion and why external radiation alone cannot lead to an inversion. The results of this study suggest that 4.8 GHz formaldehyde masers are not pumped by radiation just because it is dominant but more precisely require a path and an excitation process, which in this case is collisions, which is the corresponding process of the dominant radiative process.

Keywords: Monte Carlo; Markov chain Monte Carlo; masers: stars; stars: massive.

Contents

List of Figures

List of Tables

Table of abbreviations

A list of abbreviations used throughout the text.

CH_3OH	Methanol
CS	Monocarbon sulphide
H_2	Molecular hydrogen
H_2CO	Formaldehyde
HCN	Hydrogen cynanide
ISM	Interstellar medium
IMF	Initial mass function
LTE	Local thermodynamic equilibrium
MASER	Microwave amplification by stimulated emission of radiation
MC	Monte Carlo
MERLIN	Multi-element radio linked interferometer
NH_3	Ammonia
Non-LTE	Non-local thermodynamic equilibrium
OH	Hydroxyl
SCD	Specific column density
SED	Spectral energy density
SiO	Silicon monoxide
SiS	Silicon monosulphide
TE	Thermodynamic equilibrium
VLA	Very large array
VLBA	Very long baseline array

Chapter 1

Introduction

The chemical composition of the primordial gas of the Universe after the Big Bang consisted of approximately 91% hydrogen (H) and 9% helium (He) and traces of lithium (Li). The population III stars, the first stars to form after the Big Bang, were composed of this primordial gas. The first heavier elements after helium were formed in the supernova events of the population III stars via nucleosynthesis.

The cycle of high-mass star formation followed by supernova events gradually enriched the interstellar medium (ISM) with these heavier elements. The gradual increase of these heavier elements in the ISM had as a consequence that lower-mass stars could also form. Nucleosynthesis in low-mass stars proceeds at a slower rate, resulting in higher mass locked up in stars for longer times and, therefore, affecting the rate of the chemical enrichment of the ISM. The star formation process, therefore, determines the chemical evolution of the Universe and the physical processes that occur in the ISM. Since stars are the 'building blocks of the Universe' (Mckee and Ostriker, 2007), it is essential to understand stellar evolution and the process of star formation (Lada, 2005).

The star formation process occurs within a molecular cloud and is considered inefficient due to the fact that it appears to be slower than gravity would allow (Matzner and McKee, 2000). The star formation process is fundamental to understanding the evolution of stellar systems and galaxies, which in turn is essential to understanding the evolution of the Universe. This process shapes the Universe.

By studying a volume of space in the Universe, the distribution of stellar masses of newly formed stars is referred to as the initial mass function (IMF). The IMF describes the distribution of stellar masses of stars formed in a single event (Kroupa, 2002) and follows a universal power law originally defined by Salpeter (1955), given as,

$$\phi(m)dm \sim m^{-\alpha}dm, \tag{1.1}$$

where $\phi(m)$ is the mass function, such that $\phi(m)dm$ is the number of stars formed between

m and $m + dm$, m is the mass, and the α is the slope. Salpeter (1955) found the slope to be $\alpha = -2.35$, known as the Salpeter IMF. The universal IMF is characterised by multiple power laws, according to the data, and these power laws are separated piecewise as follows:

$$\phi(m) = \begin{cases} \alpha = -1.2 & 0.1 < M < 1.0 \\ \alpha = -2.7 & 1.0 < M < 10 \\ \alpha = -2.3 & 10 < M < 1.0. \end{cases} \tag{1.2}$$

Kroupa (2002) and Chabrier (2003) derived other sequence of power laws to approximate the universal IMF, which will not be shown here.

The high-mass stars are extremely luminous and make up a small fraction of all stars formed compared to low-mass stars. The chemical and physical formation of massive stars is still not fully understood (Mckee and Ostriker, 2007). Detailed knowledge of the formation process of these high-mass stars and their properties generally provide more insight into the star formation process, and up to the present observational techniques are used to improve this knowledge.

The reason for the poor knowledge towards understanding the formation process of young massive stellar objects (YMSOs) is twofold: first due to short-lived evolutionary timescales (10^5yr) compared to the disruption timescale of the parent molecular cloud (Harada et al., 2019), and second, the evolving YMSOs are entirely embedded within a cold opaque molecular cloud. The evolving YMSOs in this region are thus heavily obscured by the surrounding dust, making it difficult to study the early stages of high-mass star formation.

Direct optical observation of high mass star forming regions is impossible because these regions are opaque (Mckee and Ostriker, 2007). The dust is fortunately less opaque at longer wavelengths, i.e. infrared, millimetre and sub-millimetre wavelengths making it easier to observe these regions. The thermal line emission can be used to determine parameters such as the temperature and density of the interstellar molecules. In addition to the thermal line emission, there is also a strong maser emission line from several molecules. Maser emission is used to trace and study these opaque regions (Lada and Lada, 2003). Astrophysical masers are sensitive to changes in their environments, and thus, the monitoring of masers provides useful information about the physical conditions of the environment in which they operate.

1.1 Astronomical Masers

Microwave Amplification by Stimulated Emission of Radiation (Maser) is a naturally occurring astrophysical phenomenon that can be used to probe astronomical environments. Masers trace the physical and chemical conditions of star-forming regions in which they are produced (Bartkiewicz and van Langevelde, 2012). When masers probe these astrophysical

environments, conditions such as (i) temperature, (ii) density, and (iii) the proper motion of material ejected from shocks (Elitzur, 1992a), (iv) magnetic field strength (Chandler, 2005), can be determined. (v) The maser spots can be used to identify the circumstellar disks around newly formed stars, tracing how these disks are expanding and rotating. (vii) Maser emission can determine the evolutionary stages in late-type stars (Elitzur, 1992a).

Maser emission lines have been detected for various molecules, the list of these molecular species comprises of molecules such as hydroxyl (OH) (Weinreb et al., 1963), water (H_2O) (Cheung et al., 1969), silicon monoxide (SiO) (Snyder and Buhl, 1974), methanol (CH_3OH) (Barrett et al., 1971; Chui et al., 1974), ammonia (NH_3) (Madden et al., 1986), H_2CO (H_2CO) (Forster et al., 1980), CS (Highberger et al., 2000), hydrogen cyanide (HCN) (Guilloteau et al., 1987), silicon monosulphide (SiS) (Henkel et al., 1983). The list is incorporated from the most common masers studied and is not a complete list (Gray, 1999).

Different maser lines of varying maser species are observed in dissimilar environments, such as massive stars, circumstellar envelopes, supernova remnants, shocked gas, evolved stars, and galactic centres. The aforementioned indicates that different maser transitions require different excitation (pumping) conditions to establish a population inversion (Gray, 1999), and also, some molecules do not occur in every environment. Masers are pumped collisionally or radiatively, and molecular hydrogen (H_2) is the primary colliding partner.

Observational techniques allow for direct determination of maser physical properties. Reid and Menten (1990) used the VLA (Very Large Array) data set of an H_2O maser to set up the detailed fundamental physical properties and the amplification process of a maser source. The basic physical properties of maser sources were concluded to be: (i) Maser radiation is highly beamed. (ii) The maser emission of the same species can attain different properties, such as brightness in different environments, due to the kinematic geometric factor. The disparity is due to widely different geometries. (iii) Maser sources can exhibit long-term variability. (iv) Polarization of maser radiation by magnetic fields (Caswell et al., 1995). Masers amplify background radiation of background sources such as stars (Elitzur, 1992a).

Megamasers occur in the same conditions as the galactic maser for the same molecular species. These masers are 10^6 times more luminous than the galactic maser sources and are thus called megamasers. They are more powerful than galactic masers and found in high-density molecular gas (Elitzur, 1992a).

In the recent years, astrophysical masers such as CH_3OH, OH, H_2O, CS and H_2CO masers associated with high mass star forming regions have received more attention. This extensive attention is because of a need to gain knowledge of these regions that are 'short-lived' and opaque. This study will focus only on two of these maser species, specifically CS and H_2CO masers. The idea is to attempt to determine the pumping mechanism of CS and H_2CO masers using a Monte Carlo simulation and to understand why Baan et al. (2017) concluded that H_2CO maser is radiatively pumped. The H_2CO molecule has a complex

energy level structure, and it is the main focus of the study. On the other hand, the CS was used to test the numerical code.

1.2 CS Maser

The CS is a linear molecule. The molecule consists of a single rotational energy level ladder, and the energy levels are characterised by angular momentum quantum number J. In this thesis, the first 31 energy levels, as shown in Figure 1.1, will be used.

Highberger et al. (2000) discovered a vibrationally excited ($\nu = 1$) CS maser towards the carbon star IRC +10216 and detected the $J = 3 \rightarrow 2$ (146 GHz), $J = 6 \rightarrow 5$ (292 GHz) and $J = 7 \rightarrow 6$ (340 GHz) transitions and re-observed the transitions $J = 2 \rightarrow 1$ (97270.9 MHz) and $J = 5 \rightarrow 4$ (243160.8 MHz). Highberger et al. (2000) concluded that the region in which the maser appears is closer to the star just before the circumstellar shell had accelerated to its terminal velocity. They suggested that the vibrational excitation of CS could be due to infrared radiation, as the densities in IRC +10216 are not high enough to produce the excited population. Highberger et al. (2000) also concluded that the observed transition appears thermal and that $J = 3 \rightarrow 2$ (146 GHz) transition could be a weak maser and further reported that there was no detection of CS ($\nu = 0$) masers.

Ginsburg and Goddi (2019) reported the first detection of a CS maser associated with high-mass young stellar objects; they furthermore detected the maser emission in the two lowest rotational transitions, i.e. $J = 1 \rightarrow 0$ and $J = 2 \rightarrow 1$ of the vibrational ground state ($\nu = 0$) towards the high mass protostar W51 e2e. They found that these lines peaked at different locations, spatially and spectrally, with a peak brightness of $T_B \approx 7000$ K. No other maser species associated with CS maser, spatially and with velocity components, were detected. The CS masers are considered rare.

van der Walt et al. (2021) suggested that the rarity of CS masers in high-mass star-forming regions may be due to two reasons. Firstly, it may be due to the high abundance of CS molecules required, and secondly, it may be due to attenuation of the maser emission inside and outside a hot core. However, the rarity of these masers is not understood. The authors also concluded that CS ($\nu = 0$) masers are pumped collisionally.

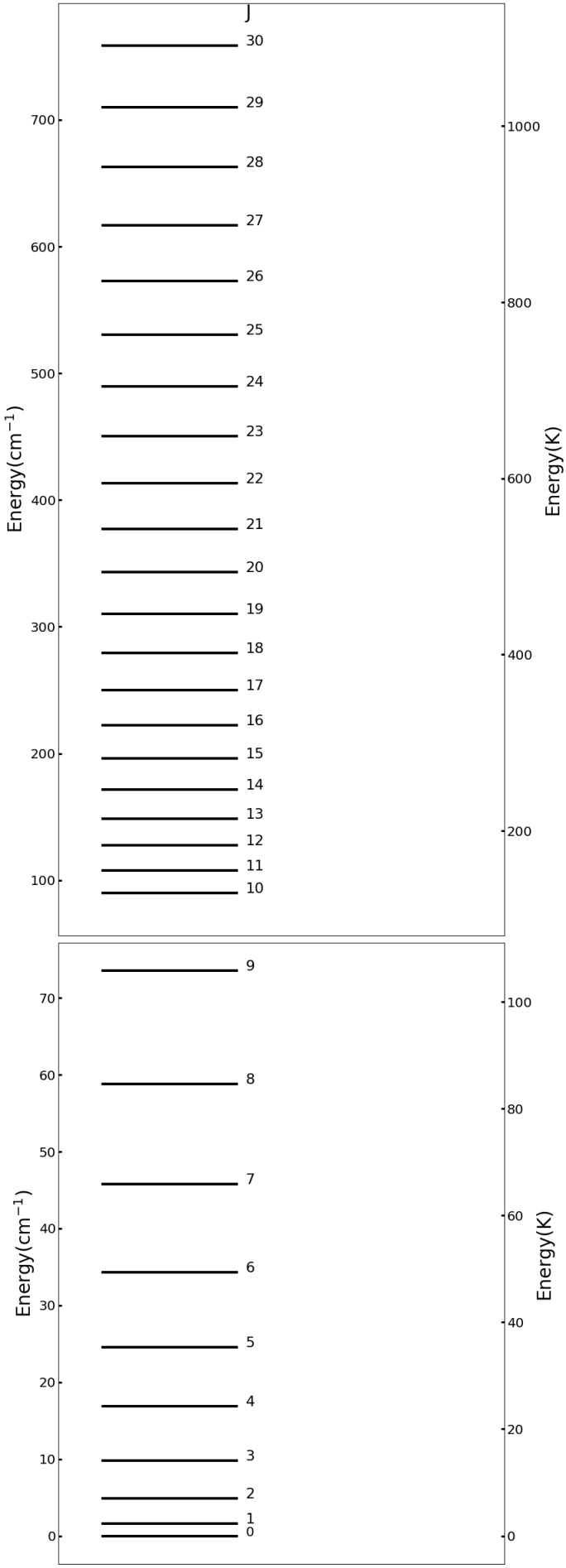

Figure 1.1: The energy level diagram of the first 31 rotational energy levels of the CS molecule.

1.3 H_2CO Maser

The H_2CO is a slight prolate asymmetric molecule. Three quantum numbers characterize the energy levels: J, K_a and K_c with J as the total angular momentum, K_a as the projection of J on the a-axis and, K_c as the projection on the c-axis. This thesis investigates the 40 energy levels of ortho-H_2CO, as shown in Figure 1.2. For an ortho-H_2CO molecule, the nuclear spin of two hydrogens is parallel, thus resulting in an odd $K_a = 1, 3$. The slight asymmetry results in the energy levels split into two energy levels, referred to as the K-doublets denoted by (K_a, K_c).

The commonly observed transition occurs between the K-doublets of the two lowest energy levels for ortho-H_2CO ($J_{K_aK_c} = 1_{10} - 1_{11}$, 4.8 GHz) (Araya et al., 2005). The maser emission line of this ubiquitous molecule is either rare or weak due to being masked by a strong absorption line associated with molecular clouds. Kutner and Thaddeus (1971) detected the first 4.8 GHz H_2CO maser line in the Orion nebula. Since the first discovery, only a further ten H_2CO masers, associated with high mass star forming regions, have been discovered in our Galaxy: NGC7538 IRS 1 (Downes and Wilson, 1974; Hoffman et al., 2003), Sgr B2 (Whiteoak and Gardner, 1983; Mehringer et al., 1994), G29.96-0.02 (Pratap et al., 1994; Hoffman et al., 2003), IRAS 18566+0408 (Araya et al., 2004b), G23.71-0.20 (Araya et al., 2006), G23.01-0.41 (Araya et al., 2008), G25.83-0.18 (Araya et al., 2008), G32.74-0.07 (Araya et al., 2015), G0.38+0.04 (Ginsburg et al., 2015) and G339.88-1.26 (Chen et al., 2017), and three extragalactic regions (Baan et al., 1986; Araya et al., 2004a).

Variability behaviour, in flux density of H_2CO masers, has been detected towards a few sources: $18566 + 0408$, Srg B2 and NGC 7538. In an attempt to explain the cause of the variability of the H_2CO 6 cm maser in G37.55+0.20, Araya et al. (2007) suggest that for a saturated H_2CO maser, the flare is conceivably caused by a change in maser gain. In the unsaturated case, the flare could be due to a change in the background 6 cm continuum radiation. The flux density variability of H_2CO maser components is poorly understood due to limited studies on this maser resulting from its rarity. Chen et al. (2017) suggest that the rarity indicates that the required physical conditions to excite the H_2CO maser are specific and short-lived. Thus, the insight into the pumping mechanism of the H_2CO maser can help understand the specific and short-lived conditions of the H_2CO maser source. The pumping mechanism of the H_2CO, however, is still yet to be understood.

After investigating the pumping mechanism, a few authors did come to some conclusions, regarding the numerical models and observations. One such conclusion, introduced by Boland and de Jong (1981), wherein a model with background free-free radio continuum radiation from a compact HII region was presented, and suggested that the H_2CO maser in NGC 7538 is pumped radiatively, and there were no further observation close to background HII regions. Based on high angular resolution VLBA (Very Long Baseline Array), MERLIN (Multi-Element Radio Linked Interferometer Network) and VLA data of NGC 7538 and G29.96-0.022 sources, Hoffman et al. (2003) suggested that the maser conceivably collisionally pumped by shocks driven by an expanding HII region.

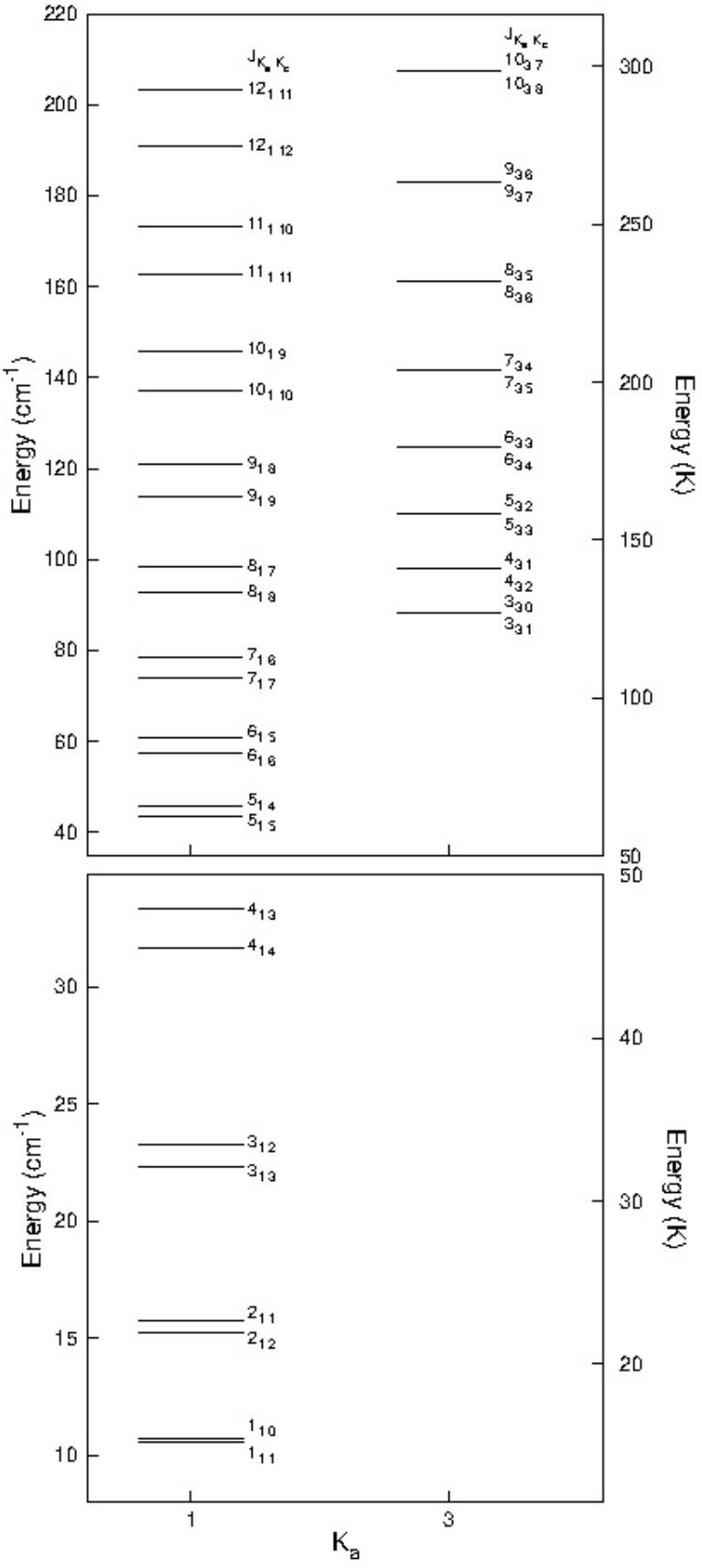

Figure 1.2: The energy level diagram of the first 40 rotational energy levels of the ortho-H_2CO molecule.

Baan et al. (2017) studied three host galaxies, specifically, IC 860, IRAS 15107+07243 and Arp 220, and concluded that the 4.8 GHz H_2CO megamasers are pumped radiatively. The conclusion drawn by the authors suggests that since the megamasers are associated with the nuclear region of the galaxy, thus the FIR radiation field is the pumping mechanism capable of pumping these megamasers because the luminosity of the maser increases as the FIR radiation field increases. Baan et al. (2017) used Leiden Atomic and Molecular Database for the molecular data and the online RADEX facility to make their calculations, and by using this facility, the radiation field is assumed to be a blackbody radiation field. Based on their reasoning, the masers are pumped radiatively, though the reason for this deduction appears inconclusive. The claim by Baan et al. (2017) was a particular stimulus for this study. van der Walt (2014) concluded that these masers are pumped collisionally and that the 4.8 GHz transition can be inverted through free-free emission from an HII region.

1.4 Aim

Even after several attempts to understand which pumping process is responsible for the inversion of H_2CO maser, the work of Boland and de Jong (1981), van der Walt (2014) and Baan et al. (2017) came to distinctive conclusions. Mehringer et al. (1994) concluded that the Boland & de Jong model is limited and fails to explain the majority of masers. The work of van der Walt (2014) presented a numerical method that solves the rate equation, and this computational method provides limited information because it does not reveal explicitly what the pumping mechanism is. Therefore, the knowledge of the pumping mechanism of the H_2CO maser is insufficient. We restrict ourselves to the 4.8 GHz ($J_{K_aK_c} = 1_{10} - 1_{11}$) transition only and from here will refer to it as just H_2CO maser.

This thesis aims to study the role of collisions and radiative excitation processes for H_2CO masers and which process is a pumping mechanism of H_2CO masers. A Monte Carlo simulation method is applied to accomplish this study. The reasons for choosing the Monte Carlo model in this study are: (1) the method focuses on the calculations of each pumping process in detail and computes the probability outcomes of each process. (2) The molecule is allowed to randomly make transitions over time without manipulating what its next transition should be. (3) With this method, the advantage of switching off the other process is to investigate the effects of the absence of the other process. The method provides a clear idea of how each process affects the level populations. Even though it is possible to switch off one of the processes, we are mindful that it does not mean that the process does not occur at all. It simply means that its effects on the maser population are significantly minimal. The second aim is to test whether the Monte Carlo method is an effective approach method for this work.

1.5 The Physical Explanation of a Monte Carlo Simulation Model

A molecule is picked and placed in a gas with a given H_2 density in a finite volume and subsequently penetrated by the radiation field. The energy density of the radiation field is the sum of the energy density of the external radiation from the dust situated locally and the internal radiation generated by excited molecules, and the radiation field is corrected by the escape probability and the optical depth. The molecule is treated as the system, and both the radiation field plus the ensemble of the H_2 molecule is treated as the reservoir.

Since a single molecule interacts with the reservoir, i.e. the canonical ensemble, thus cannot affect the properties of the reservoir. Starting with the molecule in the ground state and letting it interact with the reservoir, one can follow the route of the molecule through the levels as it interacts with the reservoir. The properties of the reservoir determine the path of the molecule. Thus, if the properties of the reservoir do not result in population inversion, the time spent on different energy levels by the molecule will reflect that. On the other hand, if the properties of the reservoir result in population inversion, then the path the molecule follows through different energy levels will show the inversion between two specific energy levels. Therefore, it is necessary to know the properties of the reservoir that results in a population inversion.

1.6 Layout

This framework comprises five chapters, including the introduction. This section is a concise summary of the chapters that follow up.

Chapter 2: Theoretical Background

The chapter provides a brief overview of radiative transfer theory because this study focuses on masers and understanding the transportation of radiation, and a brief discussion on maser theory, Einstein coefficients and the rate equation.

Chapter 3: Monte Carlo Method

The chapter discusses how the Monte Carlo numerical model was implemented.

Chapter 4: Results

This chapter details the investigation of the correctness of this model and what to expect from it using CS. The results obtained with the Monte Carlo simulation method for H_2CO

are then presented.

Chapter 5: Discussion and Conclusion

This last chapter discusses and concludes the findings of the research regarding the role of collisions and infrared radiation as a pumping mechanism for the H_2CO maser species.

Chapter 2

Theoretical Background

2.1 Introduction

In preparation for this study, the theoretical background of this thesis, is discussed in this chapter. The theory covers various topics such as radiative transfer, Einstein coefficients, rate equations, dust emission, escape probability method, interstellar molecules and their relative abundances, molecular radiation, and maser theory. However, each topic, is not discussed in detail; therefore, it simply presents a general background required to understand this study in a broader picture. Since this study focuses on understanding which pumping mechanism is responsible for population inversion, the knowledge of how molecules cycle the energy levels until inversion is established and how molecules are transported within a maser system after interacting with the radiation field is required.

2.2 Radiative Transfer

The radiative transfer theory describes how the intensity of a beam of radiation changes as it interacts with an absorbing or emitting medium. The specific intensity, I_ν, is defined as follows in terms of the energy, dE, carried by a beam of radiation with frequency in the interval $(\nu, \nu + d\nu)$ and within a solid angle $d\Omega$ that passes in a time dt perpendicular to the area, dA,

$$dE_\nu = I_\nu \, dA \, dt \, d\Omega \, d\nu. \tag{2.1}$$

The SI units of I_ν are thus W $\mathrm{m}^{-2}\,\mathrm{sr}^{-1}\,\mathrm{Hz}^{-1}$. As the radiation passes through a medium, the intensity changes over a path length ds because of the absorption and emission processes of the radiation.

2.2.1 Emission Coefficient

If we consider an emitting region with length ds, the change in intensity due to emission is given by

$$dI_\nu = j_\nu ds, \tag{2.2}$$

where j_ν is the emission coefficient with units of W m^{-3} sr^{-1} Hz^{-1}, and it is defined as the amount of energy emitted per unit time, dt, per volume, dV, per solid angle, $d\Omega$,

$$dE_\nu = j_\nu dV d\Omega dt d\nu. \tag{2.3}$$

Thus, the emission coefficient j_ν can be written in terms of emissitivity, ε_ν and density ρ

$$j_\nu = \frac{\varepsilon_\nu \rho}{4\pi}, \tag{2.4}$$

where ε_ν (W sr^{-1} Hz^{-1} kg^{-1}) is the mass emission coefficient per unit mass and j_ν is the volume emission coefficient.

2.2.2 Absorption Coefficient

For an absorbing medium, the change in intensity due to radiation lost as it propagates a distance of ds is proportional to I_ν and ds so that,

$$dI_\nu = -\alpha_\nu I_\nu ds, \tag{2.5}$$

where α_ν (m^{-1}) is the absorption coefficient, and is defined as the amount of energy absorbed. α_ν can be expressed as the product of the mass absorption coefficient κ_ν (m^2 kg^{-1}) and the density, ρ,

$$\alpha_\nu = \kappa_\nu \rho. \tag{2.6}$$

2.2.3 Radiative Transfer Equation

The change in the intensity is due to the effects of absorption, α_ν, and emission, j_ν, coefficients expressed in one equation. This results in the radiative transfer equation (Rybicki and Lightman, 1979) and is given as follows,

$$\frac{dI_\nu}{ds} = -\alpha_\nu I_\nu + j_\nu. \tag{2.7}$$

There are two cases wherein the solution for the radiative transfer equation is determined.

Emission only: $\alpha_\nu = 0$ For a medium that emits only, in the absence of an absorption process, the transfer equation is reduced to:

$$\frac{dI_\nu}{ds} = j_\nu. \tag{2.8}$$

The solution is then given by

$$I_\nu(s) = I_\nu(s_0) + \int_{s_0}^{s} j_\nu(s')ds', \tag{2.9}$$

where $I_\nu(s_0)$ is the intensity of any incident radiation, and $I_\nu(s)$ is the intensity of the radiation emitted.

Absorption only: $j_\nu = 0$ Similarly, for a medium that only absorbs radiation and there is no emission process, the change in I_ν is expressed as follows:

$$\frac{dI_\nu}{ds} = -\alpha_\nu I_\nu, \tag{2.10}$$

with the solution:

$$I_\nu(s) = I_\nu(s_0) \exp\Big[- \int_{s_0}^{s} \alpha_\nu(s')ds' \Big]. \tag{2.11}$$

Optical Depth and Source Function

Using the radiative transfer equation, we can define two other quantities: the optical depth and the source function. By using Equation 2.10, the optical depth can be defined by re-arranging the terms as follows.

$$\frac{dI_\nu}{\alpha_\nu ds} = -I_\nu \tag{2.12}$$

Then, the optical depth is defined as follows:

$$d\tau_\nu = \alpha_\nu ds \tag{2.13}$$

Thus, τ_ν is a quantity that describes the effect of matter on radiation along the path ds in which the radiation is propagating. The solution of Equation 2.12 integrated over $[0,\tau_\nu]$ is given by:

$$I_\nu(\tau_\nu) = I_\nu(0)e^{-\tau_\nu}, \tag{2.14}$$

where $I_\nu(0)$ is the incident intensity and $I_\nu(\tau_\nu)$ is the intensity at optical depth τ_ν. Equation 2.14 shows that, in an absorbing medium, the intensity decreases exponentially with the optical depth. When the value of τ_ν is significantly small ($\tau_\nu \ll 1$), $e^{-\tau_\nu} \simeq 1 - \tau_\nu$ and Equation 2.14 is given by:

$$I_\nu(\tau_\nu) = I_\nu(0)(1 - \tau_\nu) \approx I_\nu(0). \tag{2.15}$$

This condition is described as the optically thin case, meaning that the initial intensity is unattenuated as the photons propagate. When τ_ν is significantly large ($\tau_\nu \gg 1$), the condition is referred to as optically thick (Kwok, 2007), which implies that the initial intensity will undergo absorption and scattering many times.

The definition of the source function starts with the radiative transfer equation (Equation 2.7), dividing Equation 2.7 by α_ν on both sides (Rybicki and Lightman, 1979):

$$\frac{dI_\nu}{\alpha_\nu ds} = -I_\nu + \frac{j_\nu}{\alpha_\nu} \tag{2.16}$$

Using Equations 2.13 and 2.16, the radiative transfer equation is:

$$\frac{dI_\nu}{d\tau_\nu} = -I_\nu + S_\nu, \tag{2.17}$$

where S_ν is the source function and expressed as the ratio of the emission and absorption coefficients, i.e.

$$S_\nu = \frac{j_\nu}{\alpha_\nu}. \tag{2.18}$$

The definition of S_ν is a general definition of the source function. For a medium in local thermodynamic equilibrium (LTE), the source function is given, in terms of Planck's function $B_\nu(T)$, $j_\nu/\alpha_\nu = B_\nu(T)$. The relation between the emission and absorption coefficient is called Kirchoff's law which states that a strong emitter is also a strong absorber.

The general solution of the radiative transfer equation in terms of the optical depth and the source function is then,

$$I_\nu(\tau_\nu) = I_\nu(0)e^{-\tau_\nu} + \int_0^{\tau_\nu} S_\nu(\tau_\nu')e^{-(\tau_\nu - \tau_\nu')}d\tau_\nu', \tag{2.19}$$

2.3 The Einstein Coefficients

Assume that a cavity contains atoms, with quantized energy levels i and j, with energies $E_i < E_j$. Three types of transitions can occur between two energy levels, which are spontaneous emission, stimulated and absorption processes, as shown in Figure 2.1. The atomic system undergoes the absorption process by absorbing a photon, causing a transition from a lower energy level (E_i) to a higher energy level (E_j). The system spontaneously (without external influence) transitions from a higher energy level j to i. Lastly, the system (atoms) can be induced by a photon to undergo a stimulated process to make a transition from a higher to a lower energy level. The photon absorbed or emitted by the atomic system consists of energy equal to $h\nu = E_j - E_i$. The Einstein coefficients provide a simple way to describe how radiation interacts with matter via the absorption and emission process (Wilson et al., 2009).

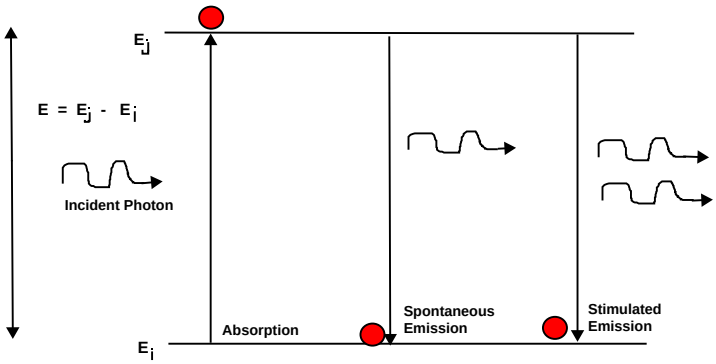

Figure 2.1: Description of absorption and emission from an atomic system between two energy levels.

Spontaneous Emission Coefficient:

The spontaneous transition, is described by the Einstein coefficient $A_{ji}(\mathrm{s}^{-1})$. Thus, A_{ji} is the probability per unit time for the occurrence of a spontaneous transition. The volume transition rate ($\mathrm{m}^{-3}\ \mathrm{s}^{-1}$) of this event is given by:

$$\frac{dn_j}{dt} = n_j A_{ji}, \tag{2.20}$$

where number density $n_j > n_i$.

Absorption Coefficient

An absorption event depends on the energy density of the radiation field U_ν, where

$$U_\nu = \frac{4\pi \bar{I}_0}{c}, \tag{2.21}$$

and $\bar{I}_0$ is the average incident intensity with the same dimensions as the intensity. The probability per unit time for an absorption event is defined as $B_{ji}U_\nu$ (s^{-1}), and the transition rate per unit volume (m^{-3} s^{-1}), is given as:

$$\frac{dn_i}{dt} = -n_i B_{ij} U_\nu, \tag{2.22}$$

with n_i as the number density in the lower energy state and n_j for an upper state.

Stimulated Emission Coefficient

Einstein found that it was necessary to include the stimulated emission process, which is proportional to U_ν to derive the Planck law, where $B_{ji}U_\nu$ (s^{-1}) is the probability per unit time for the occurrence of the stimulated emission process. The transition rate per unit volume (m^{-3} s^{-1}) is given by:

$$\frac{dn_j}{dt} = n_j B_{ji} U_\nu \tag{2.23}$$

Einstein Relations

For a two-level system in a stationary state, the rate at which absorption and emission occur must be equal. Mathematically the stationary state is expressed as,

$$n_j A_{ji} + n_j B_{ji} \bar{U} = n_i B_{ij} \bar{U}, \tag{2.24}$$

where n_i and n_j are respectively the number density of molecules in the i and j states, where $E_j > E_i$ and $\bar{U} = (\frac{4\pi}{c})B_\nu(T)$ is the energy density. For an LTE or thermodynamic equilibrium (TE), the ratio of n_j and n_i results in the Boltzmann equation:

$$\frac{n_i}{n_j} = \frac{g_i}{g_j} \exp\Big(\frac{h\nu_0}{kT}\Big), \tag{2.25}$$

where g is the statistical weight.

Solving for Equation 2.24, $\bar{U}$ is given as follows

$$\bar{U} = \frac{A_{ji}}{\frac{n_i}{n_j}B_{ij} - B_{ji}} \tag{2.26}$$

$$= \frac{A_{ji}}{\left(\frac{g_i}{g_j}e^{\frac{-h\nu_0}{kT}}\right)B_{ij} - B_{ji}} \tag{2.27}$$

In TE, $\bar{U}$ is given by the Planck function $B_\nu(T)$,

$$\bar{U} = \frac{4\pi}{c}B_\nu(T) \tag{2.28}$$

$$= \frac{8\pi h\nu_0^3}{c^3}\frac{1}{\exp\left(\frac{h\nu_0}{kT}\right) - 1} \tag{2.29}$$

Expressions 2.29 and 2.27 are identical only if

$$g_i B_{ij} = g_j B_{ji}, \tag{2.30}$$

and

$$A_{ji} = \frac{8\pi h\nu_0^3}{c^3}B_{ij}. \tag{2.31}$$

The relations between Einstein coefficients connect all three radiative transition probabilities. While deriving the Einstein relations, the cavity's thermodynamic property is not taken into account in any way; therefore, they are valid for systems presumed independent of the TE environment.

Expression for α_ν and j_ν in Terms of the Einstein coefficients and Level Populations

From the radiative transfer theory, the property of matter is expressed by the emission (j_ν) and absorption (α_ν) coefficients. The coefficients are macroscopic parameters and are related to the atomic properties of matter within a cavity. Considering the spectral line, the Einstein coefficients are used to directly link the properties of a transition responsible for the spectral line. Therefore we need the relation between the α_ν, A_{ji} and B_{ij}. Firstly, express j_ν and α_ν coefficients in terms of Einstein coefficients by substituting into Equations 2.13 and 2.18. Then, the optical depth, the source function and the level population are expressed in terms of the Einstein coefficients.

Each transition the system undergoes from the energy level j to i with energy E_j and E_i, respectively, adds the energy $h\nu_0$ distributed over a full solid angle 4π in a radiation beam. The total energy of the radiation emitted and absorbed during a transition is expressed in terms of the Einstein coefficients as follows (Wilson et al., 2009):

Spontaneous Emission: The total energy emitted spontaneously

$$dE_e(\nu) = h\nu_0 n_j A_{ji} \phi_e(\nu) d\nu \frac{d\Omega}{4\pi} dV dt \tag{2.32}$$

Stimulated Emission: The total energy due to induced emission

$$dE_s(\nu) = h\nu_0 n_j B_{ji} \frac{4\pi}{c} I_\nu \phi_e(\nu) d\nu \frac{d\Omega}{4\pi} dV dt \tag{2.33}$$

Absorption: The total energy absorbed; similarly obtained

$$dE_a(\nu) = h\nu_0 n_i B_{ij} \frac{4\pi}{c} I_\nu \phi_a(\nu) d\nu \frac{d\Omega}{4\pi} dV dt \tag{2.34}$$

where ϕ_e and ϕ_a are the line profiles for emitted and absorbed radiation respectively. The line profiles can be different, however in astrophysics it is allowed to put $\phi_e = \phi_a = \phi(\nu)$.

The total energy of the beam is given by:

$$dE = dE_e(\nu) - dE_a(\nu) + dE_s(\nu) \tag{2.35}$$

The volume element $dV = ds\ dA$, with dA as the area. The total energy of absorption, stimulated and spontaneous emission combined, can be expressed as,

$$dE = dI_\nu dA dt d\Omega d\nu \tag{2.36}$$

Substituting Equation 2.32, 2.33 and 2.34 into 2.35 and equating 2.35 to 2.36 results in:

$$dI_\nu dA dt d\Omega d\nu = \frac{h\nu_0}{4\pi} \left[n_j A_{ji} + n_j B_{ul} I_\nu \frac{4\pi}{c} - n_i B_{ij} I_\nu \frac{4\pi}{c} \right] \phi(\nu) dA dt d\Omega d\nu \tag{2.37}$$

Cancelling common factors from both sides and re-arranging the terms, the radiative transfer equation with Einstein coefficients,

$$\frac{dI_\nu}{ds} = \left(\frac{h\nu_0}{c} [n_i B_{ij} - n_j B_{ji}] + \frac{h\nu_0}{4\pi} [n_j A_{ji}] \right) \phi(\nu) \tag{2.38}$$

Thus comparing this equation with 2.7, the agreement between the two equations results in the expression for α_ν and j_ν in terms of the Einstein coefficients. Hence α_ν is expressed as (Wilson et al., 2009):

$$\alpha_\nu = \frac{h\nu_0}{c} (n_i B_{ij} - n_j B_{ji}) \phi(\nu) \tag{2.39}$$

Using the Einstein relations and re-arranging the terms, α_ν is expressed as:

$$\alpha_\nu = \frac{h\nu_0}{c} n_i B_{ij} \left(1 - \frac{g_i n_j}{g_j n_i}\right) \phi(\nu) \tag{2.40}$$

And the emission coefficient can be expressed as:

$$j_\nu = \frac{h\nu_0}{4\pi} n_j A_{ji} \phi(\nu) \tag{2.41}$$

Derivation of τ_ν and S_ν

Using the definition of the optical depth and source function as in Equation 2.13 and 2.18, respectively, these quantities can be expressed in terms of the Einstein coefficients. To determine τ_ν, firstly substitute Equations 2.30 and 2.31 into 2.40 expressing in terms of the A_{ji} to get

$$\alpha_\nu = \frac{c^2}{8\pi\nu^2} \frac{g_j}{g_i} A_{ji} n_i \left(1 - \frac{g_i n_j}{g_j n_i}\right) \phi(\nu). \tag{2.42}$$

Then multiply the terms in the bracket by $\frac{g_j}{g_i} n_i$ and 1, where $(\frac{N_{tot}}{N_{tot}}) = 1$ thus α_ν is expressed as,

$$\alpha_\nu = \frac{c^2}{8\pi\nu^2} A_{ji} \left(\frac{g_j}{g_i} \frac{n_i}{N_{tot}} - \frac{n_j}{N_{tot}}\right) \phi(\nu) N_{tot}, \tag{2.43}$$

where the total column density is defined as the total number of molecules integrated over the path length ds:

$$N_{tot} \equiv \int n_{tot} ds. \tag{2.44}$$

The fraction $n_i/N_{tot} = x_i$, where x_i is the fractional number density of molecules in the lower level.

$$\alpha_\nu = \frac{c^2}{8\pi\nu^2} A_{ji} \left(\frac{g_j}{g_i} x_i - x_j\right) \phi(\nu) N_{tot} \tag{2.45}$$

We know that $\tau_\nu = \alpha_\nu L$, with a Gaussian line profile ϕ_ν that is normalized such that, $\int_0^\infty \phi_\nu d\nu = 1$, if $\phi(\nu)$ is approximated with a box plot between a frequency width (ν_i, ν_j) given by the FWHM, thus, the approximated line profile $\phi(\nu)$ is assumed to be constant (k) and given by,

$$\int_{\nu_i}^{\nu_j} k d\nu = 1, \tag{2.46}$$

$$k \int_{\nu_i}^{\nu_j} d\nu = 1, \tag{2.47}$$

$$k(\nu_i - \nu_j) = 1, \tag{2.48}$$

$$k = \frac{1}{\Delta\nu}. \tag{2.49}$$

Therefore τ_ν can be expressed as,

$$\tau_\nu = \frac{c^2}{8\pi\nu^2} A_{ji} \left(\frac{g_j}{g_i} x_i - x_j \right) \frac{N_{tot} L}{\Delta\nu}. \tag{2.50}$$

Expressing $\Delta\nu$ in terms of velocity, Doppler broadening

$$\pm v = c \pm \frac{\Delta\nu}{\nu}, \tag{2.51}$$

then

$$\Delta v = \Delta\nu \frac{\nu}{c}. \tag{2.52}$$

Substituting Equation 2.52, then

$$\tau_\nu = \frac{c^3}{8\pi\nu^3} A_{ji} \left(\frac{g_j}{g_i} x_i - x_j \right) \frac{N_{col}}{\Delta v}. \tag{2.53}$$

The source function, is given by the ratio of α_ν and j_ν, by substituting Equation 2.30 and 2.31 into Equation 2.40 and 2.41; S_ν is expressed as:

$$S_\nu = \frac{j_\nu}{\alpha_\nu}. \tag{2.54}$$

Re-arranging the terms, then the source function is expressed as:

$$S_\nu = \frac{2h\nu_0^3}{c^2} \left(\frac{g_j}{g_i} \frac{x_i}{x_j} - 1 \right)^{-1}. \tag{2.55}$$

2.4 Collisional Process

At the microscopic level, an atomic/molecular gas is composed of particles that are constantly in motion and interact collisionally with each other. Let N be the number density of the gas particles and $dN(v)$ the number density of particles that has velocity ranging from v to $v+dv$. The velocity distribution of the gas particles is described by a probability distribution function $f(v)$, such that,

$$dN(v) = Nf(v)dv. \tag{2.56}$$

The function $f(v)$ has the dimensions of $(\mathrm{m} \cdot \mathrm{s}^{-1})^{-1}$, is normalized so that $\int_0^\infty f(v)dv = 1$ and follows a Maxwell-Boltzmann distribution in thermal equilibrium state given by,

$$f(v) = \frac{4}{\sqrt{\pi}}\left(\frac{m}{2\pi kT}\right)^{3/2} v^2 e^{-\frac{mv^2}{2kT_k}}, \tag{2.57}$$

where m is the mass of the colliding particles, k is the Boltzmann constant and T_k is the kinetic temperature (Elitzur, 1992b). This distribution is described by a single parameter T_k. For an ensemble of particles to achieve a Maxwell-Boltzmann distribution function, an exchange of energy and momentum between particles must occur, but only occurs collisionally (Kwok, 2007). The parameter T_k is proportional to the average kinetic energy of molecules/atoms and is a measure of the velocities of particles in the system. The average kinetic energy of molecules in a gas is given by:

$$E_{avg} = \frac{3}{2}kT_k. \tag{2.58}$$

The probability per particle for a collisional excitation to occur, is described by the collisional coefficient C_{ij} ($\mathrm{m}^3\ \mathrm{s}^{-1}$). The expression for the coefficient C_{ij}, can be written in terms of the cross-section, σ_{ij}, and the number of particles per unit volume with velocities between $v, v + dv$, and $f(\nu)d\nu$ which is always given by Maxwell-Boltzmann equation (Emerson, 1998). Therefore, the rate of excitation is,

$$C_{ij} = \int_0^\infty v\sigma_{ij}(v)f(v)dv, \tag{2.59}$$

Similarly, the de-excitation event is

$$C_{ji} = \int_0^\infty v\sigma_{ji}(v)f(v)dv. \tag{2.60}$$

The collisional rates then follow as the product of the collisional coefficient and the number density of the collisional partner. In this case, the collisional partner is the molecular hydrogen, H_2

$$\frac{dn_i}{dt} = n_{H_2} n_i C_{ij}, \tag{2.61}$$

$$\frac{dn_i}{dt} = n_{H_2} n_j C_{ji}. \tag{2.62}$$

For a system that is in complete equilibrium, the collisional excitation rate and de-excitation rate are equal at every energy (Emerson, 1998):

$$n_i C_{ij} = n_j C_{ji}. \tag{2.63}$$

Re-arranging the terms results in,

$$C_{ij} = \frac{n_j}{n_i} C_{ji}. \tag{2.64}$$

In TE, the principle of detailed balance states that, the level population distribution follows the Boltzmann distribution, $\frac{n_j}{n_i} = \frac{g_j}{g_i} e^{(\Delta E/kT)}$. Hence, the collisional rates can be related as follows:

$$C_{ij} = \frac{g_j}{g_i} C_{ji} \exp(-\Delta E/kT), \tag{2.65}$$

where n_j and n_i are the number density of molecules in the energy states i and j, with $j > i$. The g_j and g_i are their respective weights, ΔE is the energy difference between the two states, k is the Boltzmann constant, and T is the kinetic temperature. Whether the system is in TE or not, this relation holds under all circumstances (Emerson, 1998).

2.5 The Rate Equation

For non-LTE conditions, the level population distribution does not follow the Boltzmann distribution function. Nonetheless, statistical equilibrium can still be used to calculate the population of the system (Emerson, 1998) because a steady state system is assumed, which implies that even though the system's distribution of the state fluctuates due to variations of parameters such as energy, the number density of the population in the system remains constant.

So far, the relevant physical processes that cause population exchange between various energy states have been discussed. Determining the solution to a level population problem is a complex process because numerous energy levels are coupled, either directly or indirectly. Furthermore, the level population is coupled to the intensity of radiation that corresponds with each transition, resulting in a large system of complex equations (Elitzur, 1992b). The difficulty introduced by the effect of coupling can thus be treated by an approximation method. The most used approximation method is the escape probability method. Therefore, since the entire system is multilevel, it is advantageous to discuss the population exchange of multilevel systems.

The rate of a process that causes a transition between energy levels is given as the number of transitions per unit time. These transitions occur either radiatively (R_{ij}) or collisionally

(C_{ij}). Considering the losses and gains out and into energy level i, the rate equation is:

$$\frac{dn_i}{dt} = -n_i \sum_{j<i} A_{ij} - n_i \sum_{j<i} U_{ij} B_{ij} - n_i \sum_{j>i} U_{ij} B_{ij} - n_i \mathrm{n_{H_2}} \sum_{j<i} C_{ij} - n_i \mathrm{n_{H_2}} \sum_{j>i} C_{ij} + n_j \sum_{j>i} A_{ji} + n_j \sum_{j>i} U_{ji} B_{ji} + n_j \sum_{j<i} U_{ji} B_{ji} + n_j \mathrm{n_{H_2}} \sum_{j>i} C_{ji} + n_j \mathrm{n_{H_2}} \sum_{j<i} C_{ji} \quad (2.66)$$

For a system in equilibrium, is given by $\frac{dn}{dt} = 0$, this means that the rate out of energy level i, is equal to the rate into energy level i. The energy level j could be any level above or below a specific energy level of interest denoted by i. Therefore, the rate equation is given by

$$\sum_{j<i} n_i (A_{ij} + U_{ij} B_{ij} + \mathrm{n_{H_2}} C_{ij}) + \sum_{j>i} n_i (U_{ij} B_{ij} + \mathrm{n_{H_2}} C_{ij}) = \sum_{j>i} n_j (A_{ji} + n_j U_{ji} B_{ji} + n_j \mathrm{n_{H_2}} C_{ji}) + \sum_{j<1} n_j (U_{ji} B_{ji} + \mathrm{n_{H_2}} C_{ji}) \quad (2.67)$$

2.6 Escape Probability Method

To simplify the escape probability method, consider a transition between two energy levels, i and j. This method is applied to decouple the equation of level population from the equation of radiative transfer. The fundamental idea of this method is to introduce a multiplicative factor, β_ν, that describes the probability of a photon escaping from a medium after being generated (Elitzur, 1992b; van der Tak et al., 2007). The decoupling is achieved by treating the transfer of the radiation within a cloud solely through the escape probability, and this means that the radiation from the rate equation does not involve the intensity of the radiation but only the probability that it escapes from the source.

$$\bar{U}_\nu = \frac{4\pi}{c} S_\nu (1 - \beta_\nu). \quad (2.68)$$

Substituting the energy density expressed in terms of the source function (Equations 2.68) and 2.55 into Equation 2.66 and grouping the radiative terms into $j > i$ and $j < i$. Then the B-coefficients are expressed in terms of the A-coefficient using the Einstein relation 2.31. The rate equation is, therefore, reduced to,

$$\frac{dn_i}{dt} = -n_i \sum_{j<i} A_{ij} \beta_{ij} + \sum_{j>i} n_j A_{ji} \beta_{ji} - n_i \mathrm{n_{H_2}} \sum_{j<i} C_{ij} - n_i \mathrm{n_{H_2}} \sum_{j>i} C_{ij} + n_j \mathrm{n_{H_2}} \sum_{j>i} C_{ji} + n_j \mathrm{n_{H_2}} \sum_{j<i} C_{ji}, \quad (2.69)$$

where the first term is the radiative losses out of energy level i, the second term represents the gain into energy level i, and β accounts for the stimulated emission and absorption.

The method to estimate the escape probability is based on the assumption that β_ν depends on the optical depth τ_ν and the geometry and not on the radiation field (van der Tak et al., 2007). The average local escape probability can be calculated as:

$$\beta_\nu = \left\langle \exp(-\tau_\nu) \right\rangle \tag{2.70}$$

$$= \frac{1}{\tau_\nu} \int_0^{\tau_\nu} \exp(-\tau'_\nu) d\tau'_\nu \tag{2.71}$$

$$= \frac{1 - \exp(-\tau_\nu)}{\tau_\nu} \tag{2.72}$$

Since β_ν depends on τ_ν, the behaviour of β_ν in the limits of τ_ν is as follows: If $\tau_\nu \ll 1$, β_ν tends to be $\beta_\nu \simeq 1$. These limits explain that (for an optically thin case) photons easily escape from the source without interacting with particles within the same source. If $\tau_\nu \gg 1$, $\beta_\nu \simeq \frac{1}{\tau_\nu}$, therefore, for an optically thick case, the source is separated into τ_ν sections that sum up to unity. Consequently, a photon can escape if, and only if, it is generated in the outermost section, and the probability to escape is expressed by $1/\tau_\nu$ (Elitzur, 1992b).

2.7 Dust Emission

Dust grains are solid small particles that are completely mixed with the gas in all interstellar environments (Elitzur, 1992b). The effects of the presence of these grains in the ISM are the obscuration of visible light and emission by the grains themselves. Obscuration, known as the extinction of visible light, is a consequence of the absorption or scattering of visible light from background stars by dust grains. Extinction depends on the size of a grain, which implies the efficiency of each extinction process depends on the ratio of the wavelength to grain size. As previously mentioned, this means that grains absorb or scatter photons that are smaller in physical size compared to the grain size. In the ISM, the gas and dust densities are very low, and the gas adds little to no effect in heating and cooling the dust grain. Grain heating is then due to the absorption of diffuse starlight, and the cooling process occurs when dust re-radiates in a longer wavelength, i.e. in the infrared range (Kwok, 2007).

Dust grain formation occurs in cool environments of star-forming regions of high density, such as circumstellar environments. These grains nucleate, grow further in size and are transported into the ISM through stellar winds, shock fronts and supernova shock waves (Jones, 2001). One important question has always been, what are dust grains made of? The spectroscopy method was applied to find the answers. It has been found that

dust composition varies by environment, and the absorption line spectroscopy shows the underabundance of C, Mg, Si and Fe elements in the gas phase in the ISM. Therefore, underabundance is due to the condensation of these elements in a gas phase to form grains (Draine, 2010). Dust grains are composed of molecules, complex aromatic hydrocarbon molecules and metallic elements (Jones, 2001).

Assuming a spherical dust grain of a radius a, the absorption coefficient, is defined as:

$$\alpha_\nu = \pi a^2 n, \tag{2.73}$$

where n is the number density of dust particles. A dimensionless extinction efficiency ($Q_\nu(a)$) is introduced in the absorption process. The absorption coefficient, is thus expressed as,

$$\alpha_\nu = \pi a^2 Q_\nu(a) n. \tag{2.74}$$

The extinction efficiency is written as the sum of the absorption and scattering extinction efficiency.

$$Q_{ex} = Q_{abs} + Q_{sct}, \tag{2.75}$$

where Q_{ex} is frequency dependent and is approximated as $Q \approx (\nu/\nu_0)^p$ with $1 < p < 2$, and ν_0 is the frequency at the peak of the dust SED which is $\approx\geq 10^{12}$. Assuming a uniform temperature, the emission coefficient is related to the absorption coefficient by Kirchoff's law. Therefore, the emission coefficient is given by:

$$j_\nu = (\pi a^2 Q_\nu) n B_\nu(T_d), \tag{2.76}$$

where T_d is the dust temperature, dust emission is not that of a black body but that of a grey body. The spectral energy distribution depends on the temperature as well as the chemical composition of these grains, and thus the spectrum is given by:

$$F_{ij}^{IR} = \left(\frac{\nu}{\nu_0}\right)^p B_\nu(T_d), \tag{2.77}$$

where ν_0 is the fiducial frequency.

2.8 Relative Abundances of Interstellar Molecules

Various molecules have been detected in the ISM (Kwok, 2007) since the late 1930s. Some of these molecules are 'used' as tracers of molecular clouds in the ISM and star-forming regions. Molecular hydrogen (H_2) is the most abundant molecule in the ISM. The second most abundant molecule is Carbon Monoxide (CO) (Emerson, 1998). CO has an abundance of $\sim 10^{-4}$ relative to H_2 and is used to trace molecular gas instead of H_2. The previously mentioned is because H_2 cannot be detected directly as an emission line at long wavelengths due to lack of a dipole moment, thus emitting a weak emission. Rare molecules such as CS, NH_3 or HCN have abundances of $\sim 10^{-8} - 10^{-9}$, and are detected in dense cores of star-forming regions (Tafalla, 2011). The abundance of such rare molecules depends on the elemental abundances of a region, for example, the abundance of CS molecule is determined by the abundance of sulphur (S). Relative abundances prove that interstellar molecules are continually formed via gas phase and grain surface chemistry and destroyed via photo-dissociation (Kwok, 2007). During the collapse of cold molecular clouds, molecules in a gas phase collide with dust grains and freeze on the surfaces of these grains. Chemical reactions occur on the surface of these grains to form complex organic molecules. When the young protostar heats its surroundings, the complex organic molecules are released from the grain surfaces by thermal evaporation (Tafalla, 2011).

By 2005 more than 120 molecules were discovered (Kwok, 2007); Table 2.1 provides examples of a few other molecules found in the ISM,

Table 2.1: Interstellar molecules and their abundances relative to H_2

Molecules	Abundances
H_2O	10^{-4}
O_2	10^{-7} - 10^{-6}
SiO	4×10^{-8} - 3×10^{-7}
CO_2	10^{-6}
H_2CO	10^{-11}
CH_4	10^{-4}
CS	10^{-10} - 10^{-8}
CH_3OH	10^{-6} - 10^{-5}
CH_3CN	0.85×10^{-10}
OH	10^{-7}

Abundances of numerous molecules provide information about the physical conditions of various environments and their histories (van Dishoeck and Blake, 1998); molecules are thus, used as tracers in different interstellar environments.

2.9 Molecular Line Radiation

The discovery of molecules occurred when the optical lines were identified in absorption against the background starlight. The first molecules detected were CN (3876.84 Å), CH (4300.30 Å) and CH^+ (4232.54 Å). Later when radio receivers were available, spectroscopic observations of molecules in the radio region became possible. Therefore spectroscopic observations in the infrared and millimetre region of the spectrum made it possible to observe rotational and vibrational transitions of molecules. However, in the case of the electronic transition, the spectroscopic observations are made in the visible and near UV spectrum region.

The energy bandwidths of the electronic, vibrational and rotational states are very different. The transitions between these states are assumed to be decoupled, and their respective wavefunctions separable. For example, separating the wavefunction of nuclei and electrons results in a separate motion of the nuclei and electrons. This is referred to as the Born-Oppenheimer Approximation (Kwok, 2007), where the total wavefuction ψ_{tot} is the product of the ψ_{el}, ψ_{vib} and ψ_{rot} which are electronic, vibrational and rotational wavefunctions respectively as given by,

$$\psi_{tot} = \psi_{el}\psi_{vib}\psi_{rot}. \tag{2.78}$$

Therefore, the total energy of a molecule is given as the sum of electronic, vibrational and rotational states:

$$E^{tot} = E^{el} + E^{vib} + E^{rot}, \tag{2.79}$$

where E^{el} is the energy of the electrons, and E^{vib} and E^{rot} are the vibrational and rotational energies of the nuclei of an atom, respectively (Wilson et al., 2009).

Radiative transitions of molecules are categorized into three processes, as explained above:

- Electronic transition: This transition occurs when electrons in a molecule are excited. A transition that consists of energy that ranges from $E^{el} = (1-10)$ eV. The electronic quantum number is n.
- Vibrational transition: This transition is caused by oscillations of the relative positions of the nuclei with respect to their equilibrium positions. The energy states that result from the oscillation motions are quantized. The energy for vibrational transition to occur, ranges from $E^{vib} = (0.1 - 0.01)$ eV. The vibrational quantum number is v, and the allowed vibrational transitions, are given by the selection rule $v = \pm 1$.
- Rotational transition: These transitions are caused by the rotation of the nuclei, and the rotational states are quantized. The energy for rotational transition to occur,

is of the order of $E^{rot} \approx 10^{-3}$ eV (Wilson et al., 2009). The rotational quantum number is J, thus, the transition between allowed successive J states, is given by the selection rule $J = \pm 1$ (Kwok, 2007).

The molecular line generally results from a transition between two energy states described by different electronic, vibrational and rotational quantum numbers. The strength of these lines is used to study the temperature, density and background radiation of ISM (Wilson et al., 2009).

2.9.1 Structure of Molecule, Rotational Transition, Symmetric and Asymmetric Molecules

Rotational Transition

In general, the rotation of molecules is described by three principal moments of inertia I_a, I_b and I_c in increasing order of distance from the rotational axis (Kwok, 2007). For simplicity, a diatomic molecule will be discussed in more detail to illustrate some basic aspects of rotational energy states and the transitions between such states. The rotation of a diatomic molecule is modelled as a rigid rotor as shown in Figure 2.2, and is represented by $I_a = 0$ and $I_b = I_c$, and the cm is the centre of mass,

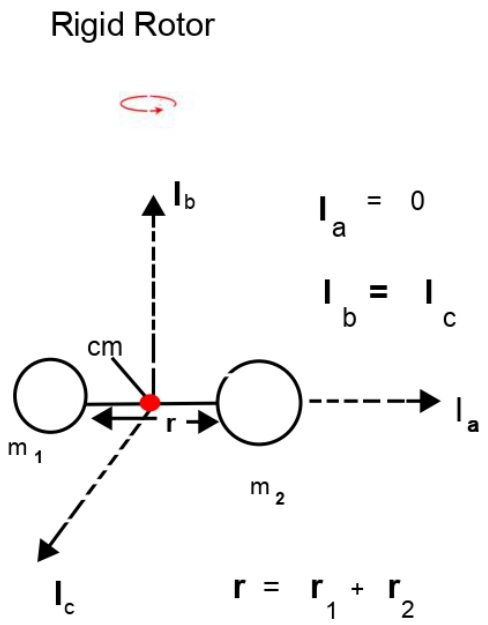

Figure 2.2: A rigid rotator model of a diatomic model

$$I = \mu r^2, \tag{2.80}$$

where μ is the reduced mass of the two nuclei,

$$\mu = \frac{m_1 m_2}{m_1 + m_2}, \tag{2.81}$$

and r is the bond length between the two nuclei. The kinetic energy of the rotation, is given by the solution to the Schrodinger equation:

$$E = \frac{\hbar^2}{8\pi^2 I} J(J+1), \tag{2.82}$$

where J is the rotational quantum number,(J $= 0, 1, 2, ...$).

Equation 2.82 applies to completely rigid molecules. For slightly elastic molecules, r is given as r_e, and increases with the rotational energy due to centrifugal stretching (Wilson et al., 2009). Centrifugal stretching results when the molecular bonds stretch, which in turn leads to the increase of the moment of inertia and the rotational energy is modified as follows:

$$E = \frac{\hbar^2}{8\pi^2 I} J(J+1) - hD[J(J+1)]^2 \tag{2.83}$$

$$= \hbar B J(J+1) - hD[J(J+1)]^2, \tag{2.84}$$

where B $= \frac{\hbar}{8\pi^2 I}$ is the rotational constant, and $D > 0$ is the centrifugal stretching constant (Wilson et al., 2009). Table 2.2 provides the values of the rotational constants. The electric dipole transition is only allowed between successive rotational states and is represented by $\Delta J \pm 1$ (Kwok, 2007):

Table 2.2: Rotational constants of CS molecule

Rotational Constants	Values
B	24,495.586(MHz)
D	42.18 (kHz)

The difference between the energies of the rigid and slightly elastic molecules is the frequency line observed for the energy with the centrifugal stretch is lower than the frequency of the rigid rotor (Burke et al., 2019).

Symmetric Top Molecules

Using the three principle moments of inertia about their axes, one can determine the shape or symmetry of a molecule. A molecule is referred to as a symmetric top when its two moments of inertia are equal and the third moment of inertia is different. The symmetric top is categorised into a prolate or oblate symmetric top (Kwok, 2007). Prolate symmetric top structures (elongated shape) result when I_a is small and $I_b = I_c$ and oblate symmetric top structures (pancake shape) where $I_a = I_b < I_c$ (Kwok, 2007). A linear molecule is

used as an example, and the rotational constants are defined as follows:

$$A = \frac{h}{8\pi^2 I_a} \tag{2.85}$$

$$B = \frac{h}{8\pi^2 I_b} \tag{2.86}$$

$$C = \frac{h}{8\pi^2 I_c}. \tag{2.87}$$

The rotational levels of the symmetric top molecule are described by J and K quantum numbers, which are the total angular momentum and the projection onto the axis of symmetry, respectively. K is a component of J, and it is given by:

$$K = 0, \pm 1, \pm 2, ..., \pm J. \tag{2.88}$$

The energy levels of a rigid rotor are expressed as:

$$E_{j,k} = BJ(J+1) + (A-B)K^2, \qquad \text{prolate top} \tag{2.89}$$

$$= BJ(J+1) + (C-B)K^2, \qquad \text{oblate top} \tag{2.90}$$

The energy of J increases with K for a prolate top molecule and decreases with K for an oblate molecule since A > B and B > C, respectively (Kwok, 2007). The energy levels of a molecule are designated to be J_K.

The selection rules are $\Delta K = 0$, $\Delta J = 0, \pm 1$. There can never be transitions between different K's; the energy levels are, thus, described by a column of K value. This column is also referred to as a ladder and the transitions within this ladder occur between adjacent J states (Kwok, 2007).

Asymmetric Top Molecule

A molecule is referred to as an asymmetric top when the three moments of inertia are different, $I_a \neq I_b \neq I_c$, with A, B and C as rotational constants. Considering a non-linear molecule such as H_2CO, the molecular structure of this molecule is quite complex (Burke et al., 2019). The rotational constants of this molecule are given in Table 2.3.

In this case, for each J state, the projection K onto the axis of symmetry is given by quantities K_a and K_c, with K_a as a component of J along the A axis and K_c along the C axis. The energy levels of a molecule are thus given as $J_{K_a K_c}$ (Kwok, 2007; Wilson et al., 2009). The K quantities act as limiting factors for a prolate and oblate symmetric top.

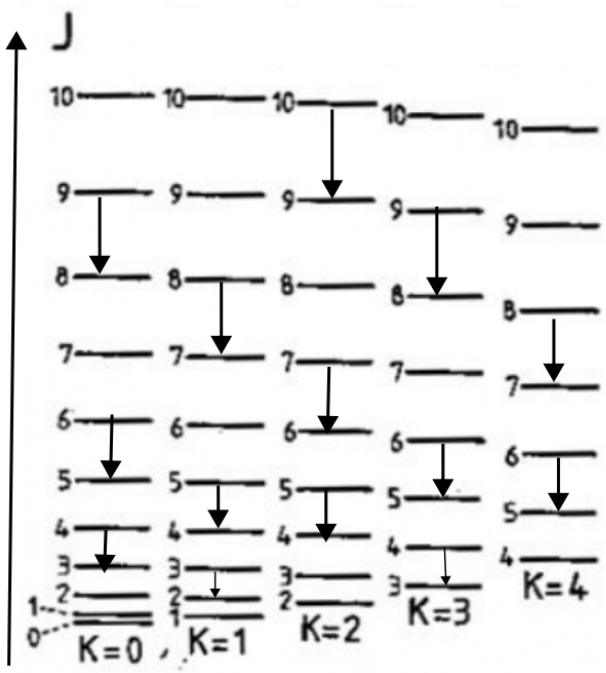

Figure 2.3: Example of the energy level diagram of a symmetric top molecule arranged in columns of constant K. The transitions in this structure occur within the K ladder.

Table 2.3: Rotational constants of H_2CO molecule

Rotational Constants	Values (MHz)
A	281,970.672
B	38,836.0455
C	34,002.2034

For example, J and K_a are quantum numbers for the prolate symmetric top and J and K_c for the oblate symmetric top. In this case, transitions are allowed between the ladders, and only between ladders, that are either in ortho or para-state (Wilson et al., 2009).

The Effects of Nuclear Spin on the Rotation Spectrum

As previously explained, the total wavefunction is the product of the electronic, vibrational, rotational and wavefunctions. The rotational wavefunction can either be symmetric or antisymmetric depending on whether J is even or odd (Kwok, 2007).

The spin wavefunction determines the allowed values of J, if the spins are parallel, that results in an ortho-state and if the spins are anti-parallel, that results in a para-state. For an asymmetric top molecule where the energy levels are described by $J_{K_aK_c}$, K_aK_c is given (Wilson et al., 2009):

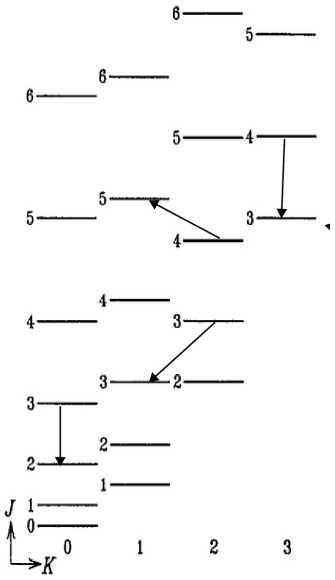

Figure 2.4: Example of the energy level structure of an asymmetric top molecule arranged in columns of constant K shows the molecule can transition between K ladders.

$$K_a K_c = \text{(even,odd)/(odd,even)} \qquad \text{For ortho-state} \tag{2.91}$$

$$= \text{(even,even)/(odd,odd)} \qquad \text{For para-state} \tag{2.92}$$

The selection rule is there can never be a cross-transition between ortho and para-state or vice versa.

Nuclear spin introduces hyperfine splitting in the energy levels of a molecule as well. For nuclear spin $S = 1$, the rotational states split into several distinct sub-levels with a definite value of J and the degeneracy $g = 2J + 1$. Degeneracy in energy states merely means a different arrangement of energy states and has the same energy in a system. When an energy state is split into two, three, or four sub-states with a definite value of J, these sub-states are termed doublets, triplets, or quartets, respectively (Draine, 2010).

2.10 Maser Theory

2.10.1 Population Inversion

In LTE, where radiation dominates the radiation field is given by black body radiation, and the Boltzmann distribution describes the level population distribution:

$$\frac{n_j}{n_i} = \frac{g_i}{g_i} e^{-E_{ji}/k_B T_B}, \tag{2.93}$$

where $E_j > E_i$ and T_B is the black body temperature. Equation 2.93 implies that $n_i > n_j$ in LTE.

For gas in thermal equilibrium collisions, the velocity distribution follows that of the Maxwell-Boltzmann velocity distribution, wherein the level population distribution follows the Boltzmann distribution, and T_k is the kinetic temperature.

$$\frac{n_j}{g_j} = \frac{n_i}{g_i} e^{-E_{ji}/k_B T_k}, \tag{2.94}$$

When the system deviates from TE, the velocity distribution and radiation distribution deviate from a Maxwellian velocity or Planck function, respectively. Therefore, the level population distribution of molecules deviates from the Boltzmann distribution as well,

$$\frac{n_j}{g_j} = \frac{n_i}{g_i} e^{-E_{ji}/k_B T_{ex}}. \tag{2.95}$$

Where T_{ex} is the excitation temperature that describes the population of each level relative to the ground state or any other level. This case leaves a chance of reaching the state of population inversion defined as:

$$n_j > n_i. \tag{2.96}$$

This state is called the population inversion. Inversion is when the upper energy level is more populated than the lower energy level. A pumping mechanism is required to establish and maintain population inversion, which is achieved when molecules cycle through energy levels. The pumping can be via radiation or collisions.

2.11 Radiation Field

Population inversion is a prerequisite for maser action. For this condition to hold, the absorption coefficient, α_ν, should be negative, which in turn makes the optical depth, τ_ν, and the source function, S_ν, to be negative. In the case of the unsaturated maser, the radiative transfer equation is necessary for studying the intensity along independent rays and, the equation is given as:

$$\frac{dI_\nu}{d\tau_\nu} = -S_\nu + I_\nu. \tag{2.97}$$

For an absorbing medium ($j_\nu = 0$, therefore $S_\nu = 0$)

$$\frac{dI_\nu}{I_\nu} = d\tau_\nu. \tag{2.98}$$

In solving for the intensity, an integration method is applied as follows:

$$\int_\tau^0 \frac{dI_\nu}{I_\nu} = \int_\tau^0 d\tau_\nu. \tag{2.99}$$

As stated above, the negative absorption coefficient produces a negative optical depth. Therefore, the specific intensity is,

$$I_\nu(0) = I_\nu(\tau)e^{\tau_\nu}. \tag{2.100}$$

In addition, it is necessary to define the total energy density of the maser system as, U_{ij}, at frequency ν_{ij} where $j > i$. The total energy density of the system is the sum of the external energy density due to dust at the local position, B_{ij}^{IR}, and the internally generated radiation, B_{ij}^{Int}. Internal radiation results from allowed transitions between different energy states of the molecule. Therefore, if β_{ij} is the escape probability the energy density is,

$$B_{ij}^{Int} = \frac{4\pi}{c} S_\nu (1 - \beta_{ij}). \tag{2.101}$$

The external radiation field from dust emission is written as $(\frac{\nu}{\nu_0})^p B_\nu(T_d)$ with $B_\nu(T_d)$ the Planck function, where β_{ij} is the probability of a photon with frequency ν_{ij} to escape. An additional factor that affects external radiation is a geometric $1/r^2$ dilution factor, W_{ij}. This factor results from the distance between the masing cloud and the external source, and thus, the energy density of the dust radiation contribution is,

$$B_{ij}^{IR} = \frac{4\pi}{c}\Big(\beta_{ij} W_{ij} \Big(\frac{\nu}{\nu_0}\Big)^p B_\nu(T_d)\Big). \tag{2.102}$$

Substituting Equation 2.55, the local energy density in the total radiation field is,

$$U_{ij} = \frac{4\pi}{c}\left[\beta_{ij} W_{ij}\Big(\frac{\nu}{\nu_0}\Big)^p B_\nu(T_d) + \frac{2h\nu_{ij}^3}{c^2}\left(\frac{g_j}{g_i}\frac{n_i}{n_j} - 1\right)^{-1}(1 - \beta_{ij})\right]. \tag{2.103}$$

2.12 Pumping of Masers

This section is the simplified version of (Elitzur, 1992b), on astronomical masers. The propagation of radiation in masing environments is assumed by studying the properties of

pumping processes. As previously stated, the pumping mechanism can be via collisions or radiative processes. The purpose of this section is to understand what exactly are the pumping mechanisms and differentiate between the pumping mechanism and pumping schemes. It is fundamentally important to understand these processes because the information regarding the physical conditions of a maser source can only be understood when the pumping schemes are understood.

2.12.1 General Idea

As mentioned above, for a system in LTE, it is expected that $n_i > n_j$ where $j > i$, and the reverse for a non-LTE. An inversion requires a system that circulates particles among various energy states. This process of circulation is called the pumping process (pumps). The pumps could either be radiatively or collisional. A pumping scheme is a dominant process responsible for exciting molecules out of the ground state to higher energy levels. The pumping mechanism is a process in which in its absence, the inversion would disappear. In many cases, the pumping process is indirect, in such a way that the particles are excited to energy levels above the higher maser level. Then, populate the maser level by radiatively cascading from a higher level.

For a process to be regarded as a pumping scheme of a maser source, it must fulfil two fundamental conditions. (1) The process must establish a population inversion of a maser transition. Since the definition of a pumping scheme is that process which, in its absence, population inversion does not hold, this mechanism does not need to be a process that dominates the pump rates. (2) The pumping scheme must be able to generate the maser luminosity observed; a high maser luminosity implies large pump rates. Pump rates cannot be increased randomly, or else the maser will saturate, the energy levels will thermalize, collisional rates will get too high, and the inversion will be destroyed, which will, in turn, destroy the maser. The powerful maser pumps operate close to thermalization. A minor increase in the pump rate, either collisionally or radiatively, will cause thermalization. Therefore limitation is the pump rates and not the energy flux.

2.12.2 Radiative Pumps

For the pumps dominated by radiative processes, collisional terms in the rate Equation 2.66 can be neglected. For pumping schemes to be considered radiatively dominated, two requirements must be satisfied for the population inversion to hold. The first condition is that the external radiation field should not be an undiluted black body. The deviation from a black body law is because of the geometric dilution factor, i.e. $(W < 1)$.

The second condition is that generally, the pumping schemes involve gain and losses of maser levels. When each maser level exchanges particles with the same level, the loss and gain rate will be equal, and population inversion becomes impossible. These two

conditions generally hold irrespective of the optical thickness of each transition (Elitzur, 1992b).

2.12.3 Collisional Pumps

Radiative terms cannot be neglected for collisional pumps, unlike radiative pumps, which can neglect the collisional terms. The deviation from thermal equilibrium requires the collisional de-excitation to compete with radiative de-excitation for at least some of the transitions. Thus collisions are assumed to be coupled to the radiative losses. If the radiative terms are neglected, the level population will thermalize with the kinetic temperature, and the inversion will not hold. Furthermore, population inversion does not hold when collisional loss rates exceed the radiative loss rate between the maser levels (Elitzur, 1992b),

$$C_{ji} \gtrsim A_{ji} \frac{kT}{\Delta E}. \tag{2.104}$$

2.13 Maser Amplification and Saturation

Consider a maser column of length L, as shown in Figure 2.5, with the population inversion. As the population inversion is established, the absorption coefficient (α_ν) becomes negative, which in turn causes the optical depth (τ_ν) to be negative and is explained in Figure 2.6, as presented from sections B to D of Figure 2.6. The propagation of the radiation within the maser column is described by the source function (S_ν) when the background radiation permeates the maser column, as shown in Figure 2.5.

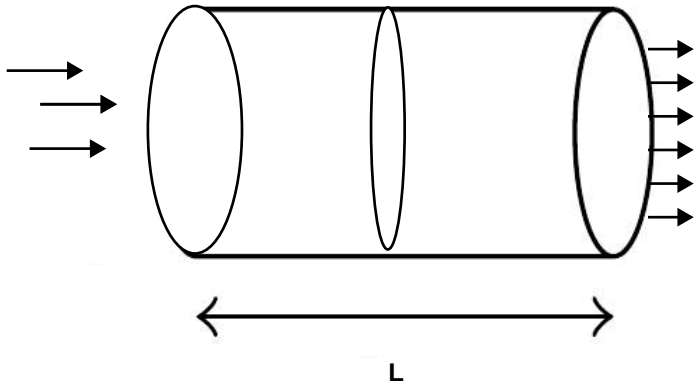

Figure 2.5: A schematic model of a maser column over distance L.

The rate of stimulated emission starts to exceed the rate of absorption. Stimulated emissions are accompanied by the emission of other photons whose properties are identical to the incident photons, exponentially increasing the number of photons in a radiation field, which means that the medium amplifies the radiation ($e^{|\tau|}$) exponentially instead of attenuating the radiation ($e^{-\tau}$). The absolute value of the optical depth, is referred to as maser gain.

The exponential growth of radiation continues to grow as long as the pumping processes maintain the inversion; with this, the maser is said to be unsaturated. The maser radiation, however, cannot continually grow exponentially because it will imply an infinite energy density resulting from a long maser. Therefore, maser action consists of a built-in self-limiting process caused by amplification being sensitive to the path length. After a certain point in the maser column, the rate of downward transition, given by $U_\nu B_{ji} + A_{ji}$ (where $U_\nu B_{ji} > A_{ji}$) becomes larger than the rate of molecules to enter and populate level j and the inversion can no longer be maintained. The maser intensity then approaches a saturation limit and saturates the maser. This feature is seen clearly in Figure 2.6 as the column density increases above 10^{11} cm^{-3} s, the population inversion is affected and decreases. In a saturated maser, the amplification of the radiation slows down and grows linearly with the path length. Section D of Figure 2.6 indicates a fully saturated region. Consider that the cgs units are used in Figure 2.6 because that is how the model is constructed. These units will be used going forward.

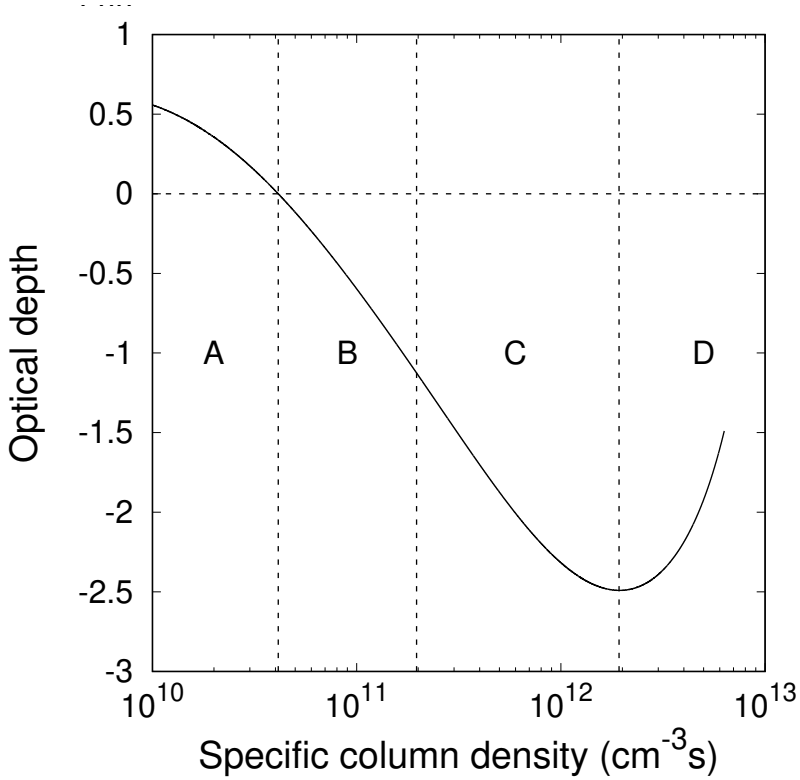

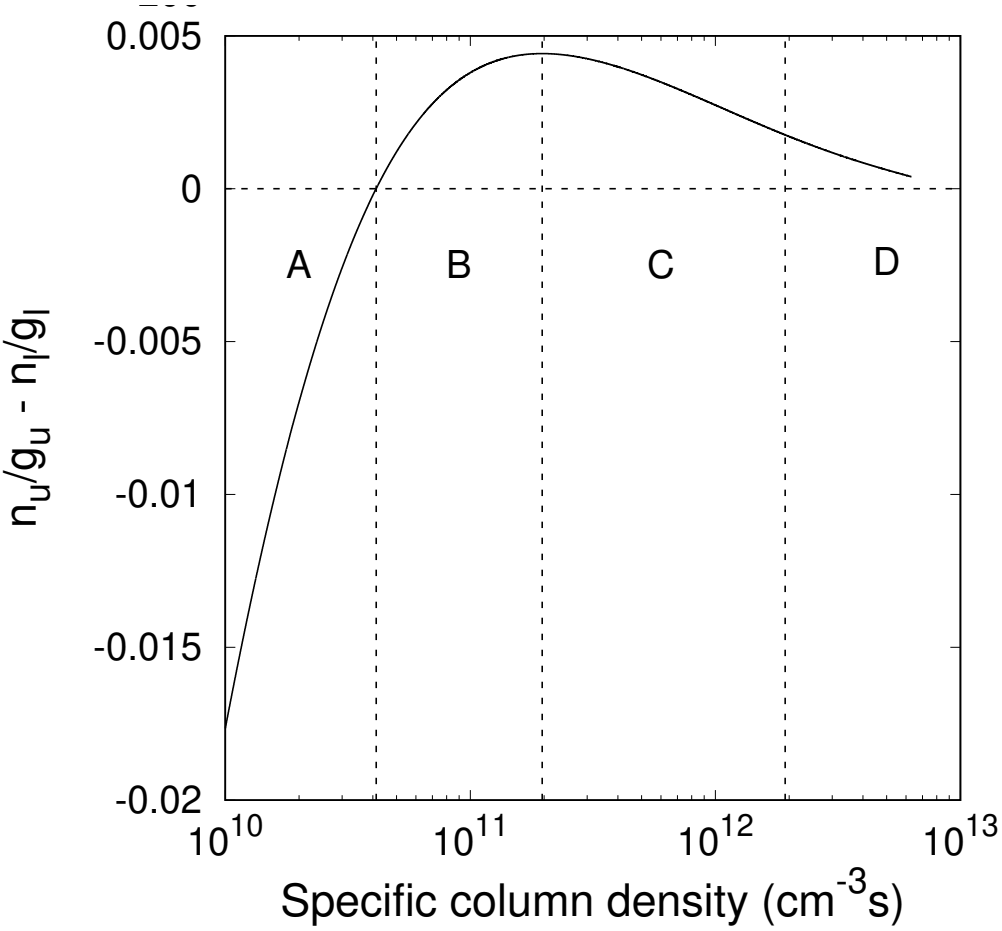

Figure 2.6: The upper panel shows how the optical depth behaves over a distance in the column density. The lower panel shows the population difference distribution behaviour in a column density of a specific length.

Chapter 3

Monte Carlo Method

As stated earlier, this thesis aims to investigate the relative roles of radiative and collisional excitation in the pumping of the H_2CO masers. Solving the rate equations numerically leads to understanding under which physical conditions a population inversion between two levels is possible. The rate equations do not explicitly carry any information on what the roles of radiative and collisional processes are in establishing the inversion. A possible way to investigate or determine the relative roles of collisional and radiative processes, is to simulate the excitation and de-excitation of a single molecule interacting with the radiation field and collisional interactions with H_2 molecules. A Monte Carlo simulation of the interaction of a single molecule with a radiation field and with H_2 would seem to be a possible way to understand the roles of radiative and collisional processes in establishing an inversion.

In this chapter, the basic background theory is presented that underlies the Monte Carlo simulation. The Monte Carlo method is based on sampling from probability distributions, and it is thus necessary to first review certain elementary aspects of probability theory. For this, various texts on probability theory (or its applications in Statistical Mechanics), e.g. Larson (1974), Fisz (1965), Gardiner (2009), Reichl (1980), Taylor and Karlin (1984), Whitney (1990) were consulted. The application of the basic concepts and definitions of probability theory will be presented in the context of this work.

3.1 Experiments, Sample Space, Events and Probabilities

Definition: An experiment is any operation whose outcome cannot be predicted with certainty.

Definition: The sample space S of an experiment is the set of all possible outcomes for the experiment.

As regards the physical situation considered for this simulation, one molecule is selected,

placed in a gas with a given number of H_2, and permeated by a radiation field; the molecule is allowed to make random radiative and collisional transitions. The molecule is treated as the system, and the radiation field plus the H_2 molecules as the reservoir.

The experiment is the random transitions by the molecule between the allowed rotational energy levels as it interacts with the reservoir, where the possible outcome is either collisional or radiative. There is no way to predict which rotational state the molecule will be in when a "measurement" is made. The sample space of the experiment consists of a set of rotational states, and it is also evident that the sample space depends on the current energy state in which the molecule is.

Since the axioms of probability theory are formulated in terms of events, the following definitions are needed.

Definition: An event occurs if one of its elements is the outcome of the experiment. It can also be a subset of a sample space.

Considering the physical situation described above, an event is a transition from the current state to any of the allowed rotational energy levels with energies less or more than the current state.

Definition: Consider an event A. The complement of A, denoted by $\bar{A}$, occurs if and only if event A does not occur; it then follows that $A \cup \bar{A} = S$.

The three fundamental axioms of probability theory are:

Axiom 1: To every random event A, there corresponds a certain number, $P(A)$, called the probability of A, which satisfies the inequality

$$0 \leq P(A) \leq 1 \tag{3.1}$$

for all $A \subset S$.

Since events are possible outcomes of experiments, it follows that experimenting must result in any event which belongs to the sample space S. Thus:

Axiom 2: The probability of the sure event equals one:

$$P(S) = 1 \tag{3.2}$$

Axiom 3: The probability of a finite sequence of pairwise exclusive events A_k, $k = 1, 2, 3 \ldots$, equals the sum of the probabilities of these events, i.e.

$$P\left(\sum_k A_k\right) = \sum_k P(A_k) \tag{3.3}$$

Axiom 3 can also be expressed more explicitly in set notation:

$$P\left(A_1 \cup A_2 \ldots \cup A_k\right) = \sum_{i=1}^{k} P(A_i) \tag{3.4}$$

if $A_i \cap A_j = \emptyset$ for all $i \neq j$.

The following theorem is also relevant to the Monte Carlo simulation:

Theorem 1: The sum of the probabilities of any event A and its complement $\bar{A}$ is one, thus

$$P(A) + P(\bar{A}) = 1, \tag{3.5}$$

and is very easy to prove since, by definition, $P(A \cup \bar{A}) = P(S) = 1$ and since $A \cap \bar{A} = \emptyset$, $P(A \cup \bar{A}) = P(A) + P(\bar{A})$ according to Axiom 3.

A simple application of Theorem 1 in the Monte Carlo simulation is that the transition out of, say, level i is either radiative or collisional. Event A can be defined as a radiative transition out of level i. It follows then that $\bar{A}$ is the event of a collisional transition out of level i.

Random Variables and Distribution Functions

To cover every aspect, a formal definition of a random variable is provided, and further explains the notation which will be used from now on.

Definition: A random variable X is a real-valued function of the elements of the sample space S. Thus, if $\omega \in S$ then, $X(\omega) \in \Re$ (the set of real numbers).

For example, when flipping a coin, the outcome can be either heads or tails. Neither of these are real numbers, but we can define X such that $X(\text{tails}) = 0$ and $X(\text{heads}) = 1$. In the simulation, the molecule of interest (CS or H_2CO) has a finite number of energy states, for example, n rotational quantum states characterized by the angular momentum quantum number J in the case of CS and J_{K_a,K_c} in the case of H_2CO. The energies of these states are known, and are arranged in increasing order of energy and label them $1, 2, 3 \ldots, n-1, n$. In the practical execution of the Monte Carlo calculation, it is simpler to work with these level numbers rather than with the energies of the different states. If the molecule is in state i at time t, it can make a transition (collisionally or radiatively) out of i to any of the remaining $n-1$ states. We can then take the sample space to be $S = \{1, 2, 3, \ldots, i-1, i+1, \ldots n\}$. The sample space, therefore, consists of a set of integers. The random variable X is then formally defined as

$$X(\omega \in S) = \omega \in \Re, \tag{3.6}$$

which is just the identity function. Since the sample space consists of a set of integers, it is clear that X can take on only certain discrete values and is therefore called a discrete random variable.

Definition: Consider a discrete random variable X which can take on a countable set of values, for example, $\{x_i\}$. The probability function for the random variable X is a function of x and is defined to be

$$p_X(x_i) = P(X(\omega) = x_i). \tag{3.7}$$

An important function used in the Monte Carlo simulation is the distribution function:
Definition: The distribution function $F_X(t)$ is defined as

$$F_X(t) = P(X \leq t), \tag{3.8}$$

with t any real-number. In the case of a discrete random variable for which the probability function is known, it follows that

$$F_X(t) = \sum_{x \leq t} p_X(x). \tag{3.9}$$

For a continuous random variable, we have

$$F_X(t) = \int_{-\infty}^{t} f_X(x)dx, \tag{3.10}$$

where $f_X(x)$, is the probability density function for X.

3.2 The Markov Process

As explained earlier, the process simulated is that of a molecule subject to a radiation field, in addition to collisional interactions with H_2. The molecule is initially in the ground state and performs a random walk between the different rotational quantum states due to radiative and collisional interactions. When in a particular state, the probability of making a radiative transition to another state depends on the Einstein A-coefficient and the energy density in the radiation field at the frequency equivalent to the difference in energy between the two states as well as on the collision coefficient for a collisional transition between the two states. These values depend only on the present state in which the molecule is and the states to which it can make a transition and not on the history of how it arrived at its current state. A stochastic process with the property that the 'future' state of the system depends only on the 'current' state is known as a Markov process, and the random walk of the molecule through the rotational quantum states is,

therefore, identified as a Markov process.

3.3 The Construction of a Monte Carlo Simulation Algorithm

3.3.1 The Description of the Monte Carlo Algorithm

This subsection discusses the algorithm used to calculate the molecule's 'trajectory' in time through the rotational states. In the Monte Carlo simulation, the molecule is in level i, and only the losses out of level i are considered. The rate equation for the losses out of level i is given by,

$$\frac{dn_i}{dt} = -n_i \sum_{j<i} A_{ij} - n_i \sum_{j<i} U_{ij}B_{ij} - n_i \sum_{k>i} U_{ik}B_{ik} - n_i \mathrm{n_{H_2}} \sum_{j<i} C_{ij} - n_i \mathrm{n_{H_2}} \sum_{k>i} C_{ik}. \quad (3.11)$$

The first term on the right-hand side of Equation 3.11 is the losses due to spontaneous emission, the second losses due to stimulated emission, the third losses due to absorption to upper levels, the fourth term is losses due to downward collisions and the fifth is losses due to upward collisions out of level i. Note that the energy density implicitly includes the escape probability terms as shown in Equation 2.103, and thus is not explicitly included in this equation. Equation 3.11 can therefore be written as

$$\frac{1}{n_i}\frac{dn_i}{dt} = -\lambda_i^{out}, \quad (3.12)$$

where

$$\lambda_i^{out} = \sum_{j<i} A_{ij} + \sum_{j<i} U_{ij}B_{ij} + \sum_{k>i} U_{ik}B_{ik} + \mathrm{n_{H_2}} \sum_{j<i} C_{ij} + \mathrm{n_{H_2}} \sum_{k>i} C_{ik}, \quad (3.13)$$

is the total probability per unit time for the molecule to transition out of level i. The solution of Equation 3.12 is given as

$$n_i(t) = n_i(t=0)e^{-\lambda_i^{out}t}, \quad (3.14)$$

which provides the number of molecules that remain in level i at time t. Therefore, $n_i(t)/n_i(t=0) = e^{-\lambda_i^{out}t}$ is the fraction of molecules from level i that have not made a transition out of level i. Thus, the probability of a molecule remaining in the level i after time t is therefore given by $e^{-\lambda_i^{out}t}$. On the other hand, the probability that the molecule

will make a transition out of level i during time t is $F_X(t) = 1 - e^{-\lambda_i^{out} t}$. As time grows larger ($t \to \infty$), it is expected that the molecule in level i would make a transition out of level i, i.e. the probability for the molecule to make a transition out of level i approaches 1.

The next step, is to determine the probability density function, which gives the probabilities per unit time for a transition out of level i. The probability density function is given by the derivative of the distribution function ($F_X(t) = 1 - e^{-\lambda_i^{out} t}$):

$$f(t) = \frac{d}{dt}(1 - e^{-\lambda_i^{out} t}) = \lambda_i^{out} e^{-\lambda_i^{out} t} \tag{3.15}$$

Note that $f(t) \to 0$ as $t \to \infty$, since at larger times the molecule would already have made a transition out of level i. Also, note that:

$$\int_{t=0}^{\infty} \lambda_i^{out} e^{-\lambda_i^{out} t} dt = 1, \tag{3.16}$$

since the molecule will definitely transition out of level i. The time $t = 0$ in Equation 3.16 is defined as the moment when the molecule "enters into level i".

The molecule can visit energy states more than once when making random transitions. One then needs to compute the time the molecule remains in a level before it makes a transition, referred to as the holding time. The accumulation of the holding times for every visit in each level is recorded; the distribution of the holding times is exponential. The probability of a molecule remaining in the energy state i at time t is given by $n_i(t)/n_i(t = 0) = e^{-\lambda t}$, and means that over time the probability of remaining in i decreases exponentially. Two approaches could be used to compute the cumulative distribution of the holding times and are discussed below.

3.3.2 First Approach

In this case, two possibilities can occur over time, the probability for a molecule to transition or alternatively remain in that particular state. The first step is to find the probability for the molecule to make a transition in the interval $(t, t + \Delta t)$ given by,

$$P(t, t + \Delta t) = \int_{t}^{t+\Delta t} \lambda_i^{out} e^{-\lambda_i^{out}} dt = e^{-\lambda_i^{out} t}(1 - e^{-\lambda_i^{out} \Delta t}). \tag{3.17}$$

The first factor on the right-hand side gives the probability that the molecule will not make a transition up to time t, and the second that the molecule will make a transition in a short time interval Δt immediately after t. Note that the probability of making a

transition out of level i in a short time interval Δt is independent of when that interval starts, i.e. it is independent of t. Therefore, generally, the probability for a molecule to make a transition in a short time interval (Δt) is given by $P(\Delta t) = 1 - \exp(-\lambda_i^{out}\Delta t)$. Thus if

$$\lambda_i^{out}\Delta t \ll 1 \tag{3.18}$$

then,

$$\exp(-\lambda_i^{out}\Delta t) \approx 1 - \Delta t, \tag{3.19}$$

which follows that,

$$P(\Delta t) = \lambda_i^{out}\Delta t. \tag{3.20}$$

This implies that, in terms of choosing Δt in the simulation code, we first need to determine λ_i^{out}. Then, in turn, determine the characteristic time $t = 1/\lambda^{out}$. **The physical meaning of the characteristic time is:** since the probability to transition in time t is $P(t) = 1 - \exp(-\lambda^{out}t)$, then set $t = \tau = 1/\lambda^{out}$ which implies that $P(\tau) = 1 - e^{-1} = 1 - 0.36788 = 0.63212$. Thus, the probability for a transition within the characteristic time is approximately 0.63.

The Choice of Δt

The choice of time interval Δt is not simple. For the probability of a transition from level i to another to occur Δt, should be chosen such that,

$$\lambda^{tot}\Delta t = (\lambda_{ij}^{sp} + \lambda_{ij}^{st} + \lambda_{ij}^{ab})\Delta t \leqslant 1 \tag{3.21}$$

$$\Delta t \ll \frac{1}{\lambda^{tot}}, \tag{3.22}$$

otherwise, the molecule will remain in the current energy level and never make a transition. Therefore, we have chosen Δt to be significantly small, for example,

$$\Delta t = \frac{0.1}{\lambda^{tot}} \tag{3.23}$$

such that,

- $0.1/A_{ij}$
- $0.1/B_{ji}U_{ij},\ j < i$
- $0.1/B_{ij}U_{ij},\ j < i$
- $0.1/n_{H_2}C_{ji}$ for *all* $j < i$. $\Rightarrow$ Collisional de-excitation
- $0.1/n_{H_2}C_{ij}$ for *all* $j > i$. $\Rightarrow$ Collisional excitation

Then, the probability of each event is:

- $P_{sp} = A_{ij}\Delta t$
- $P_{abs} = B_{ji}U_{ij}\Delta t\ j < i$
- $P_{st} = B_{ij}U_{ij}\Delta t\ j < i$
- $P_{coldown} = n_{H_2}\sum_{j<i} C_{ji}\Delta t \Rightarrow$ Collisional de-excitation
- $P_{colup} = n_{H_2}\sum_{j>i} C_{ij}\Delta t \Rightarrow$ Collisional excitation

A difficulty was encountered in choosing Δt when implementing this approach. Implementing a case of no transition for a short time is of no consequence as it involves the size of the time interval. For instance, if Δt is selected to be 'large'; it had to be carefully ensured that it would not be too large; the same applied when Δt is small (ensuring that it would not be too small), and therefore, this strategy was not pursued.

3.3.3 Second Approach

In the second approach the holding time is sampled directly from the exponential distribution. So the basic idea of this approach is to implement Equation 3.15 to sample the holding times from the probability distribution function $F_X(t)$. As previously mentioned, as time grows larger, the probability of a molecule making a transition out of the current level approaches 1, and is confirmed as:

$$\int_0^\infty f(t)dt = 1, \tag{3.24}$$

where $f(t)$ is the probability density function with $t > 0$, which further satisfies the requirement,

$$0 \leq \int_0^t f(t')dt' \leq 1. \tag{3.25}$$

The value of the probability density function at t equals the slope of the distribution function $F_X(t)$. Therefore the distribution function is such that,

$$F_X(t) = \int_0^t f(t')dt'. \tag{3.26}$$

Since the distribution function is a monotonically increasing function, it is possible to generate a random number $w(0,1)$ to sample and determine t from the distribution function such that,

$$F_X(t) = w. \tag{3.27}$$

To what extent Equation 3.27 can be inverted depends on $f(t)$, which is quite simple for an exponential distribution. Therefore,

$$w = \lambda \int_0^t e^{-\lambda t'} dt' = -e^{-\lambda t'}|_0^t = 1 - e^{-\lambda t}. \tag{3.28}$$

Thus, it follows that,

$$t = -\frac{1}{\lambda} \ln(1 - w). \tag{3.29}$$

Therefore t is the sampled holding time, with λ given by Equation 3.13. The study was continued with this approach.

3.3.4 The Monte Carlo Simulation Model

The computational model simulates the transition of a molecule from one state to the other as follows:

- The probability of radiative transition, is expressed as:

$$P_{rad} = \sum_{j<i} A_{ij}\Delta t + \sum_{j<i} U_{ij}B_{ij}\Delta t + \sum_{k>i} U_{ik}B_{ik}\Delta t \tag{3.30}$$

- The probability of collisional transitions is given by:

$$P_{coll} = \mathrm{n_{H_2}} \sum_{j<i} C_{ij}\Delta t + \mathrm{n_{H_2}} \sum_{k>i} C_{ik}\Delta t \tag{3.31}$$

- Thus, the probability of making a transition out of the energy state is such that:

$$P_{tot} = P_{rad} + P_{coll} \tag{3.32}$$

$$= \sum_{j<i} A_{ij}\Delta t + \sum_{j<i} U_{ij}B_{ij}\Delta t + \sum_{k>i} U_{ik}B_{ik}\Delta t + \mathrm{n_{H_2}} \sum_{j<i} C_{ij}\Delta t + \mathrm{n_{H_2}} \sum_{k>i} C_{ik}\Delta t \tag{3.33}$$

- First and foremost, the probability of each event is properly normalised, $P^{'}_{rad} = P_{rad}/P_{tot}$ and $P^{'}_{coll} = P_{coll}/P_{tot}$, so that $P^{'}_{rad} + P^{'}_{coll} = 1$.

- To sample the transitions a molecule makes from one state to another, a choice is made, whether the transitions will be due to radiation or collisions. To make a choice, a uniform random number, $w(0, 1)$, is generated using the GNU scientific library to sample the probability of an occurring event. In the simulation, the choice between the two events, is indicated as follows: if $w < P^{'}_{rad}$, the molecule makes a radiative transition alternately, it is a collisional transition.

- The molecule starts in the ground state, and its path, is followed as it interacts with the reservoir. After 10^9 interactions, the accumulation of holding time for each energy level is recorded. Then the holding time for each energy level is normalized over the total time of all the energy levels. The normalized total time distribution for all energy levels should be the same as the level populations used to calculate the internal radiation, optical depth and escape probability.

- Therefore, if the molecule spends a shorter time in the energy level, the probability of finding the molecule in that specific energy level is also small. On the other hand, if the molecule spends a large amount of time in an energy level, the probability of finding the molecule in that level is much higher.

Chapter 4

Results

4.1 Introduction

As previously mentioned, this work aims to investigate which process (collisionally or radiatively) is responsible for establishing a population inversion of the 4.8 GHz H_2CO maser. Therefore, to address this question, a Monte Carlo simulation is used to investigate the role of each excitation process and which process is responsible for a population inversion. In short, there is a need to understand the role of radiative and collisional excitations in achieving a population inversion of $1_{10} - 1_{11}$ transition. Four questions are asked to achieve the aim of this thesis.

1. Is the Monte Carlo simulation method the correct approach to provide the expected results?
2. To what extent is this approach reliable?
3. What is the role of each excitation process?
4. What is the pumping mechanism of the H_2CO maser?

This chapter comprises five sections, including the introduction. The second section explains the selection of the study's physical parameters. The third section presents the results for CS. The study of this molecule is to test that the proposed Monte Carlo method can indeed reproduce the expected results. The fourth section presents the results for H_2CO. In the fifth section, the Monte Carlo simulation model is used to study the results of Baan et al. (2017). In the case of radiative transitions, the effects of infrared radiation and how they affect the population inversion is studied.

4.2 Determining the Physical Parameters for the Monte Carlo Simulation Model.

Two molecules are studied under LTE and non-LTE conditions, and the parameters used for these two cases are carefully chosen. Two limiting cases are tested for LTE condition, where (a) the radiative field dominates, and (b) collisional excitation dominates. The values parameters such as the kinetic temperature (T_k) and the dust temperature (T_d) are assumed. The geometric dilution factor (W) is set to be unity, and the fractional molecular abundance is taken as $\sim 10^{-6}$. For a collisional excitation case, $T_k \gg T_d$, and the density of the H_2 molecule should be significantly larger than $\frac{A_{ji}}{C_{ij}}$. Inspecting the $J = 30 \rightarrow 29$ transition of the CS molecule, the value of A_{ji} is 6.238×10^{-2} s^{-1} and the corresponding collisional coefficient, C_{ij} is 8.170×10^{-11} cm^3 s^{-1}, thus the ratio $\frac{A_{ji}}{C_{ij}} = 7.6 \times 10^8$ cm^{-3}, thus the required density n_{H_2} is greater than 8×10^8 cm^{-3}. In the case of radiative excitation, $T_k \ll T_d$, and the H_2 density should be significantly smaller $\frac{A_{ji}}{C_{ij}}$. The A-value for the $J = 1 \rightarrow 3$ transition is A_{31} is 1.749×10^{-6} s^{-1} and the collisional rate is $C_{31} = 3.490 \times 10^{-11}$ cm^3 s^{-1}, giving a ratio $\frac{A_{ji}}{C_{ij}} = 5.0 \times 10^4$ cm^{-3}, thus, requiring the H_2 density to be less than 5×10^4 cm^{-3}. The SCD, N_{col} used in the model is calculated using the following equation:

$$N_{col} = \frac{X n_{H_2} \ell}{\Delta\nu}, \tag{4.1}$$

where the X is the fractional molecular abundance, n_{H_2} is the density of H_2, ℓ is the maser path length (10^{16} cm), and $\Delta\nu$ is the linewidth (taken as 10^5 cm s^{-1}). The idea is to start with the number density of CS molecules in the ground state given to be $n_i = 5.0 \times 10^3$ cm^{-3}. One CS molecule is then picked and followed in time as it interacts with the H_2 molecules.

In the case of non-LTE conditions, the parameters are chosen by using the solution of the numerical simulation model used by van der Walt (2014). The numerical calculation solves the set of rate equations using the 4th order Runge Kutta method, which results in the level population distribution. The calculation starts with the Boltzmann level population distribution with a small SCD and the temperatures T_k and T_d. The system is allowed to evolve with a time step of 5 seconds until equilibrium is reached, and the convergence condition attained for all levels given as $|N_i(t_{j+1}) - N_i(t_j)|/N_i(t_j) < 10^{-6}$. The final level population is used as the initial level population to compute the new level population with the new SCD. The final level populations in each specific column densities are stored and then used to calculate the optical depth. Figure 4.1 shows the variation in the behaviour of the optical depth as the SCD increases, plotted for different kinetic temperatures. The excitation is via collisions plus the external and internal radiation field.

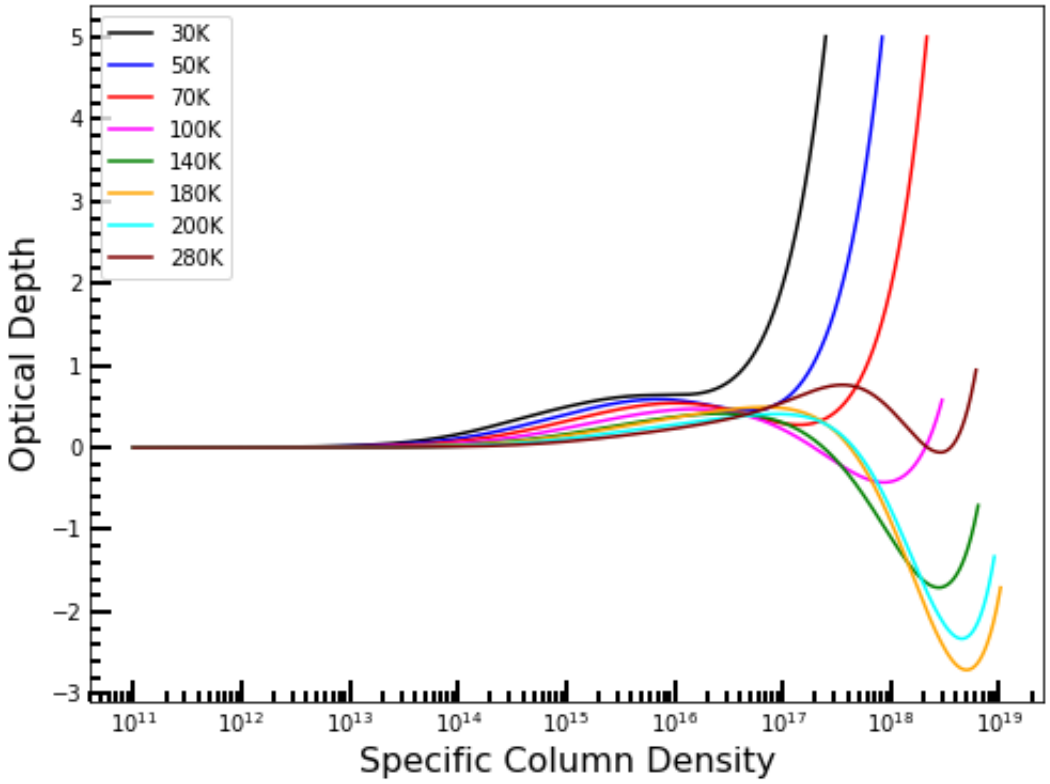

Figure 4.1: The behaviour of optical depth of 4.8 GHz H_2CO maser as the SCD increases for kinetic different temperatures.

Figure 4.1 shows the variation of the optical depth as the function of the SCD at T_k = 30, 50, 70, 100, 140, 180, 200 and 280 K. These results are obtained from the numerical simulation model that solves the rate equation as described above. These cases are examined to search for a set of physical parameters required to form an H_2CO maser in a molecular cloud; the parameters are used in the Monte Carlo simulation, and the same is done for the CS. The goal was to get the SCD where maximum inversion (when $\tau < 0$) occurs for different kinetic temperatures (T_k). Then, the Runge Kutta numerical model was used to produce the distribution of level population for the SCD where maximum inversion occurs. The level population was used in the Monte Carlo simulation method to calculate the optical depth, the source function and the energy density.

4.3 The CS Molecule.

This section provides the CS results. The aim is to test whether the Monte Carlo simulation is a good approach. The simulation code is tested for LTE conditions, and the fractional holding time per sub-level is expected to describe the Boltzmann distribution. The fractional holding time per sub-level is the holding time in seconds divided by the total time and the weight $\left(\frac{t_i}{g_j \sum_i t_i}\right)$. In addition, the simulation code is also tested for non-LTE conditions, and the holding times distribution is expected to agree with the level population distribution from the Runge Kutta model.

4.3.1 The LTE Monte Carlo Simulation Model

In LTE, the conditions are treated locally, and the system is characterised by one temperature. The LTE conditions thus possess a dominating effect, meaning either radiation or collisions dominate. For a case where radiation dominates, the local dust temperature (T_d) is given by a black body temperature and controls the level population. When collisions dominate, the local temperature is the kinetic temperature (T_k) which controls the level populations. The number of interactions used is 10^7; the reason for this large number of interactions is to ensure that the fractional holding time distribution converges statistically over the range of energy. The number of interactions were varied until equilibrium was reached.

Since we are dealing with a single molecule as a system, other molecules (of the same type) are part of the environment. The disadvantage of simulating a large number of molecules, it is difficult to track the random walk of each molecule. Two distributions were constructed to present the results of this single molecule: First, the distribution of the number of visits, which presents the probability that the molecule visits each level. Second, the distribution of time spent in each level, i.e. the holding time distribution.

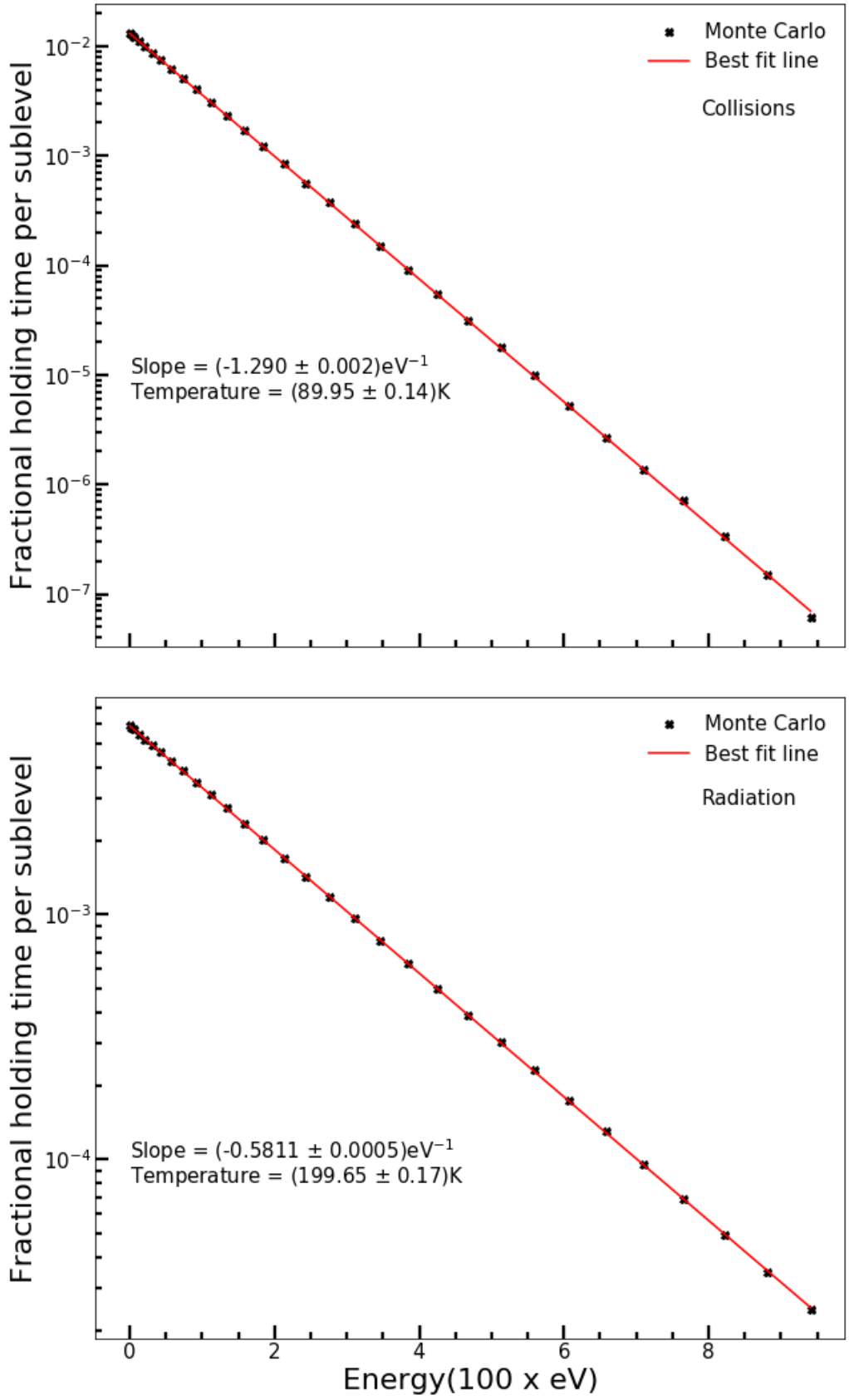

Figure 4.2: The holding time distribution of the CS molecule in thermal equilibrium. The top panel shows the distribution when collisional excitation dominates at a temperature of $T_k = 90$ K, SCD $= 2.0 \times 10^{16}$ cm^{-3}s and $n_{H_2} = 10^{12}$ cm^{-3}. The bottom panel shows the distribution when radiative excitation dominates with a blackbody temperature of $T_d = 200$ K, SCD $= 1.0 \times 10^{8}$ cm^{-3}s and $n_{H_2} = 10^{3}$ cm^{-3}.

Figure 4.2 shows the holding time distribution (black) and the line of best fit (red). The upper panel is the distribution when collisions dominate the excitation, and radiation is excluded with the temperature of $T_k = 90$ K. The bottom panel is when radiation dominates excitation, and collisions are excluded, with the input temperature of $T_d = 200$ K. Note that Figure 4.2 is the straight line plotted on the linear x-axis and logarithmic y-axis. Thus, this indicates that the distribution has an exponential dependence on the energy relative to the ground state, similar to the Boltzmann distribution of the level population when TE applies as given by,

$$\frac{n_1}{g_1} = \frac{n_0}{g_0} e^{-\frac{\Delta E}{kT}}. \tag{4.2}$$

Then

$$\ln\left[\frac{n_1/g_1}{n_0/g_0}\right] = -\left(\frac{1}{kT}\right)\Delta E, \tag{4.3}$$

which is a straight line with slope $\frac{1}{kT}$ on a log-linear scale. The linear function is fitted to the data by applying the least square method using the Python programming language. The temperature of the system can, therefore, be calculated from the slope of the straight line, i.e. $T = 1/(k \times \text{slope})$. Whether the distribution of the holding times correctly reflects the distribution of the level populations can be tested by calculating the temperature of the system from the slope and comparing it to the input temperature. When applying this to the two cases in Figure 4.2 it is found that $T_k = (89.95 \pm 0.14)$ K for the upper panel and $T_d = (199.69 \pm 0.17)$ K for the lower panel. The uncertainties of T are estimated using the propagation of errors formula:

$$\Delta T = \frac{1}{k\Delta s}, \tag{4.4}$$

where ΔT is the error of T, and Δs is the error of the slope. Both derived temperatures are in excellent agreement with the input temperatures $T_k = 90$ K for collisions and $T_d = 200$ K for radiation with a difference of less than one percent. Since there is a good agreement, it is concluded that the fractional holding times are equivalent to the level population.

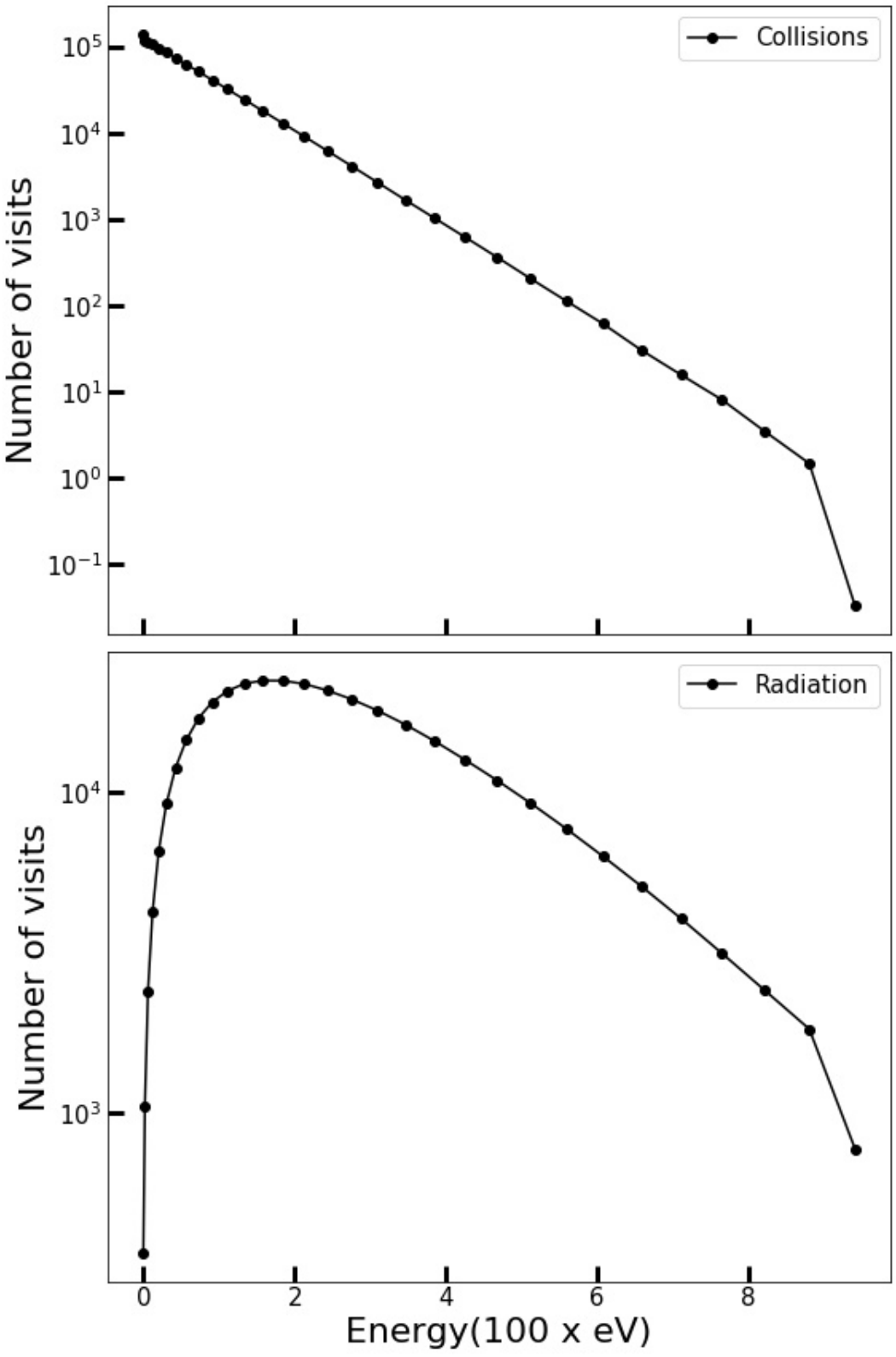

Figure 4.3: The distribution of the number of visits of the CS molecule for all energy levels. The upper panel presents the distribution for when collisions dominate for $T_k = 90$ K. The bottom panel exhibits the distribution when radiative excitations dominate for $T_d = 200$ K.

Figure 4.3 presents the distribution of the number of visits per sub-level for when collisions dominate (top panel) and when radiation dominates (bottom panel), respectively. This distribution does not indicate how long the molecule stays in a specific energy level but how many times it has visited that energy level. For collisional excitations (top panel), for 10^7 interactions, if the distribution was that of the Boltzmann, it should have been a perfectly straight line, the lowest and highest points deviate from a line. Just as from the previous example, the distribution is fitted the best line fit and the temperature is estimated to be 99.98 K. This shows that the distribution is not equivalent to the level population. In the case of radiation excitations (bottom panel), the molecule visits the lower energies more than the higher energies. The distribution of the number of visits is, therefore, not equivalent to the level population.

4.3.2 The Non-LTE Monte Carlo Simulation Model

In the case of a non-LTE condition, the energy density in the external radiation field is diluted with the dilution of $W = 0.2$, unlike in the case of the LTE condition. As derived in Chapter 2, the total radiation is the sum of the external dust radiation field and the internal radiation field where $W \neq 1$ given by:

$$U_{ij} = \frac{4\pi}{c}\left[\underbrace{W\beta_{ij}\left(\frac{\nu}{\nu_0}\right)^p B_\nu(T_d)}_{\text{External radiation}} + \underbrace{\frac{2h\nu_{ij}^3}{c^2}\left(\frac{g_j}{g_i}\frac{x_i}{x_j} - 1\right)^{-1}(1-\beta_{ij})}_{\text{Internal radiation}}\right]. \tag{4.5}$$

The internal radiation field is significantly larger than the external radiation field, as shown in Figure 4.4. Internal radiation is generated when the allowed transitions between different energy states occur, which means the radiation field is calculated from the level population.

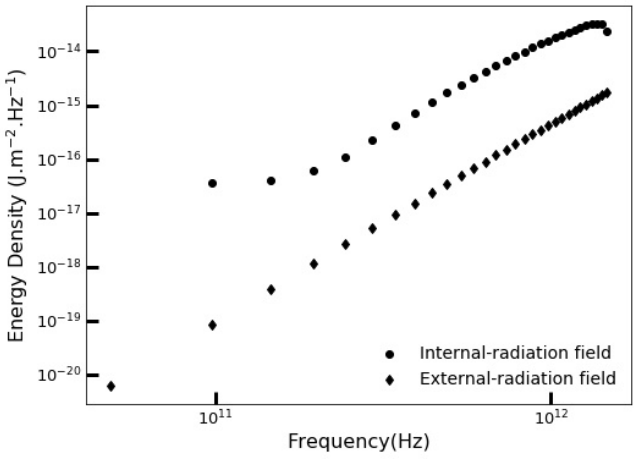

Figure 4.4: Comparison between the internal and external dust radiation field intensity.

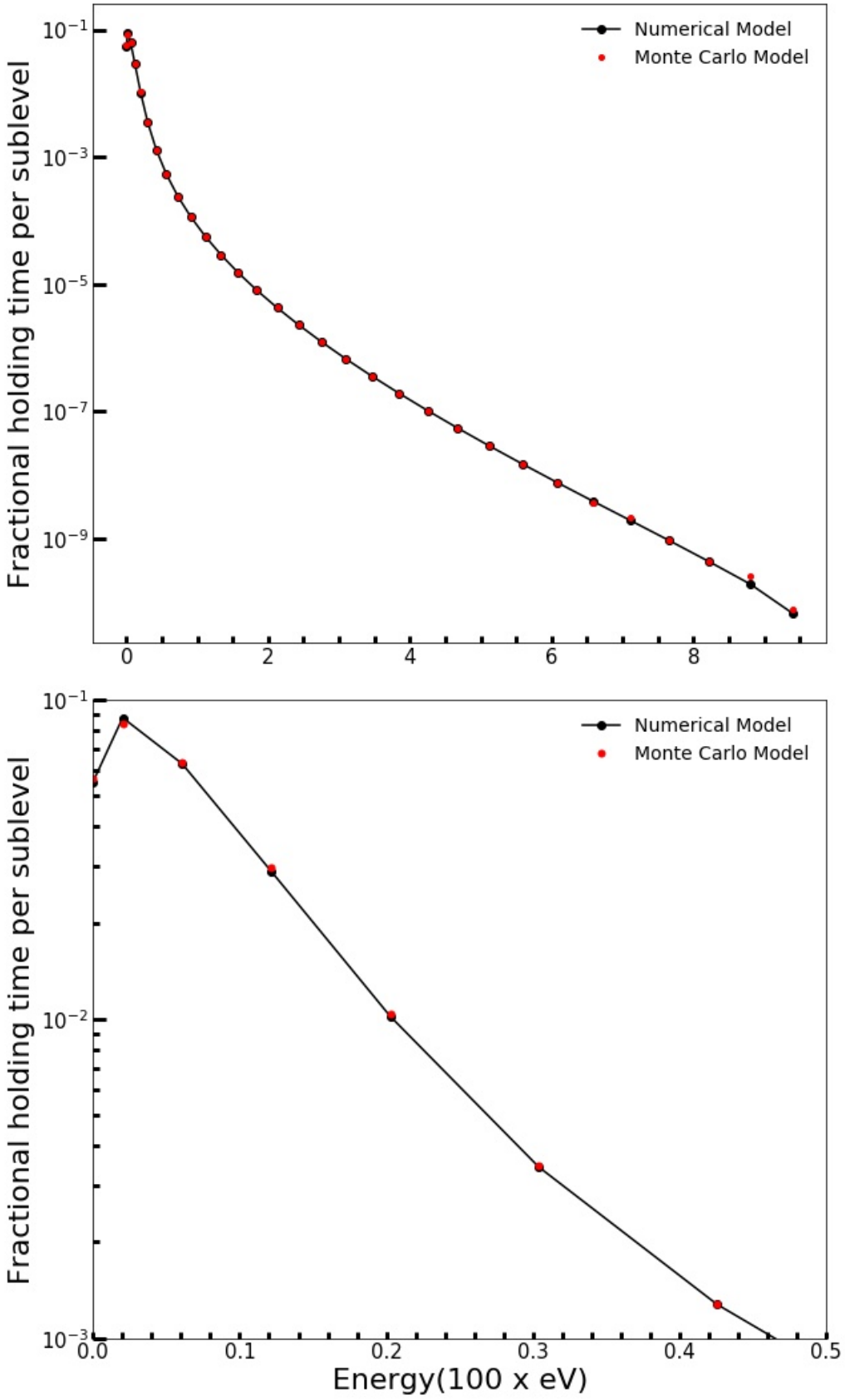

Figure 4.5: Comparing the holding time distribution (red) and the level population distribution (black) of the CS molecule. The top panel depicts the distribution for all energy levels for 10^7 interactions. The bottom panel shows the distribution above the ground state less than 0.005 eV. The physical parameters are T_k = 200 K, T_d = 50 K, SCD = 1.0×10^{14} cm^{-3} s, $n_{H_2} = 10^{4.75}$ cm^{-3}, W = 0.2 and p = 1.8.

In the case of non-LTE conditions, the goal is to test if the distribution produced reproduces an inversion of the $J = 2 - 1$ transition. The result of the Monte Carlo method is compared to that of the numerical method, that is, the distribution of the holding times and the level population, respectively. The results are reported in Figure 4.5. The bottom panel illustrates the levels with energy above the ground state of less than 0.005 eV. Figure 4.5 shows that the two models agree very well over the whole energy range. The holding time distribution behaves exactly the same as the level population. The good agreement between these two models confirms that the Monte Carlo simulation model produces the correct results and further confirms that the model is reliable to a greater extent. Therefore, the Monte Carlo simulation method is the correct approach for this work.

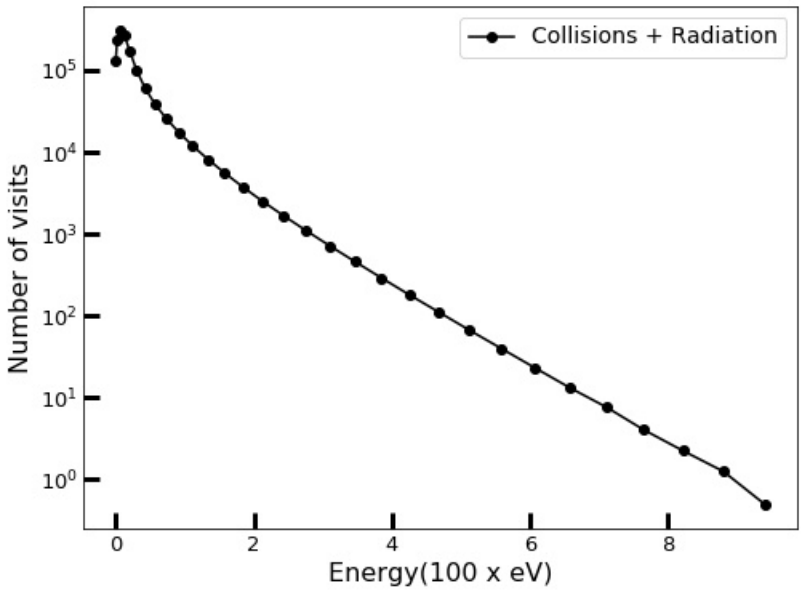

Figure 4.6: The distribution of the number of visits in each sub-level over 10^7 interactions. The physical parameters are given as $T_k = 200$ K, $T_d = 50$ K, SCD is 2.0×10^9 cm^{-3} s, W = 0.2 and p = 1.8.

Figure 4.6 shows the distribution of the number of visits for a non-LTE model. The number of visits decreases with an increase in energy. The radiation dominates the lower energies, and the collisions dominate the higher energies. It is evident that this distribution is not equivalent to the level population under the non-LTE conditions. The second energy state is the most populated when it comes to the level population distribution; yet, when it comes to the distribution of the number of visits, the third energy state is the most visited. This is a confirmation that in LTE and non-LTE cases, the distribution of the number of visits does not reflect the level population.

4.4 The H_2CO Molecule.

The pumping of the 4.8 GHz H_2CO maser is the main interest of this study. Considering the complex transitions of this molecule, the goal is to study the pumping scheme of this maser and learn what its pumping mechanism is. After implementing the Monte Carlo simulation model for the H_2CO molecule, it was necessary to start by testing the reliability of the Monte Carlo simulation for the H_2CO molecule, similar to what was done for CS. The exploration of both LTE and the non-LTE cases, are explored later. The number of interactions for the solution of the Monte Carlo simulation method to converge to a Boltzmann distribution is given by 10^8.

4.4.1 The LTE Monte Carlo Simulation Model.

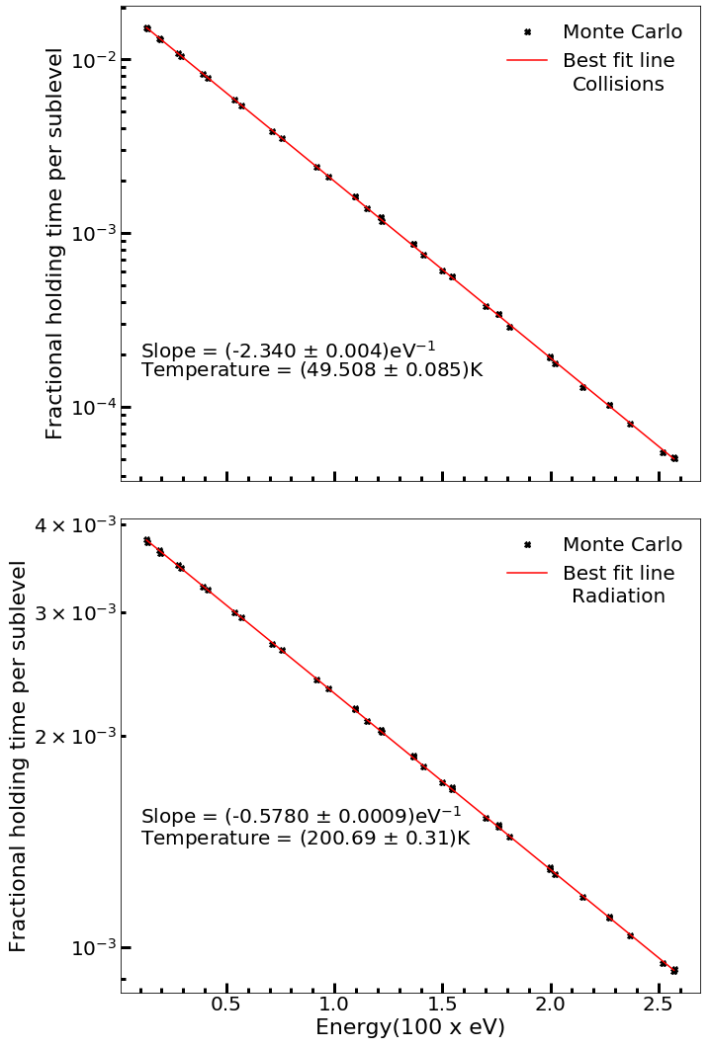

Figure 4.7: The holding time distribution of the H_2CO molecule in thermal equilibrium. The upper panel illustrates the distribution when the excitation is dominated by collisions for $T_k = 50$ K, SCD $= 1.0 \times 10^{15}$ cm^{-3}s and $n_{H_2} = 10^9$cm^{-3}. The bottom panel illustrates the distribution when radiation excitations dominate the excitation for $T_d = 200$ K, SCD $= 2.0 \times 10^9$ cm^{-3}s and $n_{H_2} = 10^3$cm^{-3}.

As mentioned above, the same approach used for the CS molecule above, is applied to the H_2CO molecule, and includes the selection of parameters discussed above. The distributions shown in Figure 4.7 present the distributions of the holding times of the molecule in TE and are fitted with the line of best fit. The temperature of the system is calculated from the slope and compared to the input temperature. For both cases in Figure 4.7 it is found that $T_d = (200.69 \pm 0.31)$ K for the upper panel and T_k is (49.508 ± 0.085) K for the lower panel. The calculated temperatures are in excellent agreement with the input temperatures, which are $T_d = 200$ K and $T_k = 50$ K, respectively with a difference of less than one percent. As in the case of CS, it is therefore concluded that the fractional holding time is equivalent to the level population.

Figure 4.8 presents the distribution of the number of visits of an LTE case for collisional and radiative excitations separately. The top panel is the distribution of the number of visits when a molecule is excited collisions only. The bottom panel is the distribution of the number of visits for a molecule only excited radiatively. It is evident that these distributions also do not reflect the level populations. However, by inspecting these figures, it is apparent that there is something to learn from these figures. In the case of radiation (bottom panel), the number of visits increases with the energy. However, it can be noticed that as the energy increases, the number of visits is larger in the K_1 than in the K_3 ladder. This is because the molecule makes fewer transitions from the K_1 to K_3 ladder. The frequency of transitions from the K_1 to K_3 ladders is low, thus resulting in lower energy density. Because of the low energy density, the absorption and stimulated rates become significantly low.

In the case of collisions (top panel), the number of visits decreases as the energy increases. Contrary to radiation (bottom panel), the number of visits to the K_1 ladder is almost equal to the K_3 ladder. The preceding indicates that the collisional rates between K_1 and K_3 are the same. Notice the number of visits distribution is not equivalent to the level population.

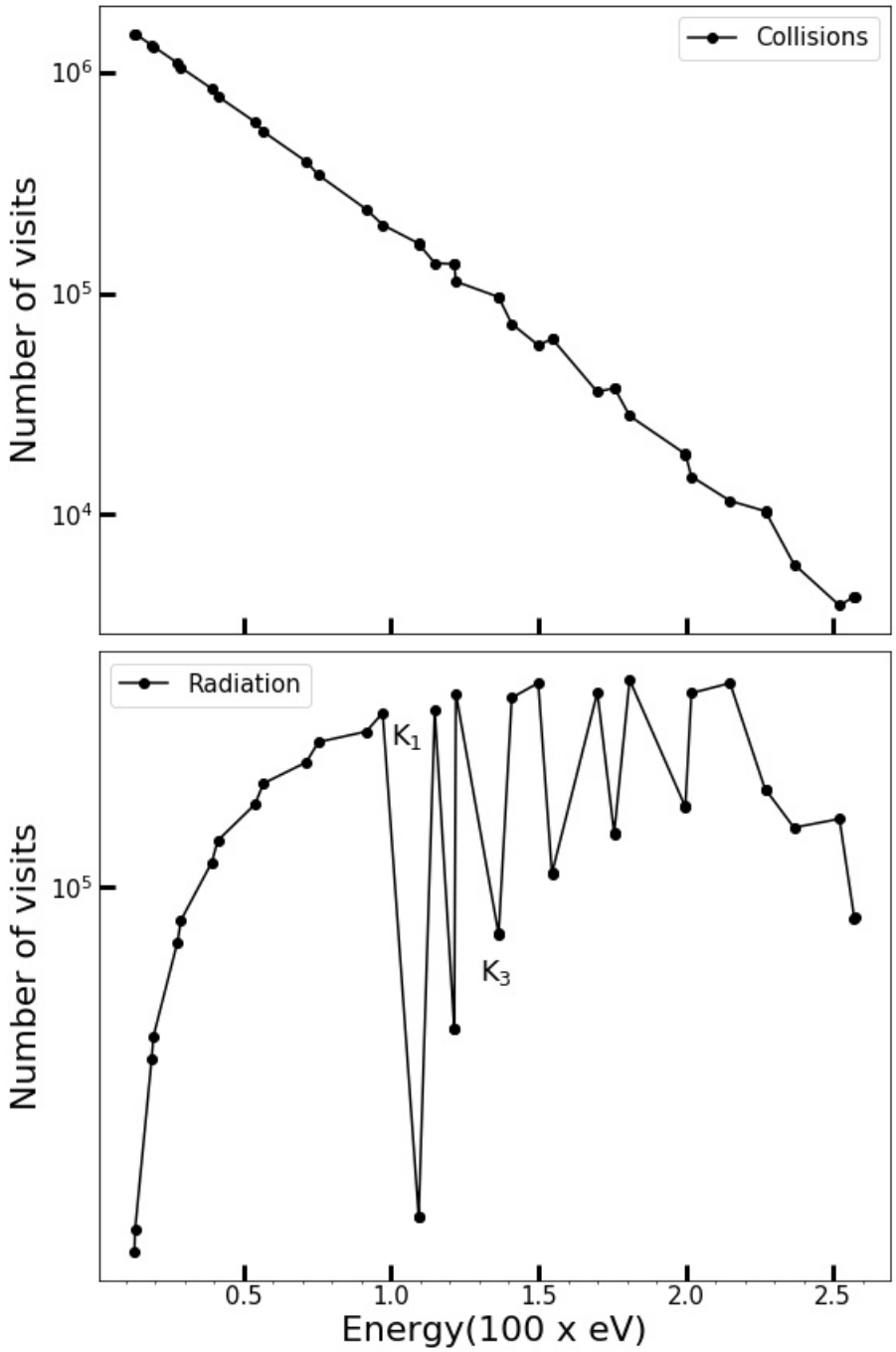

Figure 4.8: The distribution of the number of visits of the H_2CO molecule for all energy levels. The top panel shows the distribution when radiation dominates for $T_d = 200$ K. The top panel shows the distribution when collisions dominate for $T_k = 50$ K.

4.4.2 The Non-LTE Monte Carlo Simulation Model

The H_2CO molecule is simulated for a non-LTE case. Figure 4.9 the top panel shows the holding time distribution (red) of the Monte Carlo model compared to the level population (black) of the Runge Kutta calculation for an H_2CO molecule for the whole range of 40 levels, the bottom panel shows this distribution with energy above the ground state of less than 0.0035 eV. Interestingly, the Monte Carlo fits the Runge Kutta model very well, and the agreement confirms that the Monte Carlo simulation code produces the correct results, confirming that the Monte Carlo approach is reliable.

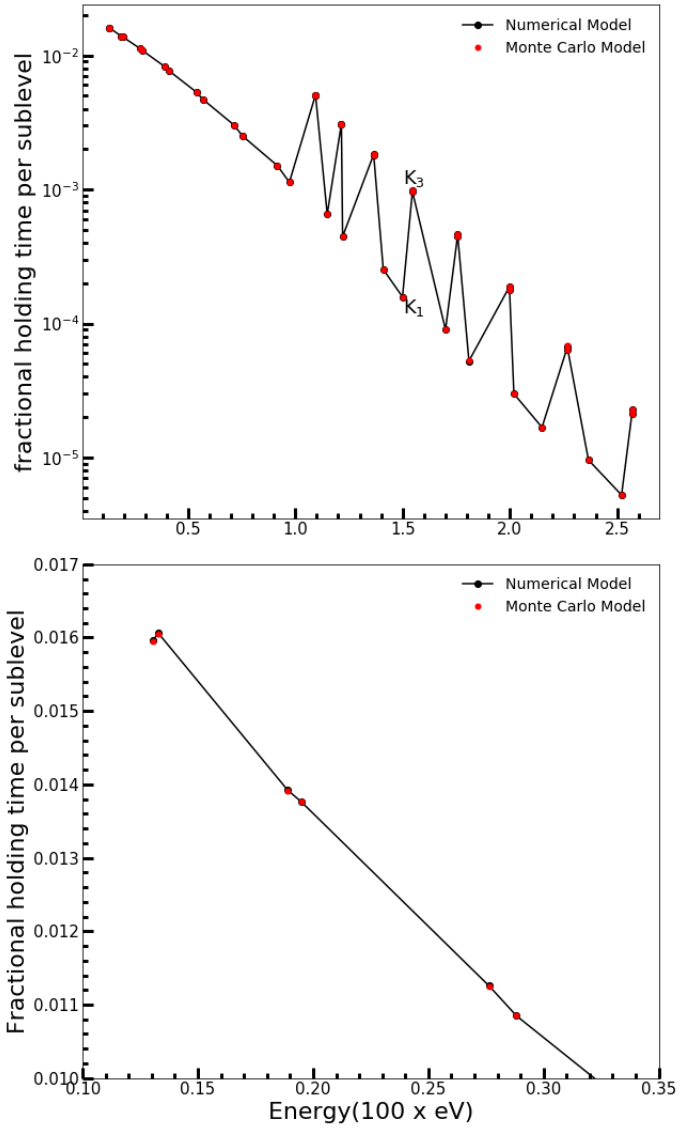

Figure 4.9: Comparing the holding time distribution (red) and level population distribution (black) of the H_2CO molecule. The top panel shows the distribution over the energy range for 10^8 interactions. The bottom panel shows the distribution above the ground state less than 0.0035 eV. The physical parameters are $T_k = 100$ K, $T_d = 180$ K, the SCD is 7.3038×10^{16} cm^{-3} s, n_{H_2} is $10^{4.25}$ cm^{-3}, W = 1 and p = 1.

Figure 4.10 shows the distribution of the number of visits for non-LTE conditions. These results confirm that the distribution of the number of visits does not reflect the level population as opposed to the holding time distribution. However, it is believed something can be learned from the number of visits that will lead to the pumping scheme of the H_2CO. Therefore, since the Monte Carlo simulation code is verified, the pumping scheme of the H_2CO molecule can thus be studied.

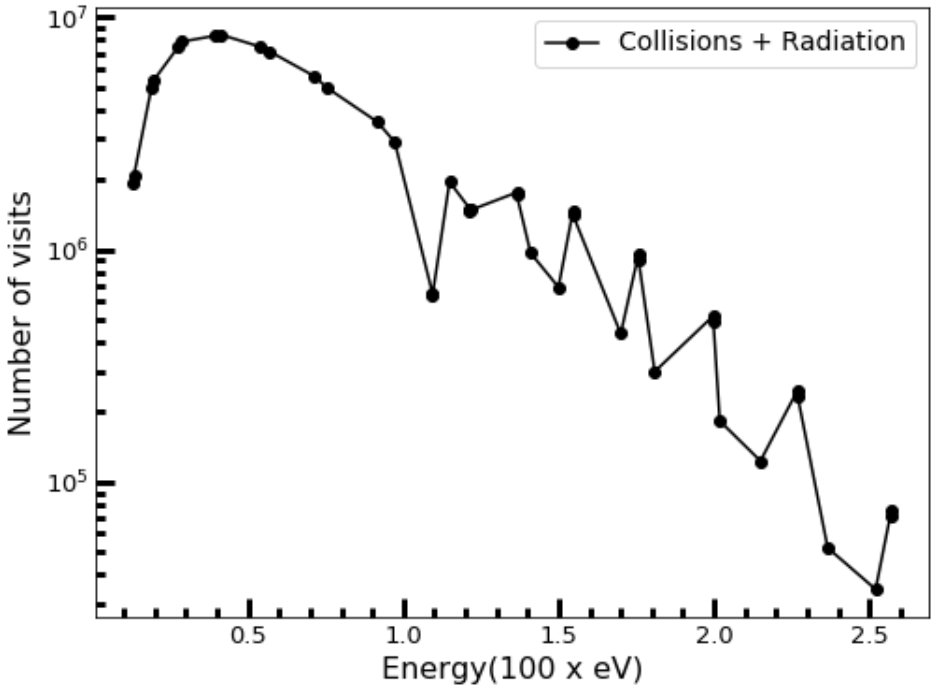

Figure 4.10: The distribution of the number of visits in each sub-level for an H_2CO molecule. The physical parameters are $T_k = 100$ K, $T_d = 180$ K, the SCD is 7.3038×10^{16} cm^{-3} s, $n_{H_2} = 10^{4.25}$ cm^{-3}, W = 1 and p = 1.

4.4.3 The Study of Pumping Schemes of the H_2CO Molecule

It is possible to study the roles of collisions and radiation as excitation processes now that the Monte Carlo code is verified to produce the correct results. In constructing a Monte Carlo simulation to work out the roles of the excitation processes, the idea was to try to learn directly from the history of a molecule as it randomly walks according to the probabilities of these two excitation processes. However, it was found to be difficult to extract any meaningful information directly from the history of the random walk. Another possible approach to studying the history of the molecule was to ask a question: with a molecule starting in level 1, what is the probability for the molecule to be in any state after the first interaction, after the second, after the third, etc.? Figures 4.11 and 4.16 present the results of the molecule followed for 100 interactions; this process is repeated 10^8 times to obtain a statistically stable result, thus resulting in a total of 10^{10} interactions.

There are ten panels in each figure, and each panel represent an interaction. The y-axis is logarithmic with a minimum of 10^{-15} (representing 0 probability), and the maximum is 10^{1}. The x-axis gives the probability for the molecule to be in a certain level for the n-th interaction.

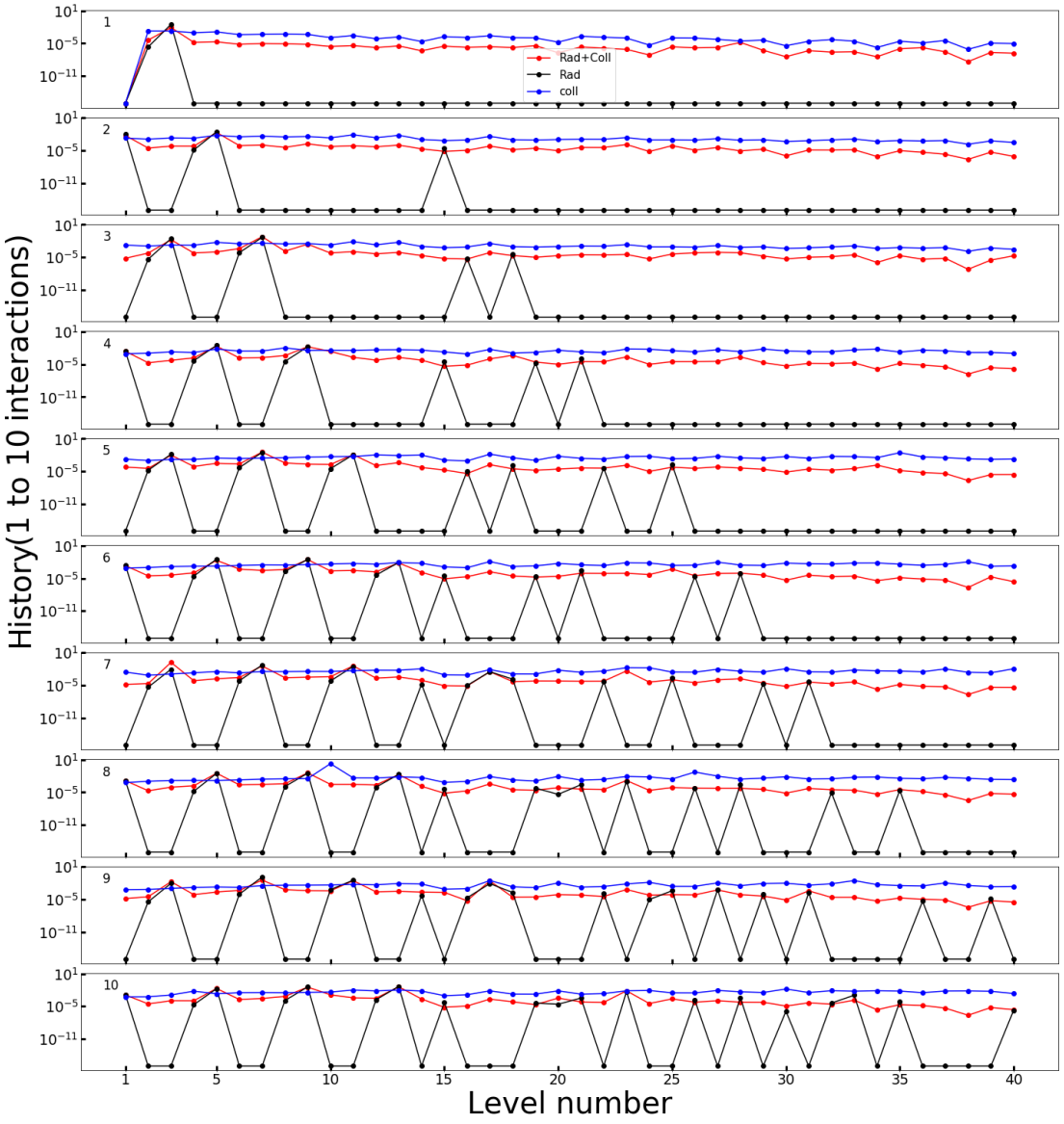

Figure 4.11: Plot showing the history of a molecule after ten interactions, when the excitation is only collisional (blue), only radiative (black), and when both radiation and collisions are considered as the excitation (red). The physical parameters for this case are given by $T_d = 100$ K, $T_k = 180$ K and $n_{H_2} = 10^{4.25}$ cm^{-3}.

Figure 4.11 illustrates the probability of the molecule being excited or de-excited into various energy levels for the first ten interactions. The red dots are for when both radiative and collisional excitations are considered. The black dots are when the excitation is only via radiation, and the blue dots are when the excitation is only through collisions. For the first interaction, it is clear that a molecule in level 1 can be excited to either level 2 or level 3 only by radiation (black). This transition is determined by the dipole selection rules. In

the other two cases where collisions are included, the molecule can be excited to any of the other energy levels. The dipole selection rules do not determine these transitions.

Comparing the case of collisional excitation only (blue) and the case where the excitation includes both collisions plus radiation (red) for the first interaction, as shown in Figure 4.12. Notice that the probabilities decrease as the level number increases. The probability of exciting the molecule from $1 \rightarrow 3$ via radiation plus collisions (red) is 2.89×10^{-5} s^{-1} and the probability of exciting the molecule collisionally (blue) which is 3.29×10^{-6} s^{-1}. Therefore, in the case of radiation plus collisions, the molecule would preferably get excited to level 3 radiatively resulting in the probability of exciting the molecule collisionally weaker.

In Figure 4.11, comparing the case of collisional excitation only (blue) to the case of radiation plus collisions (red), for the first ten interactions, there is insufficient information regarding the excitation of the molecule. Comparing the case of collisional excitations only (blue) and radiation only (black), it can be seen that collisionally the molecule is excited to any other levels, while radiatively, the molecule is excited according to the dipole selection rules. Therefore, going forward will only report on the case of radiation only (black) and radiation plus collisions (red).

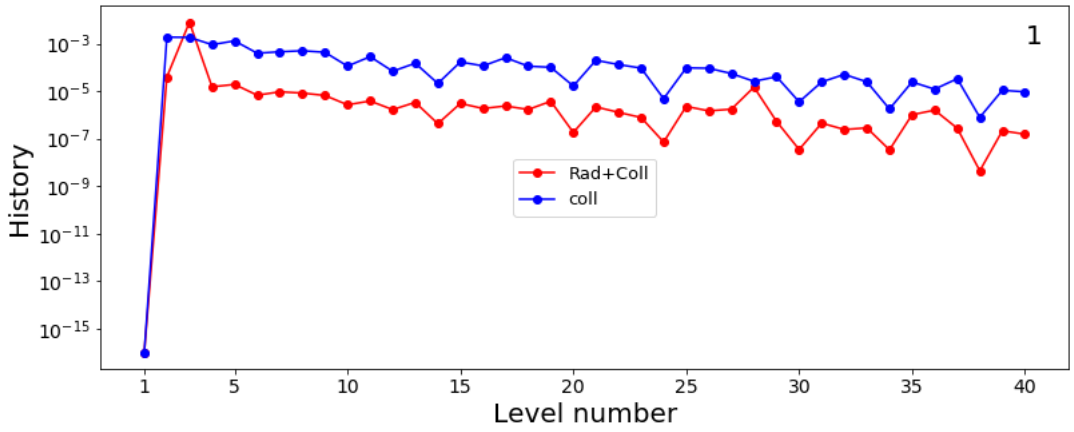

Figure 4.12: The history distribution of the molecule when collisional excitations dominate (blue), and when radiation plus collision (red), excitations dominate for the first interaction.

Similarly, comparing the cases where the molecule is excited by radiation only (black) and where the excitation is due to radiation plus collisions (red) after the first interaction, as shown in Figure 4.13. In the case of radiation excitation only, the molecule can be excited to level 2 or level 3, and the probability of being excited to level 3 is larger than the probability of being excited to level 2, with probabilities 2.2×10^{-6} and 3.1×10^{-2}, respectively. Since the spectral energy density increases with frequency, and since the frequency of the $1 \rightarrow 3$ transition is significantly larger than that of the $1 \rightarrow 2$ transition. Therefore, as a result, the absorption rate ($B_{ij}U_{\nu}$) of the $1 \rightarrow 3$ transition is higher than

that of the $1 \rightarrow 2$ transition, and similarly, in the case where the excitation is by collisions plus radiation (red), the probability of exciting the molecule to level 3 is comparably larger than level 2. In addition, it is clear that in this case, the molecule is excited to levels above level 3 caused by collisional transitions.

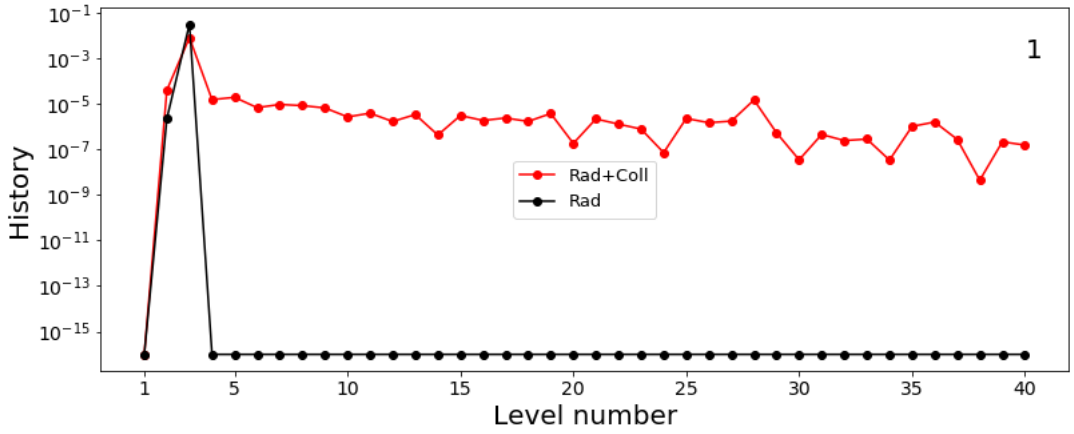

Figure 4.13: The history distribution of the H_2CO molecule, when radiative excitations dominate (black), and radiation plus collision (red) excitations dominate for the first interaction.

For the second interaction (Figure 4.14), in the case of radiative excitation only (black), the molecule can be excited from level 3 to level 5 with the probability of 2.5×10^{-2} or to level 15 with the probability of 2.3×10^{-5}, which is the lowest level of the K_3 ladder, and can similarly be excited from level 2 to level 4 with the probability of 1.1×10^{-5}. The molecule can also be de-excited to level 1, from level 2 or level 3. The probability of being excited into level 5 is significantly higher than into level 4. In the case of radiation plus collision, the molecule follows a similar trend, except that the molecule is excited to other levels, with the chance of being collisionally excited.

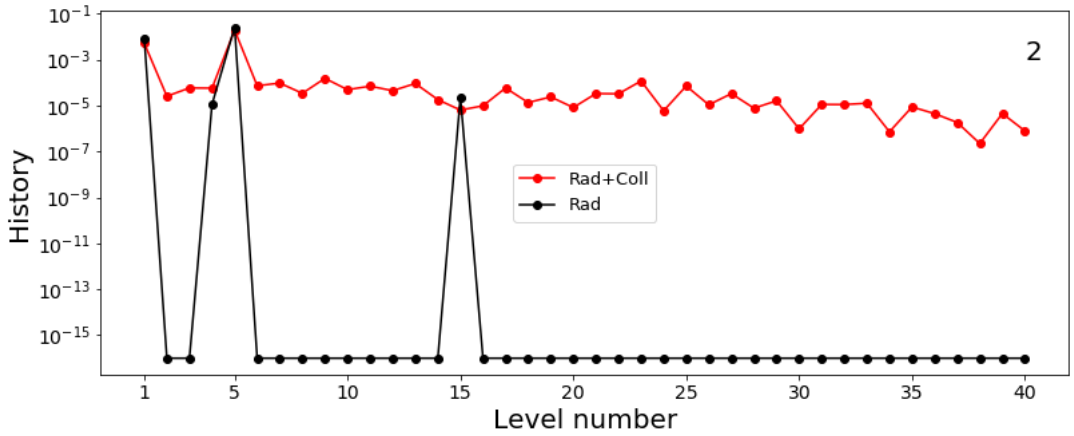

Figure 4.14: The history distribution of the H_2CO molecule, when radiative excitations dominate (black), and radiation plus collision (red) excitations dominate for the second interaction.

For the third interaction, in the case of radiation only (black), the molecule is excited from either level 4 or 5 to level 6 or 7 with a probability of 7.1×10^{-5} and 4.7×10^{-2}, respectively (illustrated in Figure 4.15), or the molecule is excited to levels 16 or 18 with a probability of 5.8×10^{-6} and 4.0×10^{-5} from levels 4 and 5, respectively. As can be seen, the probability of exciting to level 6 or 7 is much larger compared to level 16 or 18. The molecule can be de-excited to level 3 from level 5 or to level 2 from level 4; note that the $3 \rightarrow 1$ transition consists of a large probability compared to $2 \rightarrow 1$. This is because the spontaneous rate is larger due to the large A-coefficient for the $3 \rightarrow 1$ transition than that of $2 \rightarrow 1$. Also, the frequency of the $3 \rightarrow 1$ transition is larger than that of the $2 \rightarrow 1$ transition. The energy density function increases with frequency, thus increasing the rate of downward stimulated transition. In the case of radiation plus collisions (red), the probability of exciting the molecule to level 7 and de-excitation to level 3 is larger than all the transitions. This shows the effects of a strong radiation field; irrespective of that, there is a large probability of exciting the molecule to all energy levels. The radiative excitations dominate for level 7 and 3. Notice that the energy levels with large probabilities in the case of radiation plus collisions (red) are the same as those in the case of radiation only (black).

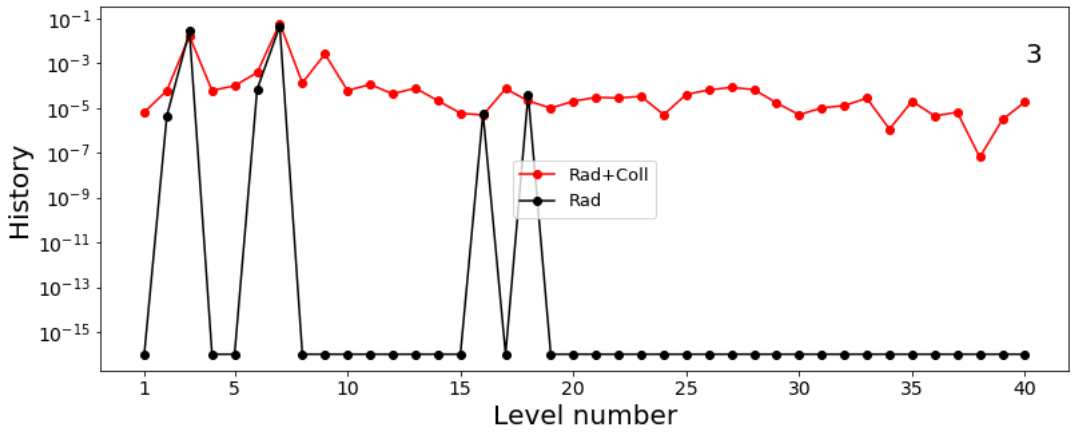

Figure 4.15: The history distribution of the H_2CO molecule, when radiative excitations dominate (black), and radiation plus collision (red) excitations dominate for the third interaction.

In Figure 4.11, it is easy to trace the molecule from the 1st to the 6th interaction. Considering the dipole selection rules, in the case of radiation only (black), it is clear that the excitation of the molecule to the $1, 3, 5, 7, 9...$ levels consists of larger probabilities compared to the $2, 4, 6, 8...$ levels. However, tracing the molecule from the eighth to the tenth interaction is difficult. Similar to the '10th to 100th' interactions in the steps of 10, as shown in Figure 4.16, the distribution converges, and it becomes complex to trace where the molecule transitioned after each interaction.

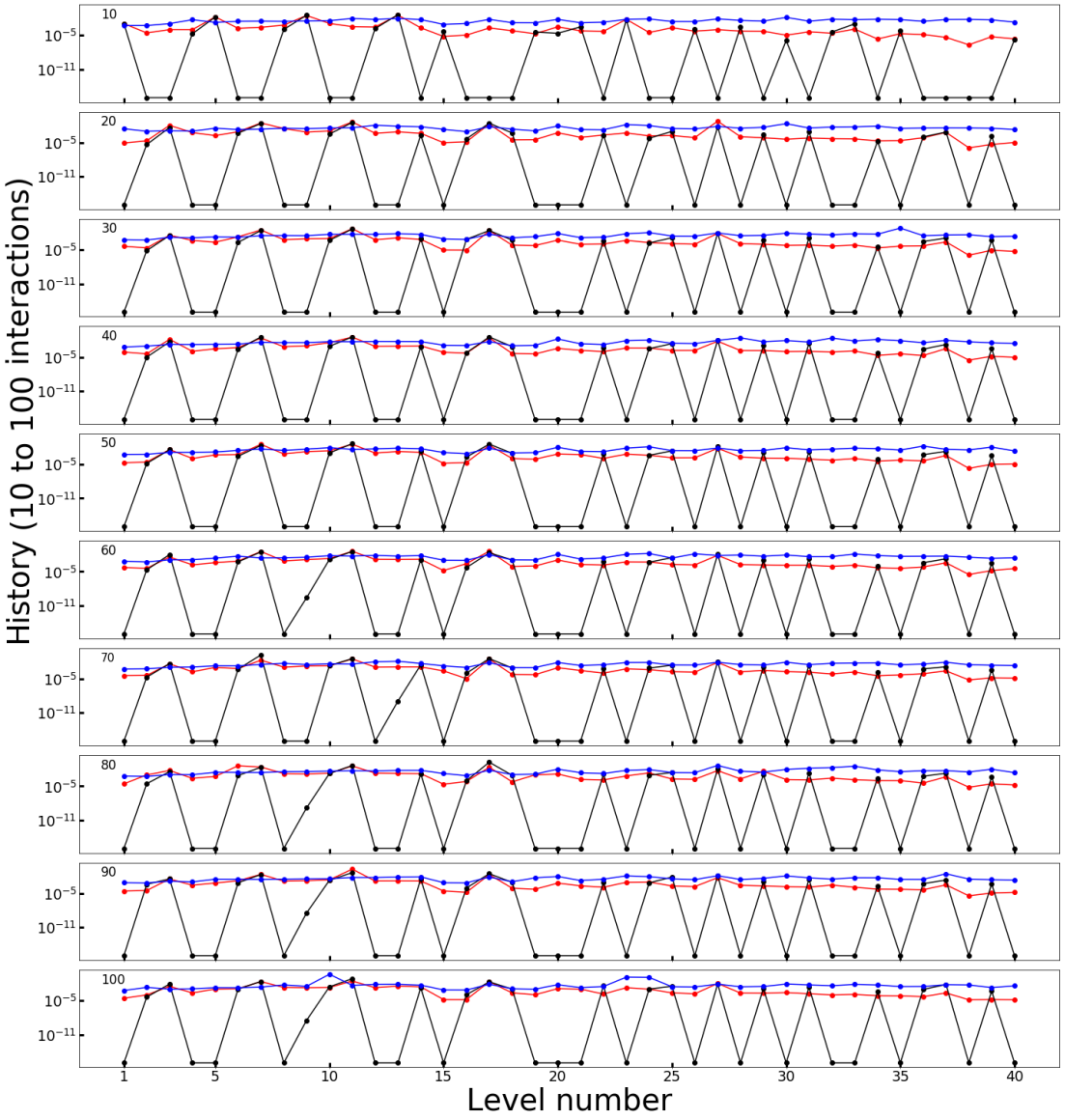

Figure 4.16: The history evolution of a molecule after 10 to 100 interactions when the excitation is only collisional (blue), only radiatively (black), and when both radiation and collisions are considered as the excitation (red).

In the case of radiation only (black), it is clear to see the possibility of how the molecule transitions for the first six interactions. Comparing the radiation-only case (black) and the case of radiation plus collisions (red), the history of the molecule is understood when excited by radiation only (black). Therefore, the effects of collisional excitation can be identified in the case of radiation plus collisions (red). The probability of exciting the molecule via radiation plus collision (red) is almost equal to that of exciting the molecule via radiation only (black). This shows that the probability of exciting the molecule via collisions in the case of radiation plus collisions (red) is significantly smaller than that of radiation. Studying Figures 4.11 and 4.16, the effects of collisions can be seen; this, however, is not sufficient to conclude the roles of the excitation process. An alternative approach, therefore, is introduced to study these transitions from a different point of view.

In the second and alternative approach, the number of interactions is fixed at 10^8. This approach determines the role of each excitation process by studying the distribution of the number of visits over all energy states. The objective in constructing the Monte Carlo simulation code is: if the molecule is in a specific known energy level, e.g. energy level 1, where would the molecule transition to, and through which process would the molecule be excited out of level 1? Figure 4.17 and 4.18 summarise a few possible transitions when the molecule is excited out of the current level, as indicated in each panel. The blue bars represent the number of visits via radiation plus collisions excitation process. The red dots represent the number of visits where the molecule is excited into various energy levels via radiation only, and the black dots represent the number of visits where the molecule is excited via collisions only.

The number of visits from a known energy level for a single transition is calculated and repeated for 10^8 interactions, thus determining how often the molecule visits any of the other 39 levels. An energy level with a large number of visits indicates a high chance of the molecule transitioning into the energy level; an energy level with fewer visits signifies a small likelihood of that transition. The energy level with the largest number of visits is, thus, manually selected as the energy level wherein the molecule is most likely to be found after the interaction; subsequently, the same calculation is performed for the selected energy level. As shown in Figure 4.17: in the top left panel, for a molecule in level 1 (i.e. the current level is 1), level 3 has the largest number of visits; therefore, it is most likely for the molecule to transition to level 3. Level 3 is thus manually selected as the current level, and the number of visits from the current level is calculated for 10^8 interactions as shown in the top right panel. The molecule, therefore, will most likely transition to level 5 or back to the ground state. Subsequently, in the second top left panel, when the molecule is in level 5, it is most likely to make a transition to level 7 or level 3 and so on. Following the excitation process explained above, the calculations propose that if a molecule is excited from the ground state into energy level 3, the succeeding radiative excitations and de-excitations (red) trap the molecule between the lower levels of the doublet states; thus, following the $1 \leftrightarrow 3 \leftrightarrow 5 \leftrightarrow 7...$ transition path.

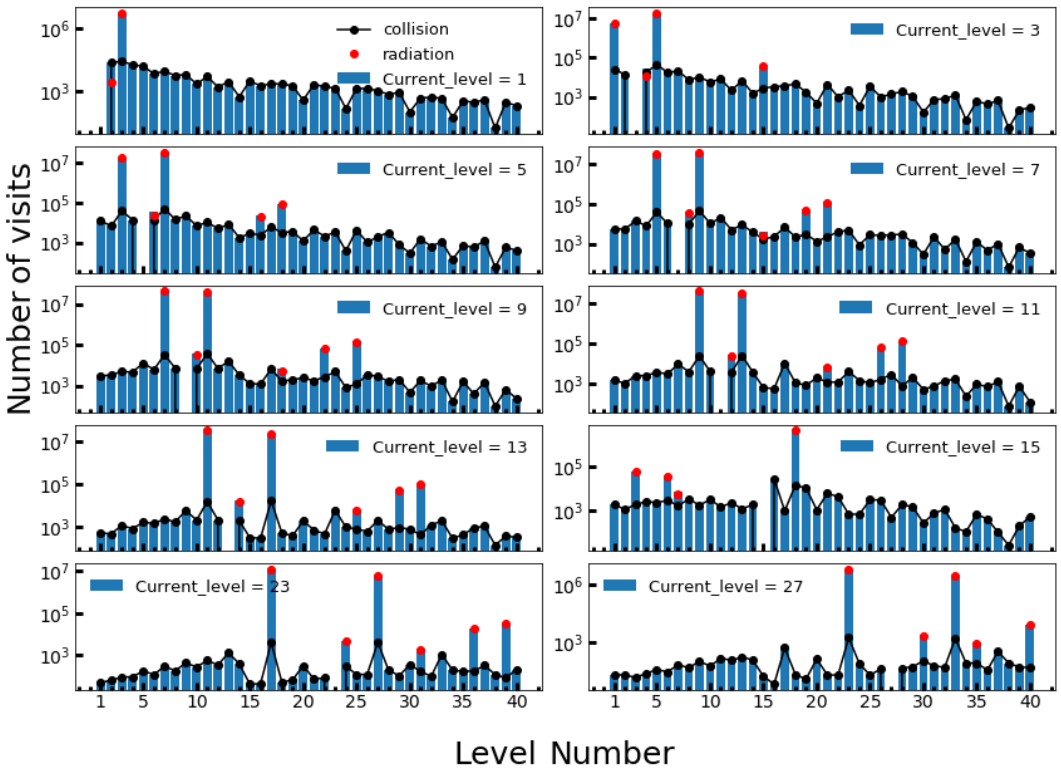

Figure 4.17: The bar graph shows the number of visits the molecule makes to 39 energy levels directly from a current level. The molecule is followed, as it is excited between lower levels of the doublets according to the probabilities of radiative and collisional excitations.

For the same number of interactions, the number of visits from level 1 to level 3 is larger than that to level 2; this confirms that the likelihood of making the $1 \rightarrow 3$ transition is larger than that of the $1 \rightarrow 2$ transition. In Figure 4.18, Level 2, however, is manually chosen as the current level (top right panel) in this calculation, to get the idea of how the successive excitations of the molecule look like. It can be seen that level 4 has the largest number of visits; therefore, it is most likely for the molecule to transition to level 4 or the ground state. Energy level 4 is thus manually selected as the current level, as shown in the second top left panel, and thus, the molecule is most likely to transition to level 6 or level 4. Subsequently, when the molecule is in level 6 (second top right panel), it is most likely to transition to level 8 or 6 and so on. The calculations propose that if a molecule is excited from the ground state into energy level 2, the succeeding radiative excitations and de-excitations (red) trap the molecule between the upper levels of the doublets, thus, following the $1 \leftrightarrow 2 \leftrightarrow 4 \leftrightarrow 6...$ transition path.

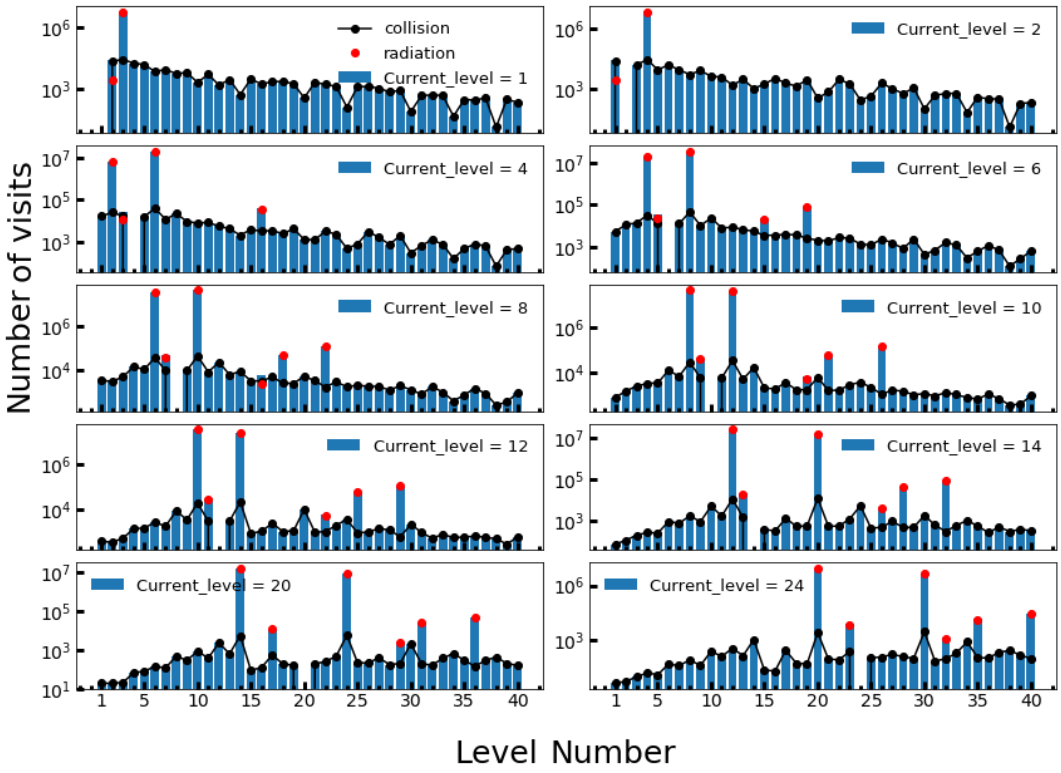

Figure 4.18: The bar graph shows the number of visits the molecule makes to 39 energy levels directly from the current level. The molecule is followed as it is excited between upper levels of the doublets according to the probabilities of radiative and collisional excitations.

Since the $1 \rightarrow 3$ transition is more likely to occur than the $1 \rightarrow 2$, it can then be argued that the $1 \leftrightarrow 3 \leftrightarrow 5 \leftrightarrow 7...$ transition path is the more likely followed path while the $1 \leftrightarrow 2 \leftrightarrow 4 \leftrightarrow 6...$ transition path is the least likely followed path. Note, even though the latter path is the least followed path, the number of visits in the upper levels of the doublet states is approximately as large as the number of visits in the lower levels. On the other hand, since collisional excitations do not follow the dipole selection rules, the collisions can excite or de-excite the molecule to any of the 39 levels.

As previously mentioned, when the molecule is excited into level 3, the succeeding excitations follow the former path; when the molecule is excited into level 2, the succeeding

excitations follow the latter path. It is as if the molecule gets "trapped" in either of the radiative transition paths, with a lower likelihood of radiatively transferring the molecule between the two paths. Collisions, however, are more likely to transfer the molecule between the two paths.

For example, when the current level is 3 (the molecule is in level 3). Radiatively, the molecule can only be excited to level 4 to be transferred to the least followed path. Collisionally, the molecule can be excited to levels 2, 4, 6, 8, 10 and more, thus increasing the likelihood of transferring the molecule collisionally. Despite the notably low chances of making collisional visits, it is noted that the transfer between the lower and upper levels of the doublet states (two paths) is more likely to occur via collisions than radiatively. It can then be argued that the role of radiative excitation is to excite and de-excite the molecule through a specific path, and the role of collisional excitations is to transfer the molecule between the abovementioned radiative paths.

4.4.4 The Effects of Change in the SED of the Dust Emission

A follow-up investigation was performed, and the effect of changing the dust emission's spectral energy distribution (SED) and how it affects the excitation processes was studied. The SED is given by $F_\nu = (\frac{\nu}{\nu_0})^p B_\nu(T_d)$, and the shape is determined by the index p. Figure 4.19 compares SED when $p = 0.5$, $p = 1.0$ and $p = 2.0$. The physical parameters, $T_d = 100$ K, $T_k = 180$ K, $n_{H_2} = 10^{4.25}$ cm^{-3} are fixed for all three cases, and the SCD is given to be 2.159×10^{17} m^{-3} s for $p = 0.5$, 7.304×10^{16} m^{-3} s for $p = 1.0$ and 1.233×10^{17} m^{-3} s for $p = 2.0$. The fiducial frequency ν_0 was taken as 3×10^{12} Hz for all cases. The SED was plotted for all radiative transitions for 40 levels. The lower frequencies ($< 10^9$ Hz) are not plotted, and higher frequencies above 10^{12} Hz were disregarded since they would not affect the transitions. Only cases when $p = 0.5$ and $p = 2.0$ are studied in more detail, and the case when $p = 1.0$ was used for comparing the SED's. Notice that the SED of $p = 0.5$ is flatter than the SED when $p = 1.0$ and steeper when $p = 2.0$; thus, the change in p affects the shape of the energy density of the radiation field. Figure 4.20 shows the plot of the radiation field's total energy density given by Equation 4.5, which is given by the sum of internal and external radiation field for $p = 0.5$, $p = 1.0$ and $p = 2.0$ for allowed radiative transitions. The energy density for $p = 0.5$ is larger than that of $p = 2.0$ across all frequencies.

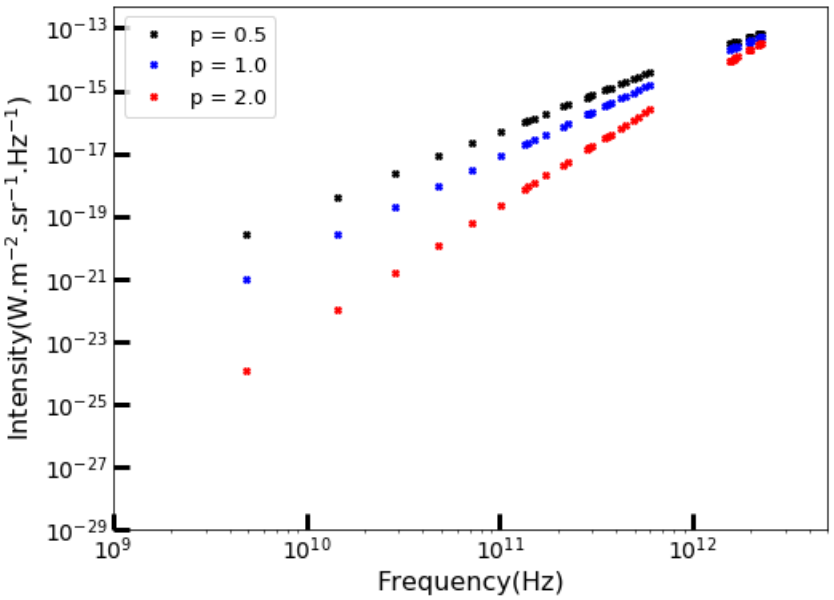

Figure 4.19: Comparison of undiluted SED's for different indices: $p = 0.5$ (black), $p = 1.0$ (blue) and $p = 2.0$ (red).

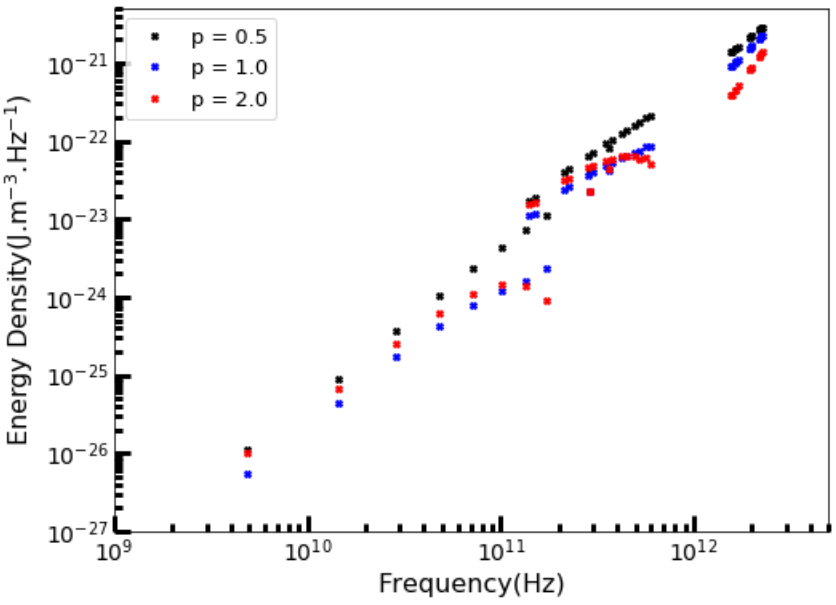

Figure 4.20: The energy density of the total radiation field according to Equation 4.5 with geometric dilution factor $W = 1$ and different indices: $p = 0.5$ (black), $p = 1.0$ (blue) and $p = 2.0$ (red).

Thus, the effect of the SED variation on the total energy density is now clear. Following that, the goal is to study the effect of the energy density on the distribution of the holding time and the number of visits. In Figure 4.21, the top panel compares the holding time distribution, and the bottom panel compares the distribution of the number of visits of the two cases. It is expected that due to the larger energy density when $p = 0.5$ than when $p = 2.0$, the two abovementioned distributions are larger when $p = 0.5$ than when $p = 2.0$.

However, Figure 4.21 shows that for lower energies, the holding times in the case of $p = 2.0$ is larger than when $p = 0.5$, and as the energy increases, the case of $p = 0.5$ increases above the case when $p = 2.0$. The reason for this different behaviour is that the total energy density is not only due to the SED but results from the sum of the internal and external radiation fields. The internal radiation field, therefore, is responsible for this behaviour. Note that the total radiation field is in equilibrium with the level population. Now, since the total energy density in the case of $p = 2.0$ is smaller, the molecule spends more time into the lower energies than when $p = 0.5$, with the low likelihood of exciting the molecule to higher energies. On the other hand, for $p = 0.5$, the total energy density is larger, and the molecule can be excited to higher energies and spend a fairly more amount of time in the upper levels compared to the case of $p = 2.0$. Furthermore, this means the number of visits is larger for $p = 2.0$ than $p = 0.5$ in lower energies, and as the energy increases, the number of visits for $p = 0.5$ increases above $p = 2.0$. This clearly shows that the transitions of a molecule depend on the behaviour of the SED.

In Figures 4.22 and 4.23, for 10^8 interactions, the number of visits to level 3 from the ground state radiatively (red) or via radiation plus collisions (blue) is $\approx 7 \times 10^6$ for $p = 2.0$ and $\approx 1 \times 10^6$ for $p = 0.5$. The number of visits collisionally to level 3 for $p = 2.0$ and $p = 0.5$ is $\approx 2 \times 10^4$ and $\approx 6 \times 10^3$, respectively. When the current level is 3, the number of visits to level 5 radiatively (red) or via radiation plus collisions (blue) is $\approx 2 \times 10^7$ and $\approx 7 \times 10^6$, for $p = 2.0$ and $p = 0.5$, respectively. Collisionally, the number of visits is $\approx 4 \times 10^4$ and $\approx 1 \times 10^4$ for $p = 2.0$ and $p = 0.5$, respectively. The number of visits is larger for $p = 2.0$ than for $p = 0.5$, as expected. Though the change in values is significant, the general behaviour remains the same for both cases, i.e. the role of each excitation process does not change. Radiatively, the molecule still follows a specific path, which is either $1 \leftrightarrow 3 \leftrightarrow 5 \leftrightarrow 7...$ or $1 \leftrightarrow 2 \leftrightarrow 4 \leftrightarrow 6...$ paths. On the other hand, collisions excite the molecule to all levels, potentially causing the molecule to deviate from the path followed by radiative transitions.

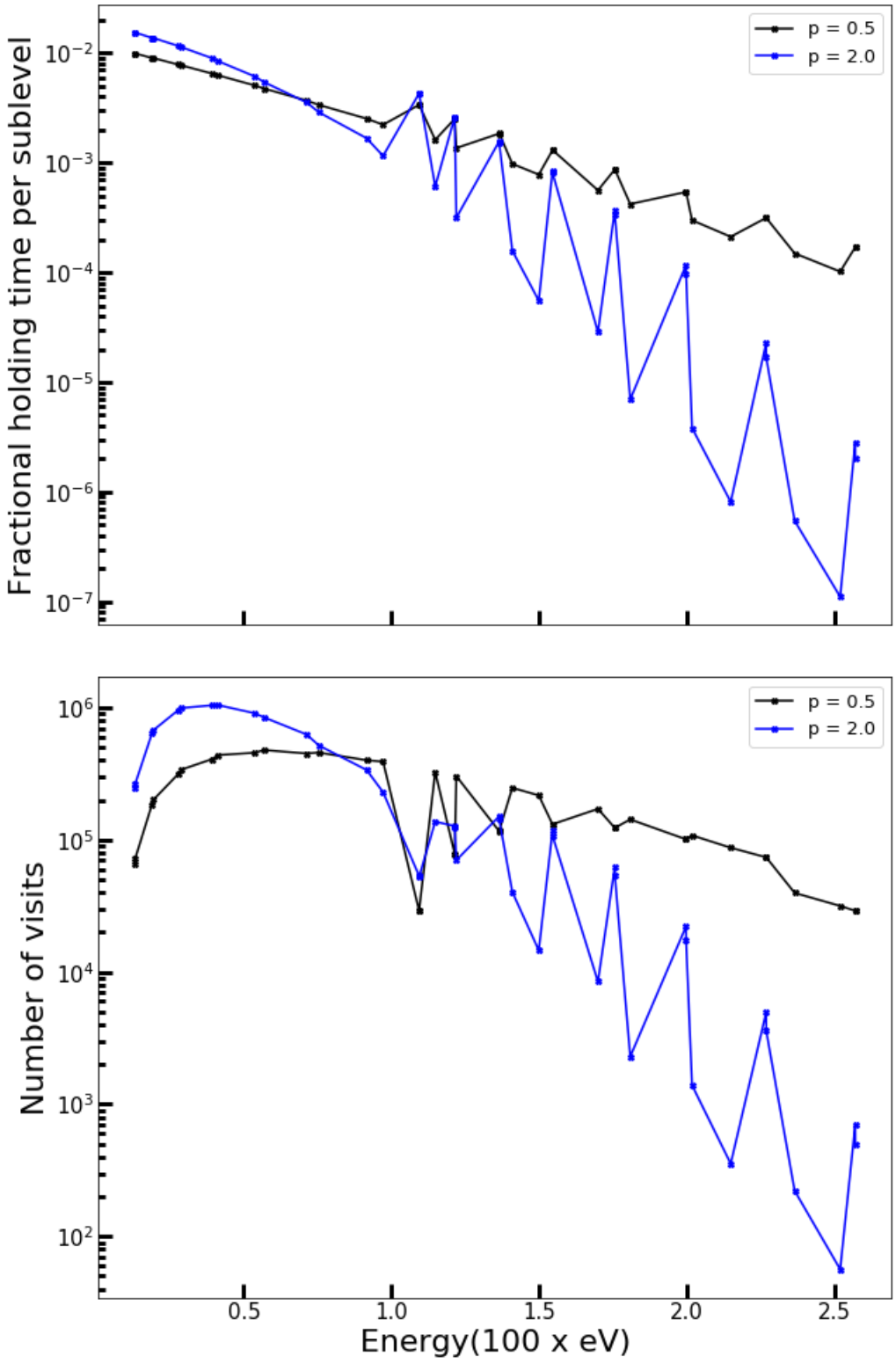

Figure 4.21: The top panel shows the holding time distributions, and the bottom panel shows the distribution of the number of visits whereby the shape of the SED is varied: $p = 0.5$ (black) and $p = 2.0$ (blue).

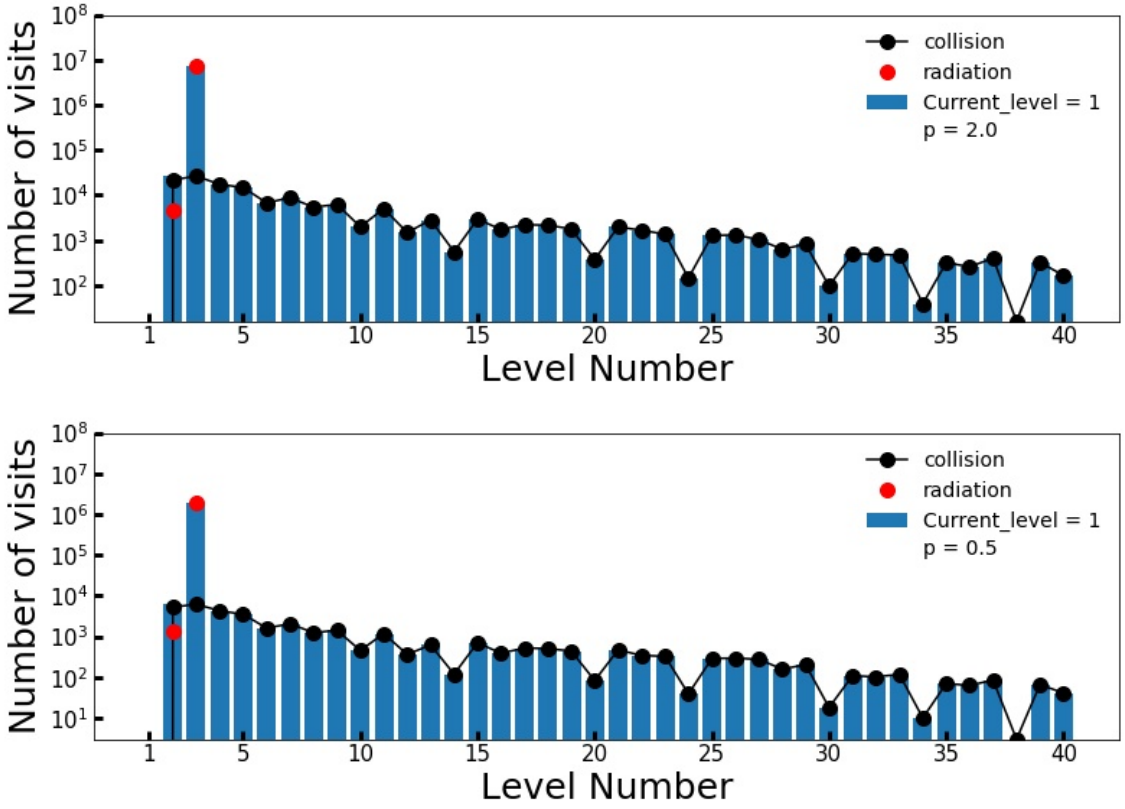

Figure 4.22: The bar graph shows the number of visits the molecule makes to 39 energy levels directly from level 1. The top panel is for $p = 2.0$, and the bottom panel is for when $p = 0.5$.

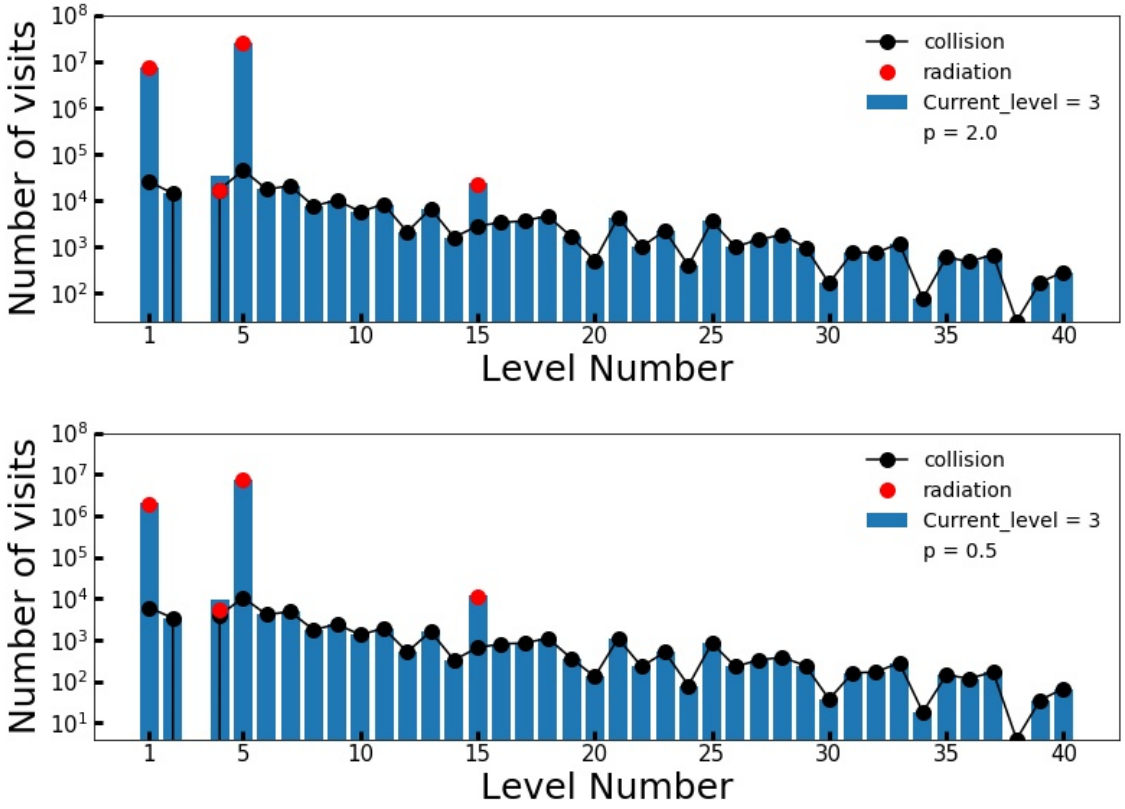

Figure 4.23: The bar graph shows the number of visits the molecule makes to 39 energy levels directly from level 3. The top panel is for $p = 2.0$, and the bottom panel is for when $p = 0.5$.

4.5 Evaluation of the Results of Baan et al. (2017).

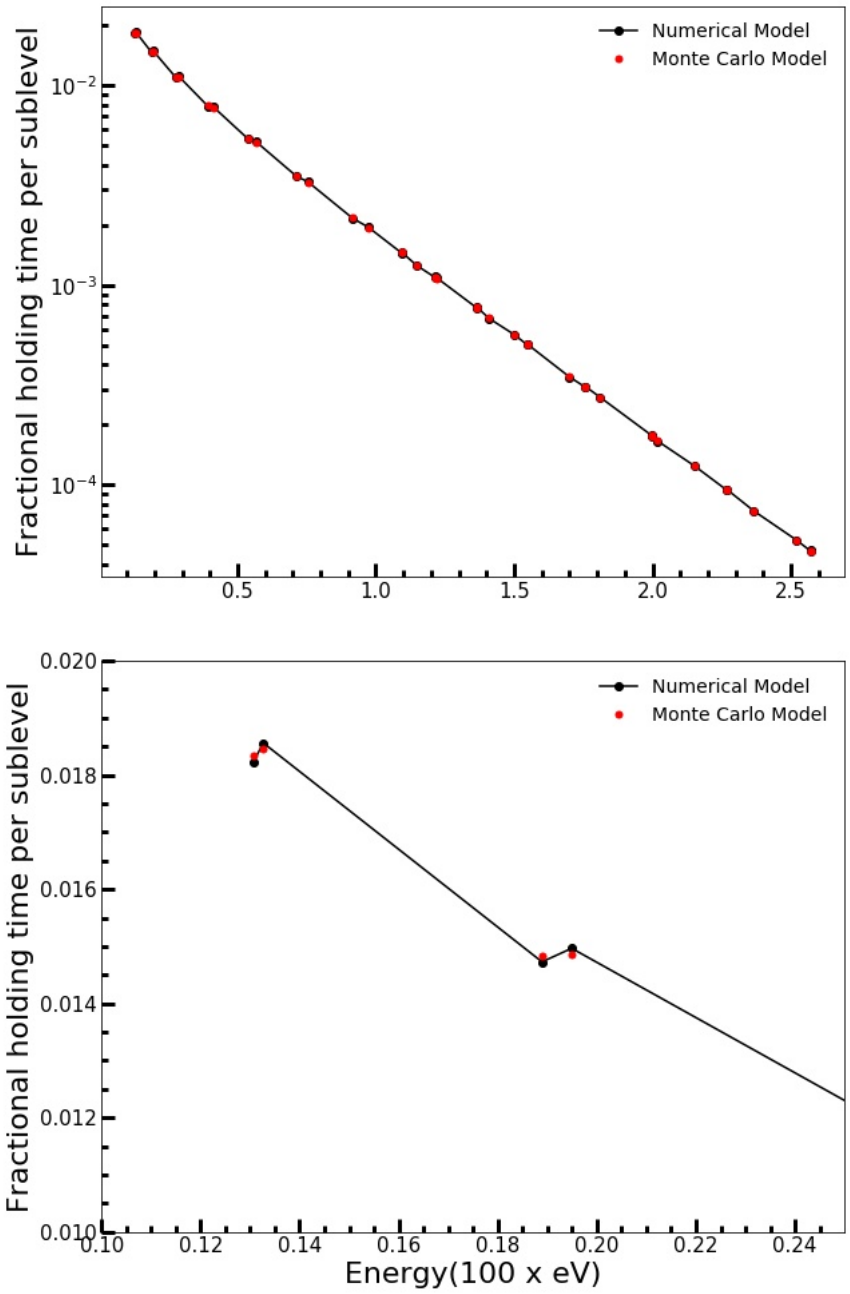

Figure 4.24: Comparing the holding time distribution (red) and the level population distribution (black) of the H_2CO molecule. The top panel shows the distribution over the whole energy range for 10^8 interactions. The bottom panel presents the first four energy states of the distribution above the ground state less than 0.0024 eV. The physical parameters are $T_k = 10$ K, $T_d = 50$ K, the SCD $= 4.699 \times 10^{16}$ cm^{-3} s , $n_{H_2} = 10^4$ cm^{-3}, W = 1 and p = 0.

Baan et al. (2017) used the online version of RADEX to make the calculations to study the H_2CO maser, using the parameter values $T_d = 50$ K and $T_k = 10$ K and $n_{H_2} = 10^4$ cm^{-3}. These authors concluded that the maser is pumped radiatively. It is important to

note that the dust radiation field used in RADEX is an unshielded blackbody radiation field. van der Walt and Mfulwane (2022) studied this case and showed that it was possible to achieve inversion under these conditions. Once more, this case is evaluated using the Monte Carlo simulation code, and an inversion is reproduced, as shown in Figure 4.24. Since the fractional holding time is equivalent to the level population distribution, the bottom panel shows that the fractional holding time of the second energy state is larger than that of the first energy state. Therefore, this implies there is population inversion since the second energy state is more populated than the first energy state. As argued by (van der Walt and Mfulwane, 2022), for $T_k = 10$ K the system is not in TE which allows for the possibility of inversion.

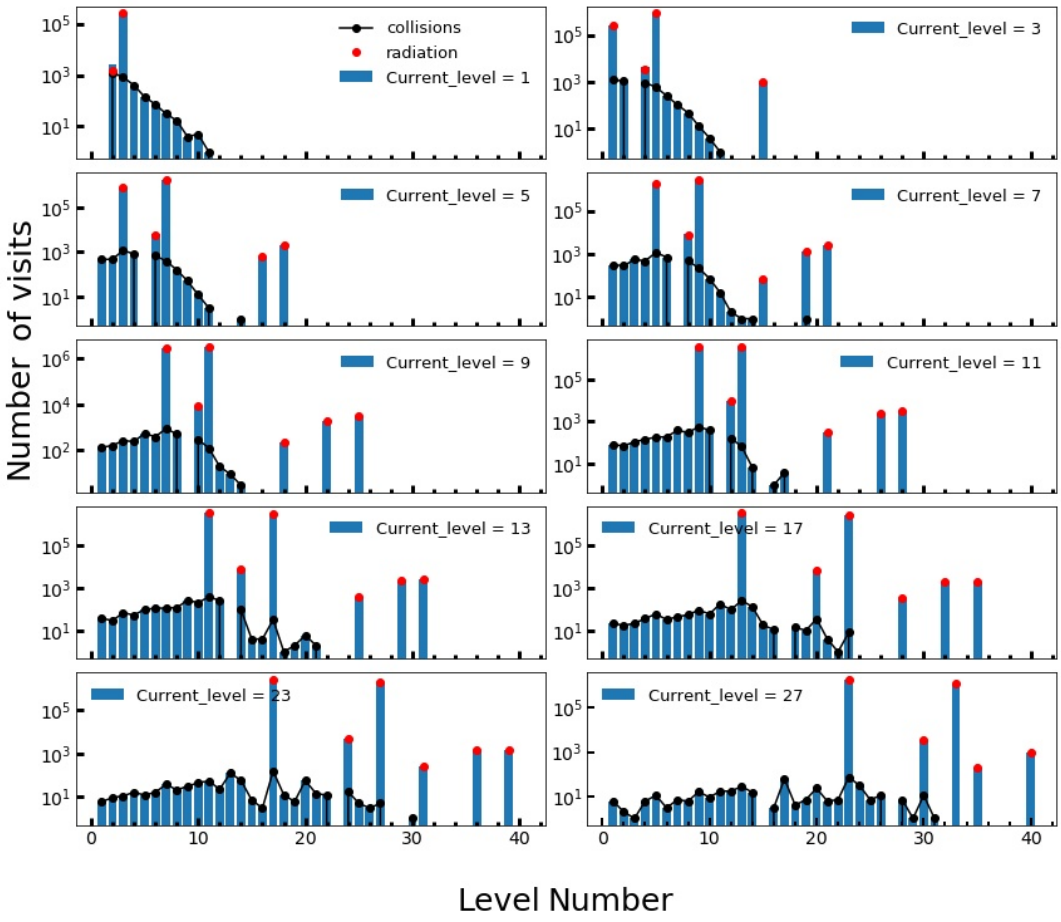

Figure 4.25: The bar graph shows the number of visits that the molecule makes to 39 energy levels directly from a current level for the Baan et al. (2017) case. The molecule is followed as it is excited between lower levels of the doublets according to the probabilities of radiative and collisional excitations.

Now that the inversion can be reproduced, the transitions of the molecule in this parameter space can be studied. Figure 4.25 summarises possible transitions when the molecule is

excited out of the current level. The number of visits via collisions is larger when the molecule is excited from any of the lower levels than when it is excited from any of the upper levels, i.e. when the molecule is in level 3 (current level equals 3), the largest number of visits collisionally go up to $\approx 1 \times 10^3$. When the molecule is in level 27, the largest number of visits collisionally goes up to $\approx 1 \times 10^1$. The number of visits via radiative excitation is larger than that via collisional excitations. Therefore, radiative excitations from the current level still have a higher chance of following the $1 \leftrightarrow 3 \leftrightarrow 5 \leftrightarrow 7...$ route than the $1 \leftrightarrow 2 \leftrightarrow 4 \leftrightarrow 6...$ route, a graph summary of the latter transitions is not shown here. Because of low kinetic temperature ($T_k = 10$ K), the molecule is not excited collisionally to all energy levels but to few compared to radiative excitations.

From Figure 4.25, radiative excitations excite the molecule upward following one of the abovementioned paths, i.e. the $1 \leftrightarrow 3 \leftrightarrow 5 \leftrightarrow 7...$ path, which is the more likely followed path. Radiatively, the molecule can be transferred to the least likely followed path by being excited to just one level. For example, when the molecule is in level 3 (top right panel), it can only be excited into level 4, while collisionally, the molecule can be excited into fewer levels, such as levels 2, 4, 6, 8 and 10. Notice that when the excitation of the molecule occurs between the levels above level 3, i.e. levels 5, 7, 9, 11, 13 and 17, the radiative number of visits to the levels of the least followed path (i.e. the upper levels of the doublet states) is significantly larger than the corresponding collisional number of visits. However, since the molecule visits one level radiatively, while collisionally, the molecule visits a few levels, the molecule is more likely to be transferred collisionally than radiatively. Increasing the kinetic temperature increases the likelihood of collisionally exciting the molecule to more levels. However, since the radiation field used is that of an undiluted black body, the population inversion will become weaker when T_k approaches T_d and destroyed when $T_k = T_d$ due to the system approaching thermodynamic equilibrium. It can be argued that radiative excitations play a role in exciting and de-exciting the molecule following a path. On the other hand, collisional excitations play a role in transferring the molecule between the abovementioned radiative paths.

Chapter 5

Discussion and Conclusion

5.1 Discussion

Figure 4.11 shows that in the case of radiation-only, the history of the molecule can be traced up to the sixth interaction. The molecule's transitions follow the dipole selection rules. From the seventh up to the 100th interaction, as shown in Figure 4.16, tracing the molecule for the rest of the interactions becomes somewhat complicated because the distributions converge to the same distribution. It is seen that when collisions are included, the molecule makes transitions between all levels. It was unclear what the roles of each excitation process were in exciting the molecule and what the pumping scheme could be. It was, however, evident that including collisions with radiation had a huge effect on the excitation of the molecule. By visual inspection, comparing the case of radiation only and the case of radiation plus collisions, the probabilities are comparable; therefore, this implies the collisional transitions are significantly smaller than the radiative transitions. Because of the limited information, the second approach was introduced to work out the pumping scheme of the H_2CO maser.

In the second approach, the results are shown in Figures 4.17 and 4.18. Each panel represent a single transition from the current level to any level repeated for 10^8 interactions, and the number of visits in each level is calculated. The level with a large number of visits implies a high chance of the molecule transitioning into that level. The molecule is more likely to transition into that level than any other for a single interaction. The lower number of visits means that the chance of the molecule visiting that level is very low or zero for a single interaction.

Figure 4.17 shows that the radiative transitions dominate over collisional transitions following $1 \leftrightarrow 3 \leftrightarrow 5 \leftrightarrow 7 \leftrightarrow 9...$ transition path, which occurs between the lower levels of the doublet states. Similarly, Figure 4.18 shows that the radiative transitions dominate following $1 \leftrightarrow 2 \leftrightarrow 4 \leftrightarrow 6 \leftrightarrow 8...$ transition path, which occurs between the upper levels of the doublet states. Inspecting the number of visits and taking into consideration the

probabilities calculated in the first approach, it was argued that the former radiative transition path is the most followed path. Whereas the latter is the least followed path. The radiative transition between the two paths (between the doublets) rarely occurs because the coupling between the doublets is weak. It is, therefore, as if the molecule gets trapped in either of the paths. However, the collisional transition between the paths occurs more often. This stems from the fact that there are more collisional visits between the paths than the radiative visits. Therefore, it can be argued that the role of radiative excitations is to excite and de-excite the molecule following a path, and the role of collisional excitations is to transfer the molecule between the paths, i.e. between the doublet states.

It has also been shown in Figures 4.22 and 4.23 that changing the shape of the undiluted external radiation field's SED changes the total radiation field, thus affecting the molecule's excitation. The molecule, however, behaves generally the same as in the case of a diluted radiation field, i.e. the roles of the excitation processes do not change. The aforementioned is similar to the case of Baan et al. (2017); the excitation of the molecule is affected, but the behaviour generally remains the same.

The pumping scheme is such that there is a path and an excitation process that the molecule follows out of the ground state. Thus, to create a population inversion for the $1-2$ transition, the rate of excitation out of level 1 should be larger than the rate at which level 2 is populated via downward transitions from upper energy levels. The radiative route the population follows from upper levels to populate level 2 is via the $10 \rightarrow 8 \rightarrow 6 \rightarrow 4 \rightarrow 2$ transition path. Considering that the most likely followed route for an upward transition from level 1 to upper levels is via $1 \rightarrow 3 \rightarrow 5 \rightarrow 7 \rightarrow 9...$ to create an inversion, a population should be transferred from the lower levels of the doublet states which are levels of the transition path above to the upper levels of the doublet states given by the levels of $1 \leftrightarrow 2 \leftrightarrow 4 \leftrightarrow 6 \leftrightarrow 8...$ transition path. The population is then radiatively de-excited via the $10 \rightarrow 8 \rightarrow 6 \rightarrow 4 \rightarrow 2$ transition path to populate level 2. It is noted that the transfer between the two radiative transition paths is more likely to occur collisionally than radiatively. In the absence of collisions, the population remain trapped in either of the radiative paths discussed above, and the population inversion is less likely to occur. The definition of a pumping process according to Elitzur (1992b) is the process in which, in its absence, the population inversion disappears. With this definition, it can, therefore, be concluded that the collisional process is the pumping process of H_2CO maser. Note that these results indicate that just because an excitation process dominates, it does not necessarily mean it is the process responsible for pumping the maser.

5.2 Conclusion

This work aimed to investigate the pumping scheme of the H_2CO maser, if the pumping mechanism is radiative or collisional, using the Monte Carlo simulation method. Multiple authors have reported on the pumping scheme and mechanism of this maser; however, it was still not understood. The results of this work conclude that the pumping mechanism

is collisional.

5.2.1 The Monte Carlo Simulation Method

The Monte Carlo simulation code was successfully implemented using the C programming language, and the molecular data was obtained from the LAMDA website for two distinct molecules: CS and H_2CO. The molecule of interest in this investigation is the H_2CO molecule, and the CS molecule is used to test the simulation method. Two tests conducted on the Monte Carlo simulation using a CS molecule proved the method reliable and accurate. The same tests were successfully repeated for the H_2CO.

The tests were performed for LTE and non-LTE conditions, and two distributions were constructed as a result: the holding time distribution and the distribution of the number of visits. The first test was done for LTE conditions, wherein it was found that the holding time distribution followed the Boltzmann distribution, whereas the distribution of the number of visits did not. The second test was carried out and accomplished for non-LTE conditions, and the holding time distribution constructed in this case was compared to the level population distribution produced by the Runge Kutta numerical method. These two distributions, therefore, showed an agreement with remarkable accuracy and the inversion between the first two levels. The holding time distribution confirmed that the Monte Carlo simulation produced the correct results, and even though the number of visit distribution did not reflect the desired results, it was likely that there is potential to learn from this distribution and that it could shed more light on determining the pumping mechanism of the H_2CO maser.

5.2.2 The Pumping Scheme of the H_2CO Maser.

To determine the pumping scheme, before anything else, it was necessary to understand the role of each excitation process. The molecule was allowed to perform a random walk between the energy levels according to the radiative and collisional probabilities to study the roles of collisional and radiative excitation processes. The molecule was followed for 100 interactions, and this process was repeated for 10^8 times under three different cases: the case where the molecule is excited by collisions only, radiation only and radiation plus collisions. However, the case of radiation only and radiation plus collisions are reported in detail.

After each interaction, the molecule is followed to determine which energy level it would be found in, as shown in Figures 4.11 and 4.16. In the case of radiative excitation only, the molecule's excitation follows the dipole selection rule. In the case of radiation plus collisions, there is a chance of the molecule being excited into all higher energy levels, and this is due to the effects of collisional excitation. The history of the molecule shows the probability of where the molecule might be excited but does not provide enough

information to conclude the precise role of the collisional and radiative excitation processes.

The second approach was successfully implemented to study the transitions of the molecule from a different view. The calculation was set so that the molecule starts from a known energy level "termed" the current level, allowing it to interact radiatively and collisionally with its surroundings. The molecule is excited from the current level to any level; each transition is repeated for 10^8, and the number of visits to each level is calculated. The excitation process which excites the molecule for each transition was determined.

After studying the results of this second approach, it was determined that radiatively, there are two possible paths that the molecule can follow, which are $1 \leftrightarrow 2 \leftrightarrow 4 \leftrightarrow 6...$ which is the least probable, and $1 \leftrightarrow 3 \leftrightarrow 5 \leftrightarrow 7...$ which is the most probable path. The former path is the transitions between the upper levels of the doublets, and the latter is between the lower levels of the doublets. Collisional excitations, on the other hand, do not follow any path and have a significantly higher likelihood of exciting the molecule between the doublets compared to the corresponding radiative transitions. The implication is that collisions are responsible for the transfer of the molecule between the paths mentioned above, and radiation is responsible for the upward excitation of the molecule.

An additional investigation was necessary to test whether the roles mentioned might change under different conditions. The first test was to change the shape of the SED. The second test was to use the same set of parameter values used by (Baan et al., 2017). The tests show that the excitation of the molecule is affected; however, the general behaviour of the molecule remains the same. Therefore, the roles of the excitation processes do not change. Once the roles of the collisional and the radiative excitation processes were established, the pumping mechanism was concluded to be collisional.

Bibliography

Araya, E., Baan, W. A., and Hofner, P. (2004a). Studies of Extragalactic Formaldehyde and Radio Recombination Lines. *APJS*, 154(2):541–552.

Araya, E., Hofner, P., Goss, W. M., Kurtz, S., Linz, H., and Olmi, L. (2006). A New Galactic 6 cm Formaldehyde Maser. *APJL*, 643(1):L33–L36.

Araya, E., Hofner, P., Kurtz, S., Linz, H., Olmi, L., Sewilo, M., Watson, C., and Churchwell, E. (2005). Discovery of an H_2CO 6 Centimeter Maser in IRAS 18566+0408. *APJ*, 618(1):339–343.

Araya, E., Hofner, P., Linz, H., Sewilo, M., Watson, C., Churchwell, E., Olmi, L., and Kurtz, S. (2004b). A Search for H_2CO 6 Centimeter Emission toward Young Massive Stellar Objects. *APJS*, 154(2):579–584.

Araya, E., Hofner, P., Sewiło, M., Linz, H., Kurtz, S., Olmi, L., Watson, C., and Churchwell, E. (2007). First Detection of an H_2CO 6 cm Maser Flare: A Burst in IRAS 18566+0408. *APJL*, 654(1):L95–L98.

Araya, E. D., Hofner, P., Goss, W. M., Linz, H., Kurtz, S., and Olmi, L. (2008). A Search for H_2CO 6 cm Emission toward Young Stellar Objects. III. VLA Observations. *APJS*, 178(2):330–338.

Araya, E. D., Olmi, L., Morales Ortiz, J., Brown, J. E., Hofner, P., Kurtz, S., Linz, H., and Creech-Eakman, M. J. (2015). Formaldehyde Masers: Exclusive Tracers of High-mass Star Formation. *APJS*, 221(1):10.

Baan, W. A., An, T., Klöckner, H.-R., and Thomasson, P. (2017). The emission structure of formaldehyde megamasers. *MNRAS*, 469(1):916–929.

Baan, W. A., Guesten, R., and Haschick, A. D. (1986). Formaldehyde Absorption and Maser Emission in Galaxies. *APJ*, 305:830.

Barrett, A. H., Schwartz, P. R., and Waters, J. W. (1971). Detection of Methyl Alcohol in Orion at a Wavelength of ~1 Centimeter. *APJL*, 168:L101.

Bartkiewicz, A. and van Langevelde, H. J. (2012). Masers in star forming regions. *Proceedings of the International Astronomical Union*, 8(S287):117–126.

Boland, W. and de Jong, T. (1981). A model for the formaldehyde maser near NGC 7538-IRS 1. *AAP*, 98(1):149–154.

Burke, B. F., Graham-Smith, F., and Wilkinson, P. N. (2019). *An Introduction to Radio Astronomy*. Cambridge University Press, 4 edition.

Caswell, J. L., Vaile, R. A., and Ellingsen, S. P. (1995). Variability of methanol masers. *PASA*, 12:37–53.

Chabrier, G. (2003). Galactic Stellar and Substellar Initial Mass Function. *PASP*, 115(809):763–795.

Chandler, C. J. (2005). Masers and Massive Star Formation. In Romney, J. and Reid, M., editors, *Future Directions in High Resolution Astronomy*, volume 340 of *Astronomical Society of the Pacific Conference Series*, page 317.

Chen, X., Shen, Z.-Q., Ellingsen, S. P., Li, X.-Q., Yang, K., Chen, H.-Y., and Dong, J. (2017). The Brightest Known H_2CO Maser in the Milky Way: G339.88-1.26. *APJL*, 851(1):L3.

Cheung, A. C., Rank, D. M., Townes, C. H., Thornton, D. D., and Welch, W. J. (1969). Detection of Water in Interstellar Regions by its Microwave Radiation. *NAT*, 221(5181):626–628.

Chui, M. F., Cheung, A. C., Matsakis, D., Townes, C. H., and Cardiasmenos, A. G. (1974). The Methanol Source in Orion at 1.2 Centimeters. *APJL*, 187:L19.

Downes, D. and Wilson, T. L. (1974). Formaldehyde Line Emission at 4.8 GHz Near NGC 7538. *APJL*, 191:L77.

Draine, B. (2010). *Physics of the Interstellar and Intergalactic Medium*. Princeton Series in Astrophysics. Princeton University Press.

Elitzur, M. (1992a). Astronomical masers. *ARAA*, 30:75–112.

Elitzur, M. (1992b). *Astronomical masers*, volume 170. Springer Dordrecht.

Emerson, D. (1998). *Interpreting Astronomical Spectra*. Wiley.

Fisz, M. (1965). *Probability theory and statistical inference*. John Wiley & Sons.

Forster, J. R., Goss, W. M., Wilson, T. L., Downes, D., and Dickel, H. R. (1980). A formaldehyde maser in NGC 7538. *AAP*, 84:L1–L3.

Gardiner, C. (2009). *Stochastic Methods: A Handbook for the Natural and Social Sciences*. Springer Series in Synergetics. Springer Berlin Heidelberg.

Ginsburg, A. and Goddi, C. (2019). First Detection of CS Masers around a High-mass Young Stellar Object, W51 e2e. *AJ*, 158(5):208.

Ginsburg, A., Walsh, A., Henkel, C., Jones, P. A., Cunningham, M., Kauffmann, J., Pillai, T., Mills, E. A. C., Ott, J., Kruijssen, J. M. D., Menten, K. M., Battersby, C., Rathborne, J., Contreras, Y., Longmore, S., Walker, D., Dawson, J., and Lopez, J. A. P. (2015). High-mass star-forming cloud G0.38+0.04 in the Galactic center dust ridge contains H_2CO and SiO masers. *AAP*, 584:L7.

Gray, M. (1999). Astrophysical masers. *Philosophical Transactions: Mathematical, Physical and Engineering Sciences*, 357(1763):3277–3298.

Guilloteau, S., Omont, A., and Lucas, R. (1987). A new strong maser : HCN. *AAP*, 176:L24–L26.

Harada, R., Onishi, T., Tokuda, K., Zahorecz, S., Hughes, A., Meixner, M., Sewiło, M., Indebetouw, R., Nayak, O., Fukui, Y., Tachihara, K., Tsuge, K., Kawamura, A., Saigo, K., Wong, T., Bernard, J.-P., and Stephens, I. W. (2019). Formation of high-mass stars in an isolated environment in the large magellanic cloud. *Publications of the Astronomical Society of Japan*, 71(2).

Henkel, C., Matthews, H. E., and Morris, M. (1983). SiS maser emission from IRC +10216. *APJ*, 267:184–190.

Highberger, J. L., Apponi, A. J., Bieging, J. H., Ziurys, L. M., and Mangum, J. G. (2000). Millimeter Observations of Vibrationally Excited CS toward IRC +10216: A New Circumstellar Maser? *APJ*, 544(2):881–888.

Hoffman, I. M., Goss, W. M., Palmer, P., and Richards, A. M. S. (2003). The Formaldehyde Masers in NGC 7538 and G29.96-0.02: Very Long Baseline Array, Multielement Radio-linked Interferometer Network, and Very Large Array Observations. *APJ*, 598(2):1061–1075.

Jones, A. P. (2001). Interstellar and circumstellar grain formation and survival. *Philosophical Transactions: Mathematical, Physical and Engineering Sciences*, 359(1787):1961–1972.

Kroupa, P. (2002). The Initial Mass Function of Stars: Evidence for Uniformity in Variable Systems. *Science*, 295(5552):82–91.

Kutner, M. and Thaddeus, P. (1971). 6-CENTIMETER Formaldehyde Absorption and Emission in the Orion Nebula. *APJL*, 168:L67.

Kwok, S. (2007). *Physics and Chemistry of the Interstellar Medium*. University Science Books.

Lada, C. J. (2005). Star Formation in the Galaxy: An Observational Overview. *Progress of Theoretical Physics Supplement*, 158:1–23.

Lada, C. J. and Lada, E. A. (2003). Embedded Clusters in Molecular Clouds. *ARAA*, 41:57–115.

Larson, H. (1974). *Introduction to probability theory and statistical inference*. John Wiley & Sons.

Madden, S. C., Irvine, W. M., Matthews, H. E., Brown, R. D., and Godfrey, P. D. (1986). New Interstellar Masers in Nonmetastable Ammonia. *APJL*, 300:L79.

Matzner, C. D. and McKee, C. F. (2000). Efficiencies of Low-Mass Star and Star Cluster Formation. *APJ*, 545(1):364–378.

Mckee, C. and Ostriker, E. (2007). Theory of star formation. *Annual Review of Astronomy and Astrophysics*, 45.

Mehringer, D. M., Goss, W. M., and Palmer, P. (1994). New Formaldehyde Masers in Sagittarius B2. *APJ*, 434:237.

Pratap, P., Menten, K. M., and Snyder, L. E. (1994). Detection of Formaldehyde Maser Emission near the Ultracompact H II Region G29.96-0.02. *APJL*, 430:L129.

Reichl, L. (1980). *A Modern Course in Statistical Physics*. University of Texas Press.

Reid, M. J. and Menten, K. M. (1990). A Subarcsecond H 2O Maser Shell Surrounding a Variable Star. *APJL*, 360:L51.

Rybicki, G. B. and Lightman, A. P. (1979). *Radiative processes in astrophysics*. Wiley-VCH.

Salpeter, E. E. (1955). The Luminosity Function and Stellar Evolution. *APJ*, 121:161.

Snyder, L. E. and Buhl, D. (1974). Detection of Possible Maser Emission Near 3.48 Millimeters from an Unidentified Molecular Species in Orion. *APJL*, 189:L31–L33.

Tafalla, M. (2011). Molecular abundances in star-forming regions. In Zapatero Osorio, M. R., Gorgas, J., Maíz Apellániz, J., Pardo, J. R., and Gil de Paz, A., editors, *Highlights of Spanish Astrophysics VI*, pages 442–453.

Taylor, H. and Karlin, S. (1984). *An introduction to stochastic modeling*. Academic Press, Inc.

van der Tak, F. F. S., Black, J. H., Schöier, F. L., Jansen, D. J., and van Dishoeck, E. F. (2007). A computer program for fast non-LTE analysis of interstellar line spectra. With diagnostic plots to interpret observed line intensity ratios. *AAP*, 468(2):627–635.

van der Walt, D. J. (2014). Pumping of the 4.8 GHz H_2CO masers and its implications for the periodic masers in G37.55+0.20. *AAP*, 562:A68.

van der Walt, D. J., Ginsburg, A., and Goddi, C. (2021). On the pumping of the CS($\upsilon = 0$) masers in W51 e2e. *MNRAS*, 501(3):3871–3882.

van der Walt, D. J. and Mfulwane, L. L. (2022). Revisiting the formaldehyde masers. *AAP*, 657:A63.

van Dishoeck, E. F. and Blake, G. A. (1998). Chemical evolution of star-forming regions. *Annual Review of Astronomy and Astrophysics*, 36(1):317–368.

Weinreb, S., Barrett, A. H., Meeks, M. L., and Henry, J. C. (1963). Radio Observations of OH in the Interstellar Medium. *NAT*, 200(4909):829–831.

Whiteoak, J. B. and Gardner, F. F. (1983). 4.8-GHz H2CO maser emission in SGR B2. *MNRAS*, 205:27P–32.

Whitney, C. (1990). *Random Processes in Physical Systems*. Wiley.

Wilson, T. L., Rohlfs, K., and Hüttemeister, S. (2009). *Tools of Radio Astronomy*. Springer Berlin, Heidelberg.